

**Physiological role of cation channels of *P. irradians*  
ciliary photoreceptors and human sperm**

Dissertation

zur

Erlangung des Doktorgrades (Dr. rer. nat.)

der

Mathematisch-Naturwissenschaftlichen Fakultät

der

Rheinischen Friedrich-Wilhelms-Universität Bonn

vorgelegt von

**Fabio Andrés Echeverry**

aus

Ibagué, Kolumbien

Bonn 2016

Angefertigt mit Genehmigung der Mathematisch-Naturwissenschaftlichen Fakultät der  
Rheinischen Friedrich-Wilhelms-Universität Bonn

1. Gutachter: Prof. Dr. U. B. Kaupp

2. Gutachter: Prof. Dr. M. Pankratz

Tag der Promotion: 09.03.2017

Erscheinungsjahr: 2017





# Zusammenfassung

Eukariotische Flagellen und Zilien sind antennenartige Strukturen, die von Mikrotubuli durchzogen und von einer spezialisierten Erweiterung der Plasmamembran überzogen sind. Sie erfüllen verschiedenste physiologische Rollen, beispielsweise in der Sinneswahrnehmung aber auch der Zellmotilität, und sind entsprechend in vielerlei Zelltypen zu finden. Um ihre Funktion zu erfüllen nutzen Zilien und Flagellen eine Reihe spezifischer Ionenkanäle und Signalmoleküle. Ich habe die Funktion verschiedener Ionenkanäle in ziliären Photorezeptoren der Bucht-Kammuschel (*P. irradians*) sowie den Flagellen humaner Spermien untersucht.

Die Stimulation mit Licht führt in den ziliären Photorezeptoren von *P. irradians* zu einer Hyperpolarisation der Plasmamembran, welche wahrscheinlich auf das Öffnen cGMP-gesteuerter  $K^+$ -Kanäle zurückzuführen ist. Dies steht in direktem Kontrast zu dem gut charakterisierten Mechanismus der lichtinduzierten Hyperpolarisation in Stäbchen und Zapfen von Säugetieren, bei welchem die Hyperpolarisation durch das Schließen cGMP-abhängiger nichtselektiver Kationenkanäle hervorgerufen wird. In dieser Arbeit zeige ich, dass ERG-, HCN- sowie CNG-Kanäle in ziliären Photorezeptoren der Bucht-Kammuschel exprimiert werden, welche ich mittels der Patch-Clamp Technik und caged cGMP im heterologen System untersucht habe.

Neben Photorezeptoren basiert auch die Physiologie der Flagellen humaner Spermien auf einer Vielzahl von Ionenkanälen. Es wurde gezeigt, dass diverse Funktionen des Spermiums wie der Flagellenschlag oder die Akrosomreaktion, direkt von der intrazelluläre Kalziumkonzentration  $[Ca^{2+}]_i$  abhängen. In Spermien der Maus und des Menschen wird der  $Ca^{2+}$ -Einstrom in die Zelle durch den CatSper-Kanal kontrolliert. Die Aktivität von CatSper hängt dabei direkt vom intrazellulären pH-Wert sowie der Membranspannung ( $V_m$ ) ab. In Spermien der Maus wird  $V_m$  durch den  $K^+$ -Kanal Slo3 reguliert, während in menschlichen

Spermien unklar ist, welcher Kanal  $V_m$  maßgeblich bestimmt. Ich habe den humanen Slo3 Kanal heterolog in CHO-Zellen exprimiert und die von Slo3 getragenen Ströme mittels der Patch-Klamp Technik untersucht und mit den  $K^+$ -Strömen menschlicher Spermien ( $I_{K_{sper}}$ ) verglichen. Beide Ströme zeigen beeindruckend übereinstimmende Eigenschaften: Sie sind durch  $Ca^{2+}$  aktivierbar, unter intrazellulärer Alkalisierung leicht verstärkt und werden durch Progesteron in mikromolaren Konzentrationen inhibiert.

# Abstract

Eukaryotic flagella and cilia are antenna-like cellular extrusions, shaped by microtubules and covered by a specialized extension of the plasma membrane. They serve several tasks, like light and olfactory sensation or cell motility and are, therefore, present in various cell types. To exert their function flagella and cilia use a specific set of ion channels and signaling molecules. I investigated the function of different ion channels in the physiology of ciliary photoreceptors of the bay scallop (*P. irradians*) and the flagellum of human sperm.

Light stimulation of *P. irradians* ciliary photoreceptors induces a hyperpolarization of the cell membrane, presumably mediated by the opening of cGMP-dependent  $K^+$  selective channels. This stands in contrast to the well characterized light response of vertebrate rod and cone photoreceptors, where light stimulation induces a closure of cGMP-gated non-selective cation channels. I provided evidence that ERG, HCN and CNG channels are expressed in ciliary photoreceptors of *P. irradians*. Furthermore, I used caged cGMP and the patch-clamp technique to investigate ERG, HCN and CNG channels of ciliary photoreceptors of *P. irradians*.

Like photoreceptors, the physiology of sperm flagella is based on the fine interplay of several ion channels. The intracellular  $Ca^{2+}$  concentration has been shown to orchestrate various sperm functions like the swimming behavior and the acrosome reaction. In human and mouse sperm,  $Ca^{2+}$  entry is mediated by the principal  $Ca^{2+}$  channel of sperm (CatSper), which is modulated by the intracellular pH and membrane voltage ( $V_m$ ). In mouse sperm,  $V_m$  is predominantly controlled by the  $K^+$  channel Slo3. In contrast, the identity of the principal  $K^+$  channel of human sperm remains elusive. By patch-clamp recordings, I investigated the  $K^+$  currents mediated by human Slo3 (hSlo3) heterologously expressed in CHO cells and compared them to the  $K^+$  currents of human sperm ( $I_{K_{sper}}$ ). My work showed striking

similarities between hSlo3 carried-currents and human  $I_{K_{sper}}$ . I showed that hSlo3 currents are: activated by  $Ca^{2+}$ , weakly enhanced by intracellular alkalization, and inhibited by progesterone in the micromolar range, which are properties remarkably similar to  $I_{K_{sper}}$  of human sperm.

# I. Table of Contents

<b>I.</b>	<b><i>Table of Contents</i></b> .....	<b>I</b>
<b>II.</b>	<b><i>List of Abbreviations</i></b> .....	<b>V</b>
<b>1</b>	<b><i>Introduction</i></b> .....	<b>1</b>
1.1	Vertebrate ciliary photoreceptors: rods and cones.....	1
1.1	Ciliary photoreceptors of the scallop .....	2
1.2	Chemotactic signaling-pathway of sea urchin sperm .....	4
1.3	Ion channels of mammalian sperm .....	5
1.4	Phylogenetic relation between voltage-dependent K <sup>+</sup> channels and cyclic-nucleotide gated (CNG) channels .....	6
1.5	Superfamily of Kv channels: functional properties .....	8
1.6	Aim of the thesis .....	11
<b>2</b>	<b><i>Materials and methods</i></b> .....	<b>13</b>
2.1	Materials .....	13
2.2	<i>E. coli</i> cell culture .....	14
2.2.1	<i>Bacteria strains and plasmids</i> .....	14
2.2.2	<i>Culture of E. coli</i> .....	15
2.2.3	<i>E. coli</i> culture for purification of plasmid DNA .....	16
2.2.4	<i>Generation of competent cells for transformation with plasmid DNA</i> .....	16
2.3	Nucleic acids protocols .....	17
2.3.1	<i>Extraction and purification of plasmid DNA</i> .....	17
2.3.2	<i>Quantitation of nucleic acids</i> .....	19
2.3.3	<i>Separation of DNA in agarose gels</i> .....	21
2.3.4	<i>Extraction of DNA from agarose gels</i> .....	22
2.3.5	<i>Molecular cloning of DNA fragments</i> .....	22
2.3.6	<i>Polymerase Chain Reaction</i> .....	24
2.3.7	<i>P. irradians</i> retina mRNA purification & cDNA synthesis.....	25
2.3.8	<i>Rapid amplification of cDNA Ends (RACE)</i> .....	25
2.3.9	<i>DNA sequencing</i> .....	25
2.3.10	<i>Transcriptome of P. irradians</i> retina .....	26
2.3.11	<i>Transcriptome and sequence analysis</i> .....	26

---

2.4	Cell culture of Chinese Hamster Ovary (CHO) cells .....	26
2.4.1	<i>Cell culture conditions</i> .....	27
2.4.2	<i>Cryopreservation and thawing of CHO cells</i> .....	27
2.4.3	<i>Poly-L-Lysine coating of cover slips for cell culture</i> .....	28
2.5	Heterologous expression of proteins in CHO cells.....	28
2.5.1	<i>Transfection of CHO cells</i> .....	28
2.5.2	<i>Protein extraction from CHO cells</i> .....	29
2.6	Western-blot analysis and antibody screening.....	30
2.6.1	<i>SDS-Polyacrylamide Gel Electrophoresis (PAGE) and Western-blot analysis</i> .....	30
2.6.2	<i>Immunological detection of proteins</i> .....	31
2.7	Immunocytochemistry .....	33
2.7.1	<i>Fixation of CHO cells for immunocytochemistry</i> .....	33
2.7.2	<i>Immunocytochemical staining of CHO cells</i> .....	33
2.8	Antibodies.....	35
2.8.1	<i>Monoclonal primary antibodies</i> .....	35
2.8.2	<i>Secondary antibodies</i> .....	37
2.9	RNA <i>in-situ</i> hybridization and immunohistochemistry in <i>P. irradians</i> eye slices.....	37
2.9.1	<i>Eye slices of P. irradians</i> .....	37
2.9.2	<i>RNA in-situ hybridization</i> .....	38
2.9.3	<i>Immunohistochemistry of P. irradians eyes</i> .....	40
2.10	Electrophysiological recordings in <i>P. irradians</i> ciliary photoreceptors .....	41
2.10.1	<i>Dissociation of photoreceptors from P. irradians for patch clamp recordings</i> .....	41
2.10.2	<i>Patch-clamp recordings in P. irradians ciliary photoreceptors</i> .....	42
2.10.3	<i>Photolysis of caged compounds in P. irradians ciliary photoreceptors</i> .....	42
2.11	Patch-clamp recordings in Chinese Ovary Hamster (CHO) cells.....	43
2.11.1	<i>Patch-clamp recordings on CHO cells transfected with PectERG, PectHCN, and PectCNG1 channels</i> .....	43
2.11.2	<i>Patch-clamp recordings of CHO cells transfected with hSlo3 channels</i> .....	43
3	<b>Results</b> .....	45
3.1	Patch-clamp recordings in ciliary photoreceptors of <i>P. irradians</i> .....	45
3.1.1	<i>Benefits of using caged compounds to study the phototransduction cascade of P. irradians ciliary photoreceptors</i> .....	45

3.1.2	<i>cGMP-gated channels in ciliary photoreceptors of P. irradians</i> .....	46
3.1.3	<i>Ciliary photoreceptors have two different cGMP-gated conductances</i> .....	47
3.1.4	<i>The light-activated ion channel and cGMP-gated outward current have the same pharmacological properties</i> .....	50
3.1.5	<i>The ion selectivity of cGMP-gated inward current is reminiscent of classical CNG channels</i> .....	51
3.2	Analysis of the transcriptome of <i>P. irradians</i> retinas .....	52
3.2.1	<i>GetORF and UFO analysis</i> .....	52
3.2.2	<i>Homology search using sea urchin CNGKs</i> .....	52
3.2.3	<i>Homology search using K<sup>+</sup>-channels pore region and CNBD of CNG channels</i> ..	53
3.2.4	<i>Molecular cloning of ERG, HCN, and CNG channels</i> .....	53
3.3	Molecular cloning of PectERG, PectHCN, and PectCNG channels .....	55
3.3.1	<i>Constructs for heterologous expression</i> .....	61
3.3.2	<i>Western-blot analysis of P. irradians ion channels expressed in CHO cells</i> .....	63
3.4	Localization of PectERG, PectHCN, and PectCNG1 channels in <i>P. irradians</i> retina .....	64
3.4.1	<i>RNA in-situ hybridization (ISH) in eye sections of P. irradians</i> .....	65
3.4.2	<i>Immunolocalization of PectERG, PectHCN and PectCNG1 channels</i> .....	68
3.4.3	<i>Immunohistochemistry in P. irradians eye sections</i> .....	74
3.5	Electrophysiology on transfected CHO-cells expressing <i>P. irradians</i> ion channels .....	75
3.5.1	<i>Patch clamp recordings on PectHCN- and PectCNG1-transfected CHO cells</i> .....	76
3.5.2	<i>Electrophysiological features of P. irradians PectERG channels</i> .....	77
3.6	Functional characterization of the human Slo3 K <sup>+</sup> channel of sperm .....	87
3.6.1	<i>Human Slo3 K<sup>+</sup> channels are activated by Ca<sup>2+</sup></i> .....	87
3.6.2	<i>Pharmacological properties of the human Slo3 channel</i> .....	90
3.6.3	<i>hSlo3 channel is inhibited by Progesterone</i> .....	94
3.6.4	<i>hSlo3-mediated currents resemble the K<sup>+</sup> currents (IK<sub>sper</sub>) of human sperm</i> .....	95
4	<b>Discussion</b> .....	99
4.1	Light-activated K <sup>+</sup> channel of ciliary photoreceptors .....	99
4.2	Functional role of classical CNG channels in <i>P. irradians</i> ciliary photoreceptors .....	103
4.3	ERG channels of <i>P. irradians</i> ciliary photoreceptors.....	105
4.4	Ion channel properties of Slo3 and Slo1: which one underlies IK <sub>sper</sub> .....	109

4.5	What is the physiological role of Slo3 channels in human sperm? .....	110
5	<i>References</i> .....	113
6	<i>Appendix</i> .....	125
	<i>Acknowledgments</i> .....	133

## II. List of Abbreviations

4-AP	4-aminopyridine
~	approximately
<i>A. punctulata</i>	<i>Arbacia punctulata</i>
ATP	Adenosine triphosphate
bp	base pairs
°C	Celsius degree
C-Terminus	Carboxyl terminal of polypeptides
cAMP	Adenosine-3',5'-cyclic monophosphate
cDNA	complementary DNA
cGMP	Guanosine-3',5'-cyclic monophosphate
CHO cells	Chinese Hamster Ovary cells
CNBD	cyclic nucleotide-binding domain
CNG channel	cyclic nucleotide-gated channel
CNGK channel	K <sup>+</sup> -selective cyclic nucleotide-gated ion channel
cNMP	Cyclic Nucleotide Monophosphate
CTX	Charybdotoxin
Da	Dalton
dk	Donkey
DMEM	Dulbecco's Modified Eagle's Medium

*D. melanogaster* *Drosophila melanogaster*

DNA Deoxyribonucleic acid

DNase Deoxyribonuclease

dNTP Deoxyribonucleotide triphosphate

DTE Dithioerythritol

DTT Dithiothreitol

EAG channel *ether-a-gogo* K<sup>+</sup> channel

*E.coli* *Escherichia coli*

EDTA Ethylenediaminetetraacetic acid

e.g example given

EGTA Ethylene glycol-bis(β-aminoethyl ether)-N,N,N',N'-tetraacetic acid

ERG channel *ether-a-gogo*-related K<sup>+</sup> channel

*et al.* *et alia*

FCS fetal calf serum

G gauge, unit to measure the size of a needle

g gram

g Normal-gravity (9,81m x s<sup>-1</sup>)

GC Guanylyl cyclase

GFP Green Fluorescent Protein

gt goat

GTP Guanosine-5'-triphosphate

h	hour(s)
HA-Tag	Hemagglutinin A Tag
HCN channel	hyperpolarization and cyclic nucleotide-activated channel
HEPES	4-(2-hydroxyethyl)-1-piperazineethanesulfonic acid
hSlo3 channel	human Slo3 K <sup>+</sup> channel
HRP	Horseradish peroxidase
I	Electrical current
IbTX	Iberiotoxin
ICC	Immuncytochemistry
J	Joule
kDa	Kilodalton
K <sub>d</sub>	Dissociation constant
K <sub>i</sub>	Inhibition constant
K <sub>1/2</sub>	Concentration of half-maximal activation
LB	Lysogeny Broth
l	Liter
min	minute(s)
ml	milliliter
M	molar
m	meter
mOsm	milliosmol

mPIC	mammalian protease inhibitor cocktail
mRNA	messenger RNA
mV	millivolt
N-Terminus	Amino terminus of a polypeptide
NaAc	Sodium Acetate
n	number of experiments
OD	Optical density
Oligo-dT	Oligodeoxythymidine
ON	Overnight
<i>P. irradians</i>	<i>Pecten irradians</i>
PAGE	Polyacrylamide-Gel Electrophoresis
pA	Picoampere
PBS	Phosphate Buffer Saline
PCR	Polymerase Chain Reaction
PDE	Phosphodiesterase
pH	negative logarithm of the proton concentration
PLL	Poly-L-Lysine
PTX	Pertussis toxin
PVDF	Polyvinylidene fluoride
R	Gas constant ( $8.3 \text{ J} \times \text{mol}^{-1} \times \text{K}^{-1}$ )
rb	rabbit

RNA	Ribonucleic acid
RNase	Ribonuclease
RT-PCR	Reverse transcription Polymerase Chain Reaction
RT	Room Temperature
rt	rat
S1-S6	Transmembrane Segments 1-6
SDS	Sodium Dodecyl Sulfate
s	seconds
TAE	Tris-Acetate-EDTA buffer
TEMED	N,N,N',N'-Tetramethylethylenediamine
TE	Tris-EDTA buffer
T <sub>m</sub>	melting temperature
Tris	Tris(hydroxymethyl)aminomethane
T	Temperature
t	time
U	Enzyme unit
μl	microliter
UV	Ultraviolet light
V <sub>h</sub>	Holding electrical potential
V <sub>m</sub>	Transmembrane electrical potential
V <sub>rev</sub>	Reversal potential

V Volt

WB Western Blot

WT Wildtype

W Watt

# 1 Introduction

Eukaryotic flagella and cilia are antenna-like cellular protuberances composed of microtubules and covered by a specialized extension of the plasma membrane (Haimo and Rosenbaum, 1981). Flagella and cilia play functional roles in cell types as diverse as sperm and photoreceptors (Khanna, 2015; Strünker et al., 2015). Sperm flagella and cilia of ciliary photoreceptors function by expressing a specific pool of signaling molecules and ion channels (Yau and Hardie, 2009b; Doerner et al., 2015; Khanna, 2015; Strünker et al., 2015).

## 1.1 Vertebrate ciliary photoreceptors: rods and cones

The photo-transduction of vertebrate rod and cone photoreceptors has been characterized in detail. Rods and cones are ciliary photoreceptors that use transducin or Gt as G-protein, a cGMP-specific phosphodiesterase (PDE) as effector enzyme, and non-selective cGMP-gated cation channels (CNG channels) as transduction channels (Kaupp et al., 1989; Kaupp and Seifert, 2002; Yau and Hardie, 2009b). Light absorption by rhodopsin activates Gt, which stimulates PDE. The PDE diminishes cGMP levels, which are elevated in the dark; the decrease of cGMP level induces the closure of CNG channels, generating the characteristic hyperpolarizing response of rods and cones (Gauss et al., 1998; Burns and Baylor, 2001).

In order to better understand the evolution of ciliary photoreceptors, it is important to have a wider phylogenetic coverage of light-sensing cells, and to characterize them in depth, both at the molecular and physiological level. Ciliary photoreceptors of the bay scallop, *Pecten irradians* present unique features that make them especially interesting.

## 1.1 Ciliary photoreceptors of the scallop

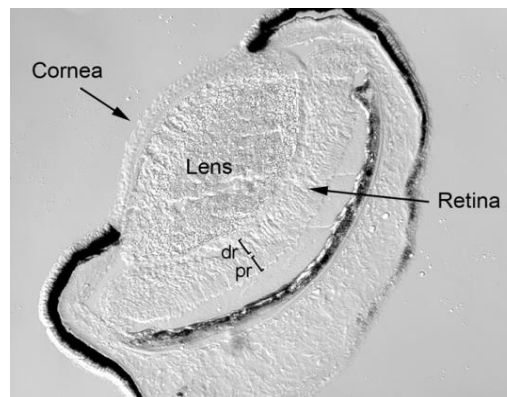


**Figure 1.1:** Micrograph showing a section of a *Pecten irradians* eye. It shows the distal (dr) and proximal (pr) retina layers.

According to the morphology, photoreceptors are classified as either microvillar or ciliary (Arendt, 2003; Arendt et al., 2009). The eye of *P. irradians* has two retinal layers: the proximal retina (pr, see Fig. 1.1), containing microvillar photoreceptors and the distal retina (dr, Fig. 1.1), containing ciliary photoreceptors (Land, 1965; Gorman and McReynolds, 1969). Ciliary photoreceptors of *P. irradians* hyperpolarize in response to light. They use cGMP as internal messenger, like vertebrate rods and cones (Gomez & Nasi, 1995). However, their hyperpolarizing light response seems to be due to an entirely different mechanism: light leads to opening of ion channels that are  $K^+$ -selective (McReynolds and Gorman, 1974; Gomez and Nasi, 1994b).

Some molecular details of the light-signaling cascade are already known in a related species (*Patinopecten yessoensis*), where an unusual rhodopsin and a G protein of subtype o ( $G_o$ ) have been identified using molecular cloning, *in-situ* RNA hybridization (ISH), and immunohistochemistry (Kojima et al., 1997). Furthermore, studies on *P. irradians* using pharmacological approaches and patch-clamp recordings showed that  $G_o$  mediates the photo-response, and that most likely the light-activated enzyme is a guanylyl cyclase (Gomez and Nasi, 2000) (Gomez & Nasi, 2000). Moreover, cGMP may directly activate a cGMP-gated

K<sup>+</sup> channel (CNGK) which is responsible for the hyperpolarization (Gomez & Nasi, 1995). However, the molecular identity of the transduction channel is not known.

The electrophysiological and pharmacological properties of the light-activated K<sup>+</sup> channels of ciliary photoreceptors have been well characterized (Gomez and Nasi, 1994b). The light-activated channels are highly K<sup>+</sup>-selective; they closely follow the calculated Nernst potential for K<sup>+</sup> ions. In addition, the selectivity sequence of the transduction channel for alkali cations is K<sup>+</sup> > Rb<sup>+</sup> > Cs<sup>+</sup> > Na<sup>+</sup>, Li<sup>+</sup> and the permeation ratio for Na<sup>+</sup> and K<sup>+</sup> ions (PNa<sup>+</sup>/PK<sup>+</sup>) is around 0.008, this means that the permeation of K<sup>+</sup> ions through light-activated channels is approximately 120-fold higher than Na<sup>+</sup> ions (Cornwall and Gorman, 1983). The high K<sup>+</sup> selectivity together with the selectivity sequence are properties reminiscent of voltage-gated K<sup>+</sup> channels. Furthermore, the transduction channels are blocked by Mg<sup>2+</sup> and Ca<sup>2+</sup> ions; which cause an outward rectification of the channel, due to a voltage dependent blockage. Ca<sup>2+</sup> blocks these channels with higher affinity than Mg<sup>2+</sup> ions (Gomez and Nasi, 2005). Removal of divalent cations causes a two-fold increase in the light-activated conductance (Gomez and Nasi, 1997a). Moreover, light-activated channels of ciliary photoreceptors of *P. irradians* are inhibited by common blockers of voltage-gated K<sup>+</sup> channels, like intracellular Cs<sup>+</sup>, TEA and, 4-aminopyridine (4-AP) (Gomez and Nasi, 1994a, 1997b). Particularly, 4-AP blocks the channels with high affinity (K<sub>1/2</sub>= 0.4 μM) (Gomez and Nasi, 1994a). Patch-clamp recordings performed on ciliary photoreceptors showed that micromolar concentrations of 8-Br-cGMP, applied through the patch pipette, activates a K<sup>+</sup>-selective conductance (Gomez and Nasi, 1995). Furthermore, increasing concentrations of the cGMP analogue diminishes the pool of ion channels available to be activated by the light-signaling cascade, suggesting that the transduction channels are directly gated by cGMP (Gomez & Nasi, 1995). In addition, L-cis Diltiazem, a CNG channel blocker, blocks both, the light and cGMP-activated K<sup>+</sup> channels with a similar affinity as the CNG channels from rod photoreceptors (Gomez and

Nasi, 1997b). The conductance activated by 8-Br-cGMP shares all the electrophysiological and pharmacological features with the  $K^+$ -conductance activated by light (Gomez & Nasi, 1995; Gomez & Nasi, 2005).

Recently the molecular identity of a  $K^+$  channel gated by cGMP (CNGK) has been elucidated (Bönigk et al., 2009). CNGK channels are involved in the chemotactic signaling-pathway that controls motility in sea urchin sperm (Strünker et al., 2015).

## 1.2 Chemotactic signaling-pathway of sea urchin sperm

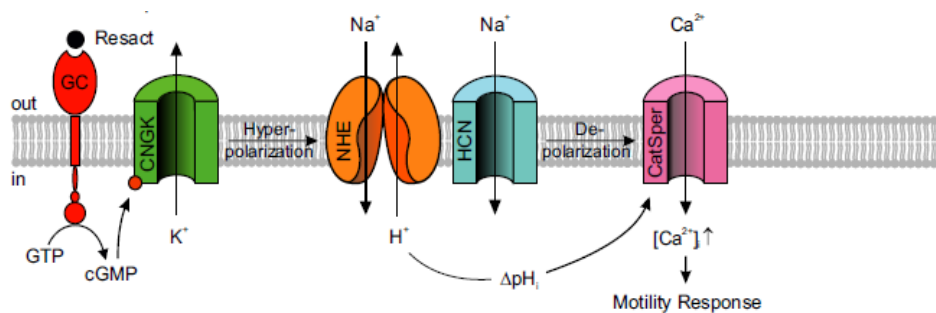


**Figure 1.2:** Chemotactic signaling pathway of sea urchin sperm, *Arbacia punctulata*. Adapted from (Seifert et al., 2015).

Sea urchins reproduce through external fertilization. Female and male animals release their gametes, eggs and sperm, respectively, into the sea. Eggs release chemical cues (chemoattractants) that guide sperm cells toward them, this process is called chemotaxis (Alvarez et al., 2014). The chemotactic signaling cascade (Figure 1.2) of sea urchin sperm, *Arbacia punctulata*, has been well characterized (Strünker et al., 2015). The chemoattractant (resact) activates a guanylate cyclase (GC) that is embedded in the membrane of the sperm flagellum. Upon activation, the GC rapidly increases the cGMP level inside the flagellum (Kaupp et al., 2003). In turn, cGMP activates a  $K^+$ -selective channel (CNGK) which hyperpolarizes the cell due to the efflux of  $K^+$  ions (Strünker et al., 2006). Subsequently, hyperpolarization elicits two different signals; rapid intracellular alkalization via  $Na^+/H^+$

exchangers (sNHE) and depolarization via HCN channels. Alkalization shifts the voltage dependence of sperm-specific  $\text{Ca}^{2+}$  (CatSper) channels to more negative values, which causes the opening of CatSper channels by the HCN channel-induced depolarization. In turn, CatSper-channel activation causes further depolarization and a concomitant increase in intracellular  $\text{Ca}^{2+}$ -concentration, modifying the flagellar beat of sperm cells (Seifert et al., 2015; Strünker et al., 2015). Sea urchin sperm are remarkably sensitive to their chemoattractant; they can sense the binding of single molecules of resact to its receptor (Pichlo et al., 2014; Strünker et al., 2015).

### **1.3 Ion channels of mammalian sperm**

During fertilization mammalian sperm use chemical, thermal and rheotactic cues to navigate and find the eggs (Lishko et al., 2012; Miki and Clapham, 2013). To effectively fertilize the eggs sperm undergo capacitation, hyperactivation and acrosome exocytosis (De Jonge, 2005). A specific combination of ion channels allows mammalian sperm to navigate the female genital tract, find and fertilize the oocytes (Lishko et al., 2012). The physiological role of ion channels in mouse sperm has been well studied (Navarro et al., 2007; Zeng et al., 2011). Intracellular pH and membrane voltage modulate the different ion channels in mouse sperm (Lishko et al., 2012). Intracellular pH modulates the sperm specific  $\text{Ca}^{2+}$  channel (CatSper) and Slo3  $\text{K}^+$  channels (Zeng et al., 2011; Lishko et al., 2012). In contrast, little is known about the role of the different ion channels of human sperm. Recent reports have shown that ion channels of mouse and human differ in their functional features. For instance, human CatSper channels are activated by progesterone, whereas mouse CatSper are not. On the other hand, Catsper channels from mouse are strongly activated by alkalization, whereas human CatSper are weakly sensitive to alkalization (Strünker et al., 2011; Lishko et al., 2012). In

addition, alkalization activates Slo3, the principal  $K^+$  channels of mouse sperm (Navarro et al., 2007; Zeng et al., 2011).

#### **1.4 Phylogenetic relation between voltage-dependent $K^+$ channels and cyclic-nucleotide gated (CNG) channels**

The superfamily of voltage-gated ion channels is one of the largest group of proteins involved in signal transduction. Voltage-gated ion channels are tetramers composed of subunits that either assemble from different polypeptides in the endoplasmic reticulum (ER) or fold from a single polypeptide (Catterall, 1995).

The most diverse members within the superfamily of voltage-gated ion channels are the voltage-gated  $K^+$  (Kv channels) channels. Members of the Kv-channel family harbor six membrane-spanning domains (S1-S6) with the N- and C-terminus of the protein located intracellularly (Jan and Jan, 2012). Furthermore, the capability to sense voltage is carried by the so called voltage-sensing (VSD) domain. VSDs are located in the fourth transmembrane segment (S4) of Kv channels and are composed of several positively charged amino acids, typically Arginines, spaced every third position throughout the entire domain (Jiang et al., 2003). The pore region is located between the fifth and sixth transmembrane (S5-S6) segments; it harbors the  $K^+$ -channel signature sequence, which corresponds to amino acids TVGYG (Thr-Val-Gly-Tyr-Gly) (Heginbotham et al., 1994). Single mutations within this region alter channel function dramatically, resulting in reduced  $K^+$ -selectivity or even lack of ion conduction (Heginbotham et al., 1994).

Although CNG channels are ligand-gated cation channels, they belong to the Kv-channel family (Kaupp et al., 1989; Kaupp and Seifert, 2002). Like Kv channels, CNG channels are tetramers made of subunits with six transmembrane domains, a voltage-sensing domain in S4 and a pore region located between S5 and S6 domains (Kaupp and Seifert, 2002). The pore region of CNG channels lacks the K<sup>+</sup>-selectivity signature (TVGYG) sequence of K<sup>+</sup>-selective channels; instead, they contain a TVGET sequence which makes them non-selective cation channels (Kaupp et al., 1989; Heginbotham et al., 1992). In addition, CNG channels harbor a cyclic nucleotide-binding domain (CNBD) in the C-terminus of the channel polypeptide. The CNBD is crucial for proper function of CNG channels, because it contains the binding site for cyclic nucleotides, which is responsible for channel gating (Kaupp et al., 1989; Kaupp and Seifert, 2002).

With regards to quaternary structure, CNG channels are heterotetrameric proteins composed of two to three different subunits. Subunit stoichiometry of vertebrate CNG channels is variable in different cell types. For instance, CNG channels of rod photoreceptors contain three alpha subunits (CNGA1) and one beta (CNGB1) (Weitz et al., 2002; Zheng et al., 2002; Zhong et al., 2002). Moreover, CNG channels of olfactory sensory neurons have a stoichiometry of three alpha subunits (two CNGA2 & one CNGA4) and one beta subunit (CNGB1) (Bönigk et al., 1999). Assembly of different CNG channel subunits produces ion channels with slightly different functional properties like differential selectivity for Ca<sup>2+</sup> or susceptibility to the CNG channel blocker L-cis-Diltiazem (Gerstner et al., 2000; Kaupp and Seifert, 2002).

Due to the structural similarities between Kv and CNG channels, it has been suggested that CNG channels have evolved from ancestral Kv channels (Biel and Michalakis, 2009). Indeed, other members of the Kv-channel family present intermediate functional properties

such as voltage-gated  $K^+$  channels harboring vestigial CNBDs (EAG-channel family) (Warmke et al., 1991; Trudeau et al., 1995), voltage-gated ion channels that are modulated by cNMPs (HCN channels) (Gauss et al., 1998), and  $K^+$ -selective CNG channels (Bönigk et al., 2009) (Bönigk *et al*, 2009). Members of the EAG-channel family are voltage-gated  $K^+$  channels that harbor a CNBD at the C-terminus; however, cNMPs neither gate nor modulate these channels (Brelidze et al., 2009). HCN channels are poorly  $K^+$ -selective channels that are gated by hyperpolarization and modulated by cyclic AMP (Gauss et al., 1998; Robinson and Siegelbaum, 2003). Recently, the CNGK channel of sea urchin sperm has been molecularly identified and functionally characterized (Strünker et al., 2006; Bönigk et al., 2009). Interestingly, CNGK channels have a similar topology as voltage-gated sodium channels; one single protein contains four repeats that are analogous to single subunits of CNG channels (Bönigk et al., 2009). Thus, functional channels result from folding of a single polypeptide instead of the assembly of four separate subunits as seen in Kv and CNG channels. CNGKs contain a TVGYG  $K^+$ -signature sequence in the pore region and a CNBD in the C-terminus (Bönigk et al., 2009) (Bönigk et al, 2009). The fact that different ion channels with intermediate properties between Kv and CNG channels exist through different animal clades, provides an excellent support to the hypothesis that CNG channels originated from ancestral Kv channels.

### **1.5 Superfamily of Kv channels: functional properties**

Despite the structural similarities between Kv and CNG channels, their functional properties are different (Heginbotham et al., 1992; Biel and Michalakakis, 2009). Due to their physiological relevance; Kv channels have been extensively studied. Kv channels are involved in physiological processes such as setting of resting potential, cell hyperpolarization and cell repolarization after depolarizing events (MacKinnon, 2003). The molecular

mechanisms of voltage sensing and gating in Kv channels are well understood. The probability of channel opening ( $P_o$ ) is regulated by the VSD, which in turn is controlled by the membrane potential. The VSD of Kv channels translates changes in membrane voltage into conformational changes that lead to channel opening (Bezanilla, 2008, 2008). A hallmark of Kv channels is their steep voltage-dependence (Bezanilla, 2008). A salient feature of  $K^+$  channels is their exquisite selectivity for  $K^+$  ions; the permeability sequence of all known  $K^+$  channels is  $Tl^+ > K^+ > Rb^+ > NH_4^+$  and they are usually blocked by intracellular  $Cs^+$ . Furthermore, Kv channel permeability of  $Na^+$  and  $Li^+$  is in most cases too low to measure (Hille, 2001).

Classical CNG channels on the other hand, are non-selective cation channels that mainly occur in sensory cells like rod and cone photoreceptors, olfactory sensory neurons (OSNs); likewise in motile cells like mammalian sperm cells (Liman and Buck, 1994; Kaupp and Seifert, 2002; Solzin et al., 2004). The first CNG channel to be molecularly identified and functionally characterized was the CNG channel of rod photoreceptors (Kaupp et al., 1989).

Regardless of the tissue of expression, all classical CNG channels poorly discriminate among cations (Dhallan et al., 1990; Gauss et al., 1998; Biel and Michalakis, 2009). Therefore, the reversal potential of CNG channels is close to 0 mV, when bathed in a physiological ion milieu (Kaupp and Seifert, 2002). Moreover, CNG channels present a voltage-dependent blockade caused by divalent cations, principally  $Ca^{2+}$ . Calcium permeation through CNG channels is of physiological importance. For instance, the ability of rods to respond to single photons and adaptation to light of rods and cones is mediated by  $Ca^{2+}$  (Burns and Baylor, 2001; Kaupp and Seifert, 2002).

Additionally, opening of CNG channels occur upon binding of cNMPs. The CNBD harbors the cNMP-binding site. Binding of cNMPs to the CNBD elicits an allosteric conformational change that gates CNG channels; fine details of this conformational change are still subject of research (Cukkemane et al., 2011). Recently, CNG channels have been grouped into two different groups based on cNMPs binding. Classical CNG channels formed by assembly of different subunits are gated by cNMPs in a cooperative fashion (Cukkemane et al., 2011). Although classical CNG channels are gated by cGMP and cAMP, different CNG-channel subunits confer differential affinities for cyclic nucleotides (Kaupp and Seifert, 2002; Biel and Michalakis, 2009). For instance, rod CNG channels are fully gated by cGMP whereas cAMP activates them only partially. Conversely, CNG channels of OSNs have higher sensitivity for cAMP than for cGMP; however in this case cGMP is a full agonist of the channel (Kaupp and Seifert, 2002). In contrast, CNGK channels are gated non-cooperatively and a single cGMP molecule is sufficient to fully activate them (Bönigk et al., 2009; Cukkemane et al., 2011).

## 1.6 Aim of the thesis

The electrophysiological and pharmacological properties of the  $K^+$  channels involved in the photo-transduction cascade of ciliary photoreceptors of *P. irradians* have been well characterized; however, the molecular identity of these ion channels remains in the dark. In addition, although the functional properties of several ion channels involved in sperm physiology have been well studied, little is known about the role of  $K^+$  channels in human sperm physiology. Thereby, the aims of my thesis are (1) to molecularly identify and localize cyclic-nucleotide-modulated ion channels in *P. irradians* retina. Likewise, (2) to electrophysiologically characterize these ion channels in a heterologous-expression system and in the native photoreceptors of *P. irradians*. Additionally, (3) to characterize the functional properties of the human Slo3  $K^+$ -channel.



## 2 Materials and methods

### 2.1 Materials

Chemicals were p.a. quality. Chemicals used were purchased from the companies AppliChem (Darmstadt, Germany), GE Healthcare Life Sciences (UK), Biozym (Hess. Oldendorf, Germany), Merck (Darmstadt, Germany), MWG Biotech (Ebersberg, Germany), Pierce (Rockford, USA), Qiagen (Hilden, Germany), Riedelde Haën AG (Seelze, Germany), Serva (Heidelberg, Germany), Sigma (Deisenhofen, Germany), Roth (Karlsruhe, Germany) and BioRad (München, Germany).

Enzymes and their buffers were purchased from Novagen (Darmstadt, Germany), Ambion (Austin, USA), GE Healthcare Life Sciences, GIBCO BRL (Eggenstein, Germany), MBI Fermentas (Vilnius, Lithuania), NEB (Germany) and Roche (Mannheim, Germany). Oligonucleotides (primers) were purchased from Eurofins MWG Operon (Ebersberg, Germany).

Bacteria media were ordered from Sigma. Chemicals and reagents for cell culture were ordered from GIBCO BRL. Secondary antibodies and reagents for immunochemical techniques were purchased from GE Healthcare Life Sciences, Invitrogen (Paisley, UK) and Jackson Immuno Research Laboratories (Suffolk, UK). Microscope slides were purchased from Menzel (Braunschweig, Germany). PVDF-Membrane Immobilon P for western blotting was purchased from Millipore (Eschborn, Germany). All solutions were prepared in double-distilled (bidest) water, unless otherwise stated. All solutions were sterilised by autoclaving (20 min, 121°C), unless otherwise stated.

## 2.2 *E. coli* cell culture

The procedures to work with *Escherichia coli* were performed as in Loogen (2009) and modified accordingly.

### 2.2.1 Bacteria strains and plasmids

The following *E. coli* K12-strain was used throughout this work:

TOP10 (Life Technologies)

Genotype: F<sup>-</sup>, *mcrA*,  $\Delta(mrr-hsdRMS-mcrBC)$ ,  $\Phi80lacZ\Delta M15$ ,  $\Delta lacX74$ , *recA1*, *araD139*,  $\Delta(ara-leu)7697$ , *galU*, *galK*, *rpsL*, (StrR), *endA1*, *nupG*)

pBluescript SK (Stratagene)

This plasmid was used for cloning and sequencing of recombinant DNA and for *in vitro* transcription experiments for *in-situ* RNA hybridization.

pcDNA3.1(+) (Life Technologies)

This plasmid was used for transient transfection and gene expression of proteins in Chinese Hamster Ovary (CHO) cells.

pc3Citrin

The plasmid pcDNA3.1(+) was genetically modified to include an expression reporter-gene. The Neomycin cassette was replaced with the gene of the fluorescent protein Citrin.

pc3QBICitrin

The pc3Citrin plasmid was genetically modified. The enhancer sequence QBI SP163 was placed before the start codon of Citrin.

**Table 2.2.1.1:** DNA constructs

Construct name	Name used on this thesis
pc3QBICitrinQBIPectERG-HA	PectERG
pc3QBICitrinQBIPectCNG1-HA	PectCNG1
pc3QBICitrinQBIPectHCN-HA	PectHCN

### 2.2.2 Culture of *E. coli*

LB medium (Carl Roth) was used to grow *E. coli* bacteria. The following are the components of the LB medium: 10 g/l Tryptone, 5 g/l Yeast extract, 5 g/l NaCl, pH 7.0. In addition, as solid growth medium LB- Agar-plates (Sigma) containing 15 g/l Agar were used. Liquid medium was placed in glass bottles and autoclaved (20 min). Bottles containing LB medium were stored at RT. LB medium containing Agar were autoclaved

and poured (25-30 ml) into sterile petri dishes. To prepare LB agar-plates with Ampicillin, before pouring into the petri dishes Ampicillin, at a final concentration of 100 µg/ml, was added to the hot (max T = 60 °C) LB medium with agar. After the agar was solid, agar plates were stored at 4 °C.

### **2.2.3 *E. coli* culture for purification of plasmid DNA**

*E. coli* bacteria were incubated at 37 °C in LB medium for 12-16 h in a rotation incubator (New Brunswick Scientific; Edison, USA). To select the bacteria that internalized the plasmid, solid or liquid LB medium with ampicillin was used.

### **2.2.4 Generation of competent cells for transformation with plasmid DNA**

In order to generate competent bacteria, a CaCl<sub>2</sub> method was used (Mandel and Higa, 1970). *E. coli* bacteria were cultured overnight, 500 µl of such a culture were transferred to 50 ml of LB medium. Bacteria were incubated at 37 °C while shaking, until it reached an optical density (at 600 nm; OD<sub>600</sub>) of 0.4. At this OD, bacteria have a concentration of 2 x 10<sup>8</sup> cells/ml. LB-medium containing bacteria was cooled down on ice. The bacteria culture was centrifuged for 10 min at 4 °C and 5,000 g, the supernatant was discarded and the pellet containing the bacteria was resuspended in 1 ml of CaCl<sub>2</sub> (0.1 M). The resuspended bacteria were diluted in CaCl<sub>2</sub> (0.1 M), to a final volume of 25 ml and incubated at 4 °C for 20 min. Afterwards, bacteria were centrifuged for 10 min at 4 °C and 5,000 g, resuspended in 1 ml of a solution of 25% glycerin and CaCl<sub>2</sub> (0.1 M), the resuspension was taken to a final

volume of 5 ml. Subsequently, the bacteria were incubated for 2 h on ice, aliquoted (50 and 100  $\mu$ l) and stored at -80 °C.

## 2.3 Nucleic acids protocols

The procedures to work with nucleic acids were performed as in Loogen (2009) and were modified accordingly.

### 2.3.1 Extraction and purification of plasmid DNA

DNA samples were reconstituted in TE-based buffers (Table 2.3.1.1) unless otherwise stated.

**Table 2.3.1.1:** DNA buffers.

Buffer	Composition
TE	10 mM Tris/HCl pH 8.0; 0.1 mM EDTA
TE/RNase	10 mM Tris/HCl pH 8.0; 0.1 mM EDTA; 4 $\mu$ l RNase-Cocktail per ml (Ambion)

### 2.3.1.1 Plasmid DNA minipreparations: alkaline lysis (Birnboim and Doly, 1979)

In order to make a plasmid DNA minipreparation, an overnight (ON) culture (4 ml) of bacteria containing the plasmid of interest was centrifuged (20,000 g; 4 °C) for 1 min. The pellet was resuspended either by pipetting or vortexing in 50 µl of solution I (Table 2.3.1.2). Next, to lyse the cells, 50 µl of solution II (Table 2.3.1.2) were added to the resuspended bacteria. To keep the genomic DNA intact, the bacteria were lysed by gently inverting the tubes several times. To precipitate debris, proteins, and genomic DNA, 50 µl of solution III (Table 2.3.1.2) was added and mixed by gently inverting the tubes several times. Afterwards, bacteria were centrifuged for 5 min at 20,000 g and 4 °C. The supernatant was carefully removed by pipetting and transferred to a clean tube. To precipitate plasmid DNA, 500 µl of ethanol (4 °C) was added and then centrifuged (20,000 g; 4 °C) for 5 min. Subsequently, the supernatant was discarded, 500 µl of 70% ethanol was added and centrifuged (20,000 g; 4 °C) for 5 min. The pellet was air-dried in a hot plate (37 °C) for approx. 10 min. Next, 10 µl TE/RNase buffer (Table 2.3.1.1) was added and the pellet was resuspended by shaking (700 rpm; 37 °C) for 10 min.

**Table 2.3.1.2.** Solutions for plasmid-DNA minipreparation

Solution I	Solution II	Solution III
25 mM Tris/HCl pH 7.5	0.2 M NaOH	3 M KAc pH 4.8
10 mM EDTA	1% SDS	

### **2.3.1.2 Plasmid-DNA preparation: NucleoBond Xtra Kit (Macherey - Nagel)**

To achieve the purity and quantity needed for transfection of cultured cells, the NucleoBond Xtra Midi Kit (Macherey-Nagel) was used following the manufacturer's instructions. To achieve a higher yield, the plasmid DNA was washed in isopropanol and centrifuged (15,000 g; 4°C) for 30 min. Afterwards, the pellet was washed in 70% Ethanol, air-dried and resuspended in 100 µl of TE buffer (Table 2.3.1.1).

### **2.3.1.3 DNA purification using SureClean (BIOLINE)**

The DNA sample was mixed with an equal volume of SureClean (Bioline). The mixture was incubated at room temperature (RT) for 10 min, and then centrifuged for 10 min at 14,000 g. The supernatant was carefully removed by aspiration. A volume of 70% ethanol equal to two times of the original sample-volume was added and vortexed for 10 s. The sample was then centrifuged (14,000 g) for 10 min, the supernatant was removed by aspiration and the pellet was air-dried to ensure complete removal of ethanol. The pellet was resuspended in the desired volume of TE buffer (Table 2.3.1.1).

## **2.3.2 Quantitation of nucleic acids**

### **2.3.2.1 Spectrophotometric measurement of nucleic-acid concentration**

To determine the concentration of nucleic acids using spectrophotometry, the sample was diluted (1:1000) in double-distilled (bidest) water, the optical density at 260 nm ( $OD_{260}$ ) was measured. Bidest water was used as blank sample. The  $OD_{260}$  values shown in table 2.3.2.1.1 were used to calculate the concentration of nucleic acids in the sample. The purity

of the sample was assessed using the OD ratio at 260 and 280 nm ( $OD_{260/280}$ ), for the sample to have a high purity the  $OD_{260/280} \geq 1.85$ .

**Table 2.3.2.1.1:** Values used to calculate the concentration of nucleic acids

---

<b>Double-stranded DNA <math>OD_{260} = 1</math></b>	50 $\mu\text{g/ml}$
<b>RNA <math>OD_{260} = 1</math></b>	40 $\mu\text{g/ml}$

---

### **2.3.2.2 Determination of nucleic-acid concentration in agarose gels**

To estimate the amount of DNA on agarose gels, the sample was compared to the Lambda DNA ECORI HindIII marker 3 (MBI Fermentas) which contained a known amount of DNA per band. The following is the fragment size (in bp) and amount of DNA (in ng) per 10 µl of ladder loaded: 21.226 bp (~292 ng), 5.148 bp (~71 ng), 4.973 bp (~68 ng), 4.268 bp (~59 ng), 3.530 bp (~49 ng), 2.027 bp (~28 ng), 1.904 bp (~27 ng), 1.584 bp (~24 ng), 1.375 bp (~19 ng), 947 bp (~13 ng), 831 bp (~11 ng), 564 bp (~8 ng), 125 bp (~2 ng). The sample together with the DNA ladder were run in an agarose gel containing Ethidium Bromide (EtBr), which binds to nucleic acids and glows under UV light, then the gel was visualized on a UV transilluminator.

### **2.3.3 Separation of DNA in agarose gels**

Analysis and separation by size of nucleic acids was performed using agarose gel electrophoresis. To separate nucleic acids ranging from 500 to 10,000 bp, 0.75-1 % agarose gels were used. To separate nucleic acids smaller than 500 bp, 1.5-2 % agarose gels were used. Agarose was dissolved in TAE buffer (Table 2.3.3.1) by heating. The agarose solution was cooled down to 60 °C and EtBr (1 µg per ml of solution) was added. The agarose solution was poured into a gel chamber; the loading wells were formed using a gel comb. The electrophoresis was performed in TAE buffer, using a constant voltage (120 V) for 20 min. Nucleic acids were visualized using a UV transilluminator.

**Table 2.3.3.1:** Solutions for agarose gel electrophoresis

---

<b>Solution</b>	<b>Contents</b>
TAE (50x)	2 M Tris/Acetate pH 7.5; 50 mM EDTA
Loading buffer (10x)	10x TAE; 50% Glycerin; 0.25% Xylencyanol

---

### **2.3.4 Extraction of DNA from agarose gels**

To extract DNA fragments from agarose gels, the Nucleospin and PCR clean-up gel extraction kit (Macherey-Nagel) was used, following the manufacturer's instructions.

### **2.3.5 Molecular cloning of DNA fragments**

Molecular cloning was performed as described in (Loogen, 2009)

#### **2.3.5.1 Restriction analysis of DNA**

To digest DNA with restriction enzymes, DNA and restriction enzymes were mixed with the recommended reaction buffer (NEB or Roche) and incubated at the optimal temperature for each restriction enzyme. Restriction analysis of DNA was performed in a volume of 10  $\mu$ l and digested for 2-4 h, unless otherwise specified. The digested DNA-fragments were separated using agarose-gel electrophoresis. DNA fragments were gel purified (section 2.3.4).

### 2.3.5.2 Ligation of DNA fragments

For ligation reactions, a 1:5 ratio of vector:DNA-fragment was used. Aprox 50 ng of linearized vector was used per ligation reaction. A reaction volume of 10  $\mu$ l was used. The recommended Ligation Reaction Buffer (Table 2.3.5.2.1) for the T4-ligase (Roche or NEB) was used. Ligation reactions containing: vector, DNA fragments, reaction buffer and T4 ligase were mixed in a micro-centrifuge tube and incubated for at least 1 h, at RT.

**Table 2.3.5.2.1:** Buffers for ligation reactions

Buffer			Contents (mM)
NEB	Ligase	Reaction	500 Tris/HCl pH 7.5; 100 MgCl <sub>2</sub> ; 100 DTT; 10 ATP
		Buffer (10 x)	
Roche	Ligase	Reaction	600 Tris/HCl pH 7.5; 50 MgCl <sub>2</sub> ; 10 DTE; 10 ATP
		Buffer (10 x)	

### 2.3.5.3 Bacteria transformation with plasmid DNA

To transform bacteria, 5  $\mu$ l of ligation reaction (section 2.3.5.2) were mixed with 5  $\mu$ l of 10x CM (100 mM CaCl<sub>2</sub>, 400 mM MgCl<sub>2</sub>); bidest water was used to fill the volume to 50  $\mu$ l and the sample was placed on ice for 10 min. Competent bacteria were thawed on ice. 50  $\mu$ l of competent bacteria were added to the sample, carefully mixed by pipetting and incubated on ice for 20 min. Afterwards, bacteria were heat-shocked at 42 °C for 60 s and returned to ice

(10 min) for recovery. Then, 200 µl of pre-warmed LB medium was added to the transformed bacteria and then placed in a shaker (300 rpm) at 37 °C for 30 min. Finally, 150 µl of transformed bacteria were spread onto LB-agar plates and incubated ON at 37 °C.

To amplify purified plasmid-DNA, 1 µl of plasmid DNA was used instead of the ligation sample and the protocol mentioned above was followed.

### 2.3.6 Polymerase Chain Reaction

The Polymerase Chain Reaction (PCR) was used to amplify DNA fragments. Several cycles allow the template DNA to denature; in turn, the oligonucleotides (primers) hybridize with the template DNA and a heat-stable DNA polymerase extends the fragments, which amplifies the regions flanked by the primers (Mullis et al., 1986). PCR fragments can be sub-cloned into vectors using restriction enzymes.

#### 2.3.6.1 PCR: reaction conditions

The PCR reactions were performed using a Labcycler (SensoQuest, Göttingen). Previous to the first cycle, DNA was denatured at 94 °C. Afterwards, each cycle consisted of denaturation (94 °C for 30 s), annealing (25-30 s) and extension steps (72 °C for 20-120 s). The temperature of the annealing step was determined by the primer with the lowest melting temperature ( $T_m$ ). Equation 2.3.6.1 was used to calculate  $T_m$ .

$$T_m = ((G/C) \times 4 \text{ °C} + (A/T) \times 2 \text{ °C} - (\text{Mismatch pairing}) \times 4 \text{ °C}) - 4 \text{ °C}$$

**Equation 2.3.6.1:** G: Guanine, C: Cytosine, A: Adenine and T: Thymine. The time of the extension step was determined by the size of the amplicon (20 s per 1 Kb). KOD Hot Start DNA-Polymerase (Novagen) was used. Reaction volumes were 25 or 50 µl. A typical PCR

(50 µl) contained the following: 1-10 ng Plasmid-DNA or 2 µl cDNA, 75 ng of each primer, 5 µl of 10x KOD Hot Start DNA-Polymerase Buffer, 5 µl of dNTPs (2 mM), 2 µl MgSO<sub>4</sub> (25 mM), 1 U KOD Hot Start DNA-Polymerase.

### **2.3.6.2 Purification of PCR products**

PCR products were purified using SureClean (section 2.3.1.3). In cases, where a PCR produced multiple bands, the amplified product of the expected size was purified from the agarose gel (section 2.3.4).

### **2.3.7 *P. irradians* retina mRNA purification & cDNA synthesis**

poly(A) mRNA was isolated from *P. irradians* retina using magnetic microbeads covalently attached to oligo(dT) (Dyna). For reverse transcription and cDNA synthesis, the SMART RACE (rapid amplification of cDNA ends) kit (Clontech) was used, which yields 5' and 3' RACE-ready cDNAs with anchor sequences added at either end. 5' and 3' RACE-ready cDNAs were used for both PCR and RACE experiments.

### **2.3.8 Rapid amplification of cDNA Ends (RACE)**

To perform RACE reactions, the instructions recommended in the user manual of the SMART RACE kit (Clontech) were followed. 5' and 3' RACE cDNA was used as template in RACE reactions. Gene specific primers for RACE were designed as recommended by the SMART RACE kit.

### **2.3.9 DNA sequencing**

DNA samples were sequenced by Eurofins MWG Operon (Ebersberg). Plasmid DNA from minipreparations were diluted (50-150 ng/μl) in bidest water and 15 μl per sample were sent for sequencing.

### **2.3.10 Transcriptome of *P. irradians* retina**

The transcriptome of *P. irradians* retina was obtained by sequencing of a normalized cDNA library using 454 pyrosequencing and it was assembled with Roche GS *de-Novo* Assembler.

### **2.3.11 Transcriptome and sequence analysis**

To obtain all the possible open reading frames (ORFs) of each assembled contig present in the *P. irradians* retina-transcriptome, the open software GetORF available in the European Molecular Biology Open Software Suite (EMBOSS) was used. Subsequently, GetORF output was run in the open source software UFO (Meinicke, 2009), which predicts conserved domains present in the ORFs submitted to analysis. Contigs of interest found in *P. irradians* retina transcriptome were analyzed using BLAST (Pubmed). The software PCSuppWin (Dr. W. Bönigk, Forschungszentrum caesar) and Bioedit were used for sequence analysis.

## **2.4 Cell culture of Chinese Hamster Ovary (CHO) cells**

The procedures to work with cell lines were performed as in Loogen (2009) and were modified accordingly.

For the heterologous expression of proteins, the K1-ATCC strain of CHO cells was used.

### **2.4.1 Cell culture conditions**

CHO cells were cultured in petri dishes (Ø 9 cm). The F12 culture medium was used at 37 °C, 5% CO<sub>2</sub> and 95% relative humidity.

### **2.4.2 Cryopreservation and thawing of CHO cells**

To cryopreservate CHO cells, cells in the logarithmic growth phase (60-70% confluent) were used. CHO cells were washed with sterile PBS and incubated for 2-3 min at 37 °C in 1 ml of 0.05% trypsin-EDTA (Life Technologies) to detach the cells from the culture dish. CHO cells were centrifuged (200 g) for 5 min and the pellet was resuspended in cryopreservation medium. Cells were placed in cryogenic (1 ml) vials ( $2 \times 10^6$  cells/ml) and gradually frozen to -80 °C at a rate of 1 °C per min, using an isopropanol-filled container (5100 Cryo 1 °C Freezing Container, Nalgene, Thermo Scientific, USA). To culture these cells again, cells were briefly warmed up in a water bath (37 °C) until the solution was completely thawed. Cells were carefully re-suspended by pipetting in culture medium. To remove the DMSO present in the cryopreservation medium, cells were centrifuged (200 g) for 5 min and re-suspended in 1 ml of pre-warmed (37 °C) culture medium. 600 µl of the cell suspension were placed on petri (Ø 9 cm) dishes.

### **2.4.3 Poly-L-Lysine coating of cover slips for cell culture**

To perform immunocytochemical and functional assays, cells were cultured on glass cover slips (Ø 5 mm and Ø 13 mm). To induce cell attachment, cover slips were placed in multiwell plates (4- and 24-well plates) and treated for at least 30 min with a solution (0.1 mg/ml) of Poly-L-Lysine (PLL) at RT.

## **2.5 Heterologous expression of proteins in CHO cells**

### **2.5.1 Transfection of CHO cells**

To express proteins heterologously in CHO cells, cells (70% confluent) were transfected with Lipofectamine 2000 (Life Technologies). Plasmid DNA and Lipofectamine 2000 were pipetted in two separate microcentrifuge tubes containing OptiMEM medium (Life Technologies). Both solutions were incubated for 5 min at RT. Next, both solutions were mixed and further incubated for 20 min at RT. In the meantime, the culture medium was removed from CHO cells, washed with sterile PBS and OptiMEM medium was added. After 20 min, the DNA:Lipofectamine 2000 solution was added to the cells. Cells were incubated (4-6 h) at 37 °C, 5% CO<sub>2</sub> and 95% of relative humidity. Afterwards, the OptiMEM medium was removed and replaced with F12 culture medium containing 1% Penicillin/Streptomycin (Life technologies). To enhance the expression of the heterologous protein, Na<sup>+</sup>-Butyrate (final concentration: 5 mM) was added to the cells and subsequently incubated for 16 to 48 h. For immunocytochemistry or electrophysiology experiments, cells were cultured and transfected on multiwell plates with PLL-treated cover slips

## 2.5.2 Protein extraction from CHO cells

To extract proteins for Western blot, CHO cells were transfected two days before the protein extraction. Culture medium from transfected CHO cells was removed and cells were washed (2x) with sterile PBS. Cells were mechanically detached from the petri (Ø 9 cm) dish using a rubber spatula. Subsequently, cells were centrifuged (2,000 g) for 5 min at RT. The supernatant was discarded and the pellet was resuspended in 0.5 ml of buffer A (Table 2.5.2.1). To lyse the cells, the cell suspension was pipetted up and down (20x) through a gauge needle (24G, Braun). The sample was centrifuged (18,000 g) for 20 min at 4 °C. The supernatant was transferred to a 1.5 microcentrifuge tube. The pellet containing membrane proteins was resuspended by pipetting in buffer B. Then, the sample was centrifuged (8,000 g) for 10 min at 4 °C and the supernatant was transferred to a clean 1.5 microcentrifuge tube. The protein concentration was measured using the BCA assay.

**Table 2.5.2.1:** Buffers for protein extraction

<b>Buffer A</b>	<b>Buffer B</b>
25 mM HEPES pH 7.5	50 mM HEPES pH 7.5
10 mM NaCl	200 mM NaCl
2 mM EDTA	1 mM DTT
1 mM DTT	mPIC (1:500 dilution)
mPIC (1:500 dilution)	0.5% Triton X-100

## **2.6 Western-blot analysis and antibody screening**

### **2.6.1 SDS-Polyacrylamide Gel Electrophoresis (PAGE) and Western-blot analysis**

Proteins were separated using SDS-PAGE and transferred to PVDF membranes (Immobilion P, Millipore) (Towbin et al., 1979). Protein transfer (Western blot) was performed using a Milliblot-Graphite Electroblotter System (Millipore). The manufacturer's instructions for the semi-dry protocol were followed. Typically, the transfer time was about 40 min. The current per area was calculated to be  $2.4 \text{ mA/cm}^2$ . A pre-stained protein ladder (Novex Sharp Pre-stained Protein Standard, Life Technologies) was used to check for complete protein transfer.

## 2.6.2 Immunological detection of proteins

The immunological staining of immobilized proteins in PVDF membranes was performed as follows. First, the membrane was treated with blocking solution (30 min) at RT to avoid unspecific antibody binding. Second, the membrane was incubated (1 h) at RT with the primary antibody. Then the membrane was incubated (1 h) at RT with the secondary antibody, which specifically binds the primary antibody, coupled to a Horseradish Peroxidase (HRP). After every blocking and incubation step, the membrane was washed. All the washing and incubation steps were performed on a rocker. The solutions and procedures used for Western blotting are shown in Table 2.6.2.1 and 2.6.2.2. The antibody reaction was visualized using ECL Western Blot Detection Kit (AppliChem).

**Table 2.6.2.1:** Solutions used in Western blot analysis.

<b>Solution name</b>	<b>Contents</b>
Blocking solution	PBS, 0.05% Tween-20; 0.5% Milk powder
Washing solution I	PBS, 0.05% Tween-20
Washing solution II	PBS
Antibody solution	Antibody in PBS, 0.05% Tween-20

**Table 2.6.2.2:** Steps used for Western blot analysis.

<b>Procedure</b>	<b>Incubation time (T)</b>	<b>Solution</b>
Blocking	45 min (RT) or ON (4 °C)	Blocking solution
Incubation primary antibody	45-60 min (RT)	Antibody solution
Washing	2 x 10 min (RT)	Washing solution I
Incubation secondary antibody	45-60 min (RT)	Antibody solution
Washing	2 x 10 min (RT)	Washing solution I
Washing	2 x 10 min (RT)	Washing solution II

## **2.7 Immunocytochemistry**

### **2.7.1 Fixation of CHO cells for immunocytochemistry**

CHO cells used for immunocytochemistry were transfected in multi-well plates with cover slips (section 2.5.1). After 16-48 h of transfection, cells were washed with sterile PBS and fixed (5 min) with 4% paraformaldehyde in PBS. Afterwards, cells were washed (3x) for 5 min with PBS.

### **2.7.2 Immunocytochemical staining of CHO cells**

To block unspecific binding sites, fixed cells were incubated in washing solution (Table 2.7.2.1). Then, the cells were incubated with the primary antibody. Afterwards, the cells were incubated with a fluorophore-coupled secondary antibody. Tables 2.7.2.1 & 2.7.2.2 show the solutions and procedures used. The cover slips with the immune-stained cells were impregnated in mounting media (Aqua Poly/Mount; Polysciences), transferred and sealed onto a microscope slide. Immuno-stained cells were imaged on a confocal microscope LSM FV 1000 (Olympus).

**Table 2.7.2.1:** Solutions used in immunocytochemistry.

<b>Solution Name</b>	<b>Contents</b>
Blocking solution	PBS, 0.5% (w/v) Triton X-100, 5% (v/v) Chemiblocker (Millipore)
Primary antibody solution	Primary antibody in PBS, 0.5% (w/v) Triton X-100, 5% (v/v) Chemiblocker (Millipore)
Secondary antibody solution	Secondary antibody in PBS, 5% (v/v) Chemiblocker (Millipore)

**Table 2.7.2.2:** Steps used for immunocytochemistry.

<b>Procedure</b>	<b>Incubation time</b>	<b>Solution</b>
Blocking reaction	30 min (RT)	Blocking solution
Incubation first antibody	1 h (RT)	First antibody solution
Washing	2 x 10 min (RT)	PBS
Incubation secondary antibody	30 min (RT)	Secondary antibody solution
Washing	2 x 10 min (RT)	PBS

## **2.8 Antibodies**

### **2.8.1 Monoclonal primary antibodies**

Monoclonal antibodies were raised in collaboration with Frau Dr. E. Kremmer (Institut für Molekulare Immunologie, Helmholtz-Zentrum München) by immunizing mice and rats with MBP fusion-proteins. Primary supernatants were tested by Western blot. Hybridomas that produced positive supernatants were recloned. The recloning was performed by splitting of single cells until every single cell in the culture reacted to the antigen (positive cells). The positive cells were cultured and the supernatants containing the secreted monoclonal-antibodies were collected. The monoclonal antibodies used in this work are summarized in Table 2.8.1.1

**Table 2.8.1.1:** Antibodies used in western blot (WB), immunocytochemistry (ICC) and immunohistochemistry (IHC)

Abbreviation	Antibody name	host species	Antigen	Dilution in WB	Dilution ICC & IHC	Manufacturer		
$\alpha$ -HA	Anti tag	HA- Rat	HA-tag	1:1,000	1:100	Frau	Dr.	E.
						Kremmer		
33	PCNG 7G4 MG3	Mouse	PectCNG1 C-terminus	undiluted	undiluted	Frau	Dr.	E.
						Kremmer		
34	PCNG 7C1 MG3	Mouse	PectCNG1 C-terminus	undiluted	undiluted	Frau	Dr.	E.
						Kremmer		
37	PCNG 8D7 M2a	Mouse	PectCNG1 C-terminus	undiluted	undiluted	Frau	Dr.	E.
						Kremmer		
56	FE1 4B10 M2a	Mouse	PectERG C-terminus	undiluted	undiluted	Frau	Dr.	E.
						Kremmer		
63	FE1 2F11 M2a	Mouse	PectERG C-terminus	undiluted	undiluted	Frau	Dr.	E.
						Kremmer		
74	FE2 1F8 M2a	Mouse	PectERG C-terminus	undiluted	undiluted	Frau	Dr.	E.
						Kremmer		
79	FE2 1C5 M2a	Mouse	PectERG C-terminus	undiluted	undiluted	Frau	Dr.	E.
						Kremmer		

## 2.8.2 Secondary antibodies

The secondary antibodies used throughout this work are summarized on Table 2.8.2.1

**Table 2.8.2.1:** Secondary Antibodies

<b>Antibody</b>	<b>Manufacturer</b>	<b>Dilution</b>
Mouse- $\alpha$ -Rat-HRP	Frau Dr. E. Kremmer	1:5,000
Rat- $\alpha$ -Mouse G3-HRP	Frau Dr. E. Kremmer	1:1,000
Rat- $\alpha$ -Mouse 2a-HRP	Frau Dr. E. Kremmer	1:1,000
Rat- $\alpha$ -Mouse 2b-HRP	Frau Dr. E. Kremmer	1:1,000
Donkey- $\alpha$ -Rat-Cy3	Jackson	1:400
Donkey- $\alpha$ -Mouse-649	Jackson	1:400

## 2.9 RNA *in-situ* hybridization and immunohistochemistry in *P. irradians* eye slices

### 2.9.1 Eye slices of *P. irradians*

Whole eyes of *P. irradians* were excised and fixed overnight in 90% ASW containing 4% paraformaldehyde at 4°C. Following permeabilization (PBS-0.2% Triton-X, 5 min on ice) three steps of sucrose impregnation (10% for 3h; 20% for 3–4 h; 30% ON) were performed. Then, eyes were embedded in gelatin (7.5% -15% sucrose), chilled to -20°C, and sectioned at 8-15  $\mu$ m in a cryostat. Finally, eye slices were plated onto electrostatically charged glass slides (Fisher Scientific Superfrost Plus), dried, and kept at -20°C for subsequent use.

## 2.9.2 RNA *in-situ* hybridization

### 2.9.2.1 RNA probes for *in-situ* hybridization

The procedure for RNA *in-situ* hybridization was performed as described by Gomez et al., 2011

Target sequences containing suitable unique restriction sites were amplified by PCR, digested with restriction enzymes, and directionally ligated into pBluescript SK (Stratagene). Plasmids were linearized using restriction enzymes. *In-vitro* transcription of RNA was performed using Digoxigenin RNA Labeling Mix (Roche). A typical transcription reaction is shown in Table 2.9.2.1.1. The reaction was stopped with EDTA, pH 8.0. To check for RNA synthesis, a sample (1  $\mu$ l) of the transcription reaction was run in an agarose-gel electrophoresis. Afterwards, the probe was diluted in 600  $\mu$ l of ethanol, 25  $\mu$ l of sodium acetate (3M), and 240  $\mu$ l of DEPC-treated water. The sample was incubated 5 min on ice. Then, the sample was centrifuged (14,000 g; 4°C) for 30 min, dried in a SpeedVac, and resuspended in 20  $\mu$ l of DEPC-treated water. RNA concentration was measured using a spectrophotometer; the sample was diluted in hybridization buffer to 10x stock concentration (20  $\mu$ g/ml) and stored at -20°C.

**Table 2.9.2.1.1:** RNA probe synthesis for RNA *in-situ* hybridization

<b>Reagent</b>	<b>Antisense probe</b>	<b>Sense probe</b>
Nuclease-free water	1.6 $\mu$ l	1.6 $\mu$ l
DIG RNA Labeling Mix 10x (Roche)	2 $\mu$ l	2 $\mu$ l
T7 transcription Buffer 10x (Ambion)	2 $\mu$ l	--
T3 transcription Buffer 10x (Ambion)	--	2 $\mu$ l
1 $\mu$ g linearized plasmid DNA	11.4 $\mu$ l	11.4 $\mu$ l
T7 RNA Polymerase 20 U/ $\mu$ l (Ambion)	2 $\mu$ l	--
T3 RNA Polymerase 20 U/ $\mu$ l (Ambion)	--	2 $\mu$ l
RNase inhibitor	1 $\mu$ l	1 $\mu$ l
<b>Total volume</b>	<b>20 <math>\mu</math>l</b>	<b>20 <math>\mu</math>l</b>

### **2.9.2.2 RNA hybridization and probe detection**

Eye slices of *P. irradians* were sequentially washed in PBS, methanol, and PBS + Tween 20 (PTw). After treatment with proteinase K in PTw and washing with glycine in PTw (2 mg/ml), the eye slices were refixed in 4% paraformaldehyde in PBS for 15 min. Following washing, they were placed in hybridization buffer, and prehybridized for 45 min at 60°C. Subsequently, the probe was added and incubated overnight at the required temperature for every particular probe, in a hybridization oven. Eye slices were washed repeatedly (3x), and rinsed in NTE (0.5 M NaCl, 10 mM Tris pH 8.0, 1 mM EDTA). The slides were incubated with RNase A and RNase T1 in NTE, washed again, and transferred to a humidified dark container. Sections were blocked off with a PAP pen, and rocked in the presence of levamisole and Boehringer Mannheim Blocking Reagent. The solution was replaced with anti-digoxigenin alkaline phosphatase (AP) antibody (1:2000, sheep- $\alpha$ -IgG; Roche) and incubated overnight. For probe detection, the slides were washed and incubated in AP substrate solution (Roche), followed by a final wash.

### **2.9.3 Immunohistochemistry of *P. irradians* eyes**

After gelatin removal by immersion for 5 min in PBS warmed to 36°C, eye slices were blocked for 30 min with 1% goat or horse serum (depending on the antibodies to be used), diluted in PBS and supplemented with 0.02% Triton-X. Next, slices were incubated with primary antibodies (dilution 1:1000 to 1:200) in PBS + 0.5% BSA (40 min to 2 h) and washed (2x) in PBS. To detect antibody binding, the ABC Elite kit (Vector Labs, USA) following the manufacturer's instructions was used. Eye slices were treated with biotinylated secondary antibodies for 30 min and then incubated with streptavidin-conjugated peroxidase

for 30 min. Eye slices were washed and developed in Vector VIP substrate, then washed with distilled water. The slices were dehydrated with ethanol in several steps (30%, 50%, 70%, 95%, and 2x 100%) and incubated twice in Xylenes (5 min each) before mounting with Permunt. Slices were imaged using an upright confocal microscope (LSM 510, Carl Zeiss).

## **2.10 Electrophysiological recordings in *P. irradians* ciliary photoreceptors**

Isolation and electrophysiological recordings of photoreceptors was performed as described (Gomez and Nasi, 1994b).

### **2.10.1 Dissociation of photoreceptors from *P. irradians* for patch clamp recordings**

Specimens of *P. irradians* were obtained from the Marine Resources Center (MRC) of the Marine Biological Laboratory. A piece of mantle containing several eyes was attached to a Sylgard-coated petri dish on the stage of a stereomicroscope illuminated with dim red light ( $\lambda > 650$  nm). A circular incision was done around the edge of the eye to remove the cornea, the lens, and the pigmented mantle. The exposed retina was carefully lifted from the argentea layer and separated from the optic nerve. Then, retinas were incubated in pronase (1,000 U/ml; Sigma) for 50-60 min at 22°C. Subsequently, retinas were washed in sea water supplemented with 3% fetal calf serum, and gently triturated with a fire-polished pasteur pipette. An aliquot of the resulting cell suspension was transferred to the recording chamber. To promote cell adhesion, the chamber was pre-treated with concanavalin A (Sigma).

### **2.10.2 Patch-clamp recordings in *P. irradians* ciliary photoreceptors**

Whole cell currents were recorded with a Cairn Research Optopatch amplifier. A 4-pole Bessel low-pass filter was used; the cutoff frequency was usually set at 1 KHz, but was increased up to 5 KHz for measuring latencies. Data were digitized at 3–15 KHz (DT9834, Data Translation). The recording chamber was perfused via a multiport manifold to change the bath solution. Solutions: intracellular solution (in mM): 100 KCl, 200 K-aspartate, 12 NaCl, 5 Na<sub>2</sub>ATP, 5 MgCl<sub>2</sub>, 15 HEPES, 1 EGTA, and 300 sucrose, pH 7.3 adjusted with KOH. Extracellular solution, artificial sea water (ASW) in mM: 480 NaCl, 10 KCl, 10 CaCl<sub>2</sub>, 49 MgCl<sub>2</sub>, 10 HEPES, 5.4 Glucose, pH 7.8 pH was adjusted with NaOH. For blocking of the light-activated channel, the potassium channel blocker 4-aminopyridine was dissolved in ASW and applied extracellularly.

### **2.10.3 Photolysis of caged compounds in *P. irradians* ciliary photoreceptors**

BCMACM-cGMP was dissolved in the intracellular solution at a final concentration of 1 mM. A high-intensity, collimated 365 nm LED (OptoFlash, Cairn Research or Thorlabs) was used for photolysis; UV and epi-fluorescence beams were combined via a 440-nm cutoff dichroic reflector (Omega Optical).

## **2.11 Patch-clamp recordings in Chinese Ovary Hamster (CHO) cells**

### **2.11.1 Patch-clamp recordings on CHO cells transfected with PectERG, PectHCN, and PectCNG1 channels**

CHO cells were transfected (Section 2.5.1) with the PectERG construct. Seals between pipette and cell were performed in standard extracellular solution (ES) containing (in mM): 140 NaCl, 5.4 KCl, 1 MgCl<sub>2</sub>, 1.8 CaCl<sub>2</sub>, 10 Glucose, and 5 HEPES adjusted to pH 7.4 with NaOH. For the recordings in high K<sup>+</sup> solution, NaCl was exchanged by KCl and pH was adjusted to 7.4 with KOH. The following pipette (4-5 MΩ) solution was used (in mM): 10 NaCl, 130 KAsp, 2 MgCl<sub>2</sub>, 2 Na<sub>2</sub>ATP, 1 EGTA, 5 HEPES, pH 7.4 (adjusted with 1 M of KOH). Osmolarity 292. For recordings using cyclic nucleotides, cyclic nucleotides were dissolved in the intracellular solution at the desired concentration. Series resistance and cell capacitance were compensated to 70-85%. Voltages were corrected for the liquid junction potential. All recordings were performed at 20-22 °C. Data were analysed using pClamp 10 and Origin Pro 9.0 software.

### **2.11.2 Patch-clamp recordings of CHO cells transfected with hSlo3 channels**

CHO cells were co-transfected (Section 2.5.1) with hSlo3 and hLRRC52-mCherry constructs (obtained from Dr. Wolfgang Bönigk, Forshungszentrum Caesar). Seals between pipette and cell were performed in standard extracellular solution (ES) containing (in mM): 140 NaCl, 5.4 KCl, 1 MgCl<sub>2</sub>, 1.8 CaCl<sub>2</sub>, 10 Glucose, and 5 HEPES adjusted to pH 7.4 with NaOH. For the recordings in high K<sup>+</sup> solution, NaCl was exchanged by KCl and pH was adjusted to 7.4 with KOH. To study activation of Slo3 by alkalization, the following pipette (4-5 MΩ)

solution was used (in mM): 130 K-aspartate, 10 NaCl, 1 EGTA, 5 HEPES, 15 Glucose, pH was adjusted either to 6.2 or 7.3 using KOH. To study the activation of hSlo3 by  $\text{Ca}^{2+}$ , the following pipette (2-3 M $\Omega$ ) solutions were used (in mM): divalent-free solution: 130 KAsp, 10 NaCl, 1 EGTA, and 20 HEPES adjusted to 7.3 using KOH; 70  $\mu\text{M}$   $\text{Ca}^{2+}$  intracellular-solution: 130 KAsp, 10 NaCl, 0.5  $\text{CaCl}_2$ , 1 NTA, and 20 HEPES adjusted to pH 7.3 using KOH, the final  $\text{Ca}^{2+}$  concentration was confirmed using the  $\text{Ca}^{2+}$  dye Mag-Fura 2; 1 mM  $\text{Ca}^{2+}$  intracellular-solution: 130 K-aspartate, 10 NaCl, 1  $\text{CaCl}_2$ , and 20 HEPES adjusted to pH 7.3 using KOH. Series resistance and cell capacitance were compensated to 70-85%. Voltages were corrected for the liquid junction potential. All recordings were performed at 20-22 °C. Blockers were dissolved in extracellular solution and bath applied. Data were analysed using pClamp 10 and Origin Pro 9.0 software.

## 3 Results

### 3.1 Patch-clamp recordings in ciliary photoreceptors of *P. irradians*

#### 3.1.1 Benefits of using caged compounds to study the phototransduction cascade of *P. irradians* ciliary photoreceptors

To identify the second messenger involved in the photo-transduction cascade of ciliary photoreceptors different cyclic nucleotide analogues (8-Br-GMP and 8-Br-cAMP) have been applied through the recording pipette in patch-clamp experiments (Gomez and Nasi;1995 1997). The results indicate that cGMP plays a key role in the photo-transduction cascade of

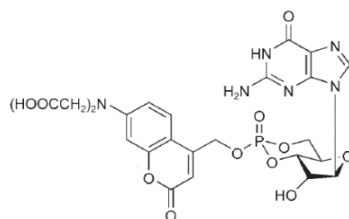


Figure 3.1.1.1: Chemical structure of BCMACM-cGMP (adapted from Hagen et al; 2006).

ciliary photoreceptors, most likely by directly activating the light-dependent channels (Gomez and Nasi;1995 1997). However, the time course of these experiments is long (seconds) compared with that of the light-response (tens of milliseconds). This discrepancy inevitably reflects a technical constraint, namely, the inherent sluggishness of the dialysis via the patch pipette; it is difficult to disentangle direct activation of channels from other cGMP-dependent processes that might be activated while the cell is dialyzed with cGMP.

### 3.1.2 cGMP-gated channels in ciliary photoreceptors of *P. irradians*

In order to unequivocally test whether cGMP directly activates the photo-transduction channels, I used caged cGMP (BCMACM-cGMP) (Figure 3.1.1.1). Because of its high extinction coefficient ( $\epsilon=18000 \text{ M}^{-1} \text{ cm}^{-1}$ ), quantum yield (0.25), and photochemical rate ( $6 \times 10^8 \text{ s}^{-1}$ ), a jump in cGMP concentration can be attained in microseconds using light intensities typically available in a standard epi-illumination light source; furthermore, the BCMACM caging group has the additional advantage that upon photo-release, its emission fluorescence (Excitation 376 Emission 479 nm) increases allowing the direct measurement of the uncaging efficiency and its kinetics (Hagen et al., 2005). One caveat of using caged cyclic nucleotides to study photoreceptors is the fact that photoreceptors are specialized in sensing light and the near-UV photolysis wavelength is capable of triggering robust physiological photoresponses. Thus, releasing a caged cyclic nucleotide can trigger more than one response, the photoresponse and, possibly, a second response that is due to uncaging of the cyclic nucleotide. One way around this complexity is to impair the photo-transduction cascade. The photo-transduction cascade of ciliary photoreceptors of *P. irradians* uses Go proteins, which harbors a cysteine in the fourth position of the C-terminus, the hallmark for susceptibility to ADP ribosylation (Mangmool and Kurose, 2011); as such, they are inhibited by Pertussis Toxin (PTX). In fact, a previous report has shown that PTX abolishes up to 60% of the photo-response of these photoreceptors without having any apparent effect on the ion channels (Gomez and Nasi, 2000).

### 3.1.3 Ciliary photoreceptors have two different cGMP-gated conductances

To impair the photo-transduction cascade of *P. irradians* ciliary photoreceptors, I incubated *P. irradians* retinas with PTX (20 ng/ml; overnight). Subsequently, I performed whole-cell recordings in dissociated (sections 2.10.2, 2.10.3) ciliary-photoreceptors with and without

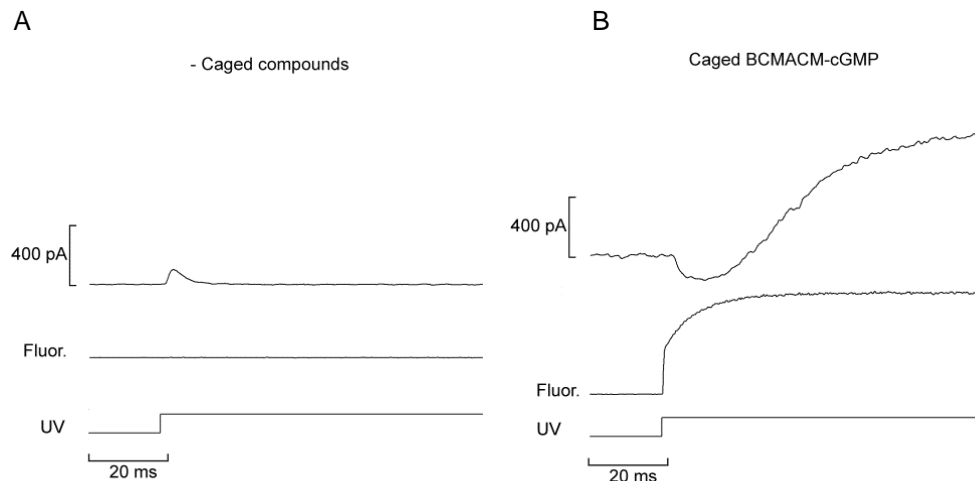


**Figure 3.1.3.1:** cGMP uncaging in *P. irradians* ciliary photoreceptors treated with 20 ng/ml Pertussis toxin (PTX). A: Voltage-clamp recordings ( $V_h = -30$  mV) of *P. irradians* ciliary photoreceptors treated with PTX. Caged compounds were not present. There is no light activated current, due to the impairment of the photo-transduction cascade by PTX. B: Voltage-clamp recordings ( $V_h = -30$  mV) of *P. irradians* ciliary photoreceptors treated with PTX. BCMACM-cGMP (1 mM) was diluted in the intracellular solution and applied through the recording pipette. Fluor.: Fluorescence registered by the photomultiplier during uncaging of BCMACM-cGMP. A UV-light pulse of 100 ms applied through the epifluorescence port of the microscope was used.

BCMACM-cGMP in the recording pipette. UV-light alone did not activate any conductances in PTX-treated ciliary photoreceptors (Figure 3.1.3.1-A). The little bump in Figure 3.1.3.1-A is the so called early receptor current (ERC), which represents the photo-isomerization current of rhodopsin due to the high intensity of the light stimulus. This indicates that the photo-transduction cascade is indeed, impaired. In contrast, uncaging of BCMACM-cGMP with UV-light activated two different conductances in ciliary photoreceptors (Figure 3.1.3.1-B), an early inward-current and a delayed outward-current. The early inward-current had an

average amplitude of  $368.3 \pm 234.6$  pA,  $n = 3$ , whereas the outward current had an average amplitude of  $806 \pm 657.2$  pA,  $n = 3$ . It is noteworthy that the latency of current activation was extremely short  $1.8 \pm 0.2$  ms compared to the latency of the photoresponse of ciliary photoreceptors (7-40 ms) (McReynolds and Gorman, 1970) consistent with the notion that cGMP likely acts directly on the light-sensitive conductance. Although there was a direct correlation between the activation of the currents and the increase in fluorescence upon BCMACM-cGMP uncaging, which suggests that cGMP activates both conductances; the fact that the inward current always precede the outward current does not allow to completely rule out activation of the delayed outward-current by a downstream effect of cGMP.

To assess the dose-dependence of photo-released cGMP, I used UV-light pulses with increasing durations in *P. irradians* ciliary photoreceptors under voltage clamp. cGMP activated both conductances in a concentration-dependent manner (Figure 3.1.3.2).

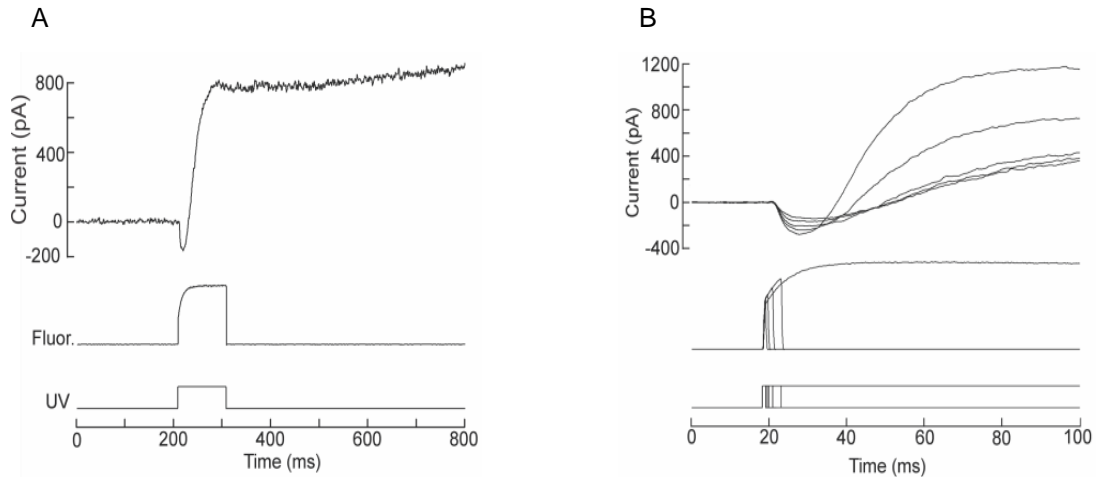


**Figure 3.1.3.2:** cGMP activates two different ion channels in a concentration dependent manner. A: Voltage clamp recordings in ciliary photoreceptors of *P. irradians* treated with 20 ng/ml PTX. Photoreceptors were voltage clamped at 0 mV. UV-light (100 ms) uncaging of BCMACM-cGMP (1 mM). B: Voltage clamp recordings in ciliary photoreceptors of *P. irradians* incubated overnight with 20 ng/ml PTX. Photoreceptors were voltage clamped at 0 mV. UV-light pulses of different durations (0.6, 1.2, 2.4, 5, 10 and 200 ms) were used to photo-release an increasing amount of cGMP.

### 3.1.4 The light-activated ion channel and cGMP-gated outward current have the same pharmacological properties

Previous reports have shown that 4-aminopyridine (4-AP) specifically blocks the light-activated channels ( $K_d = 2 \mu\text{M}$ ) of *P. irradians* ciliary photoreceptors (Gomez and Nasi, 1994; 1997). To test whether the cGMP-gated outward current has the same pharmacological properties as the light-activated current, I performed voltage-clamp recordings and cGMP uncaging in ciliary photoreceptors in the presence and absence of 4-AP. Extracellular application of 4-AP ( $10 \mu\text{M}$ ) blocked the cGMP-gated outward but not the inward current (Figure 3.1.4.1). Of note, after blockade of the cGMP-gated outward current the cGMP-gated inward current remained active (Figure 3.1.4.1), suggesting that the transient nature of the inward current recorded in absence of 4-AP (Figure 3.1.3.2-A) is not due to inactivation of those channels, but to competition with the delayed, larger outward current.

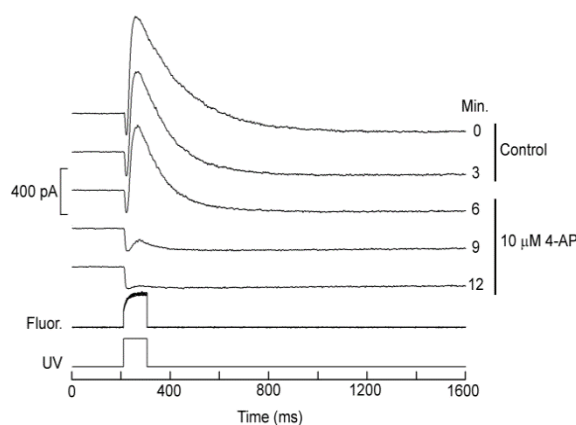


**Figure 3.1.4.1:** Specific blockade of the cGMP-gated outward current by 4-AP. Voltage-clamp recordings in ciliary photoreceptors. Currents were activated by BCMACM-cGMP uncaging using UV-light. BCMACM-cGMP (1 mM) was diluted in the intracellular solution and applied through the patch pipette. UV-pulses of 100 ms were applied every three minutes. ASW containing  $10 \mu\text{M}$  of 4-AP was used to perfuse voltage-clamped ciliary photoreceptors.

### 3.1.5 The ion selectivity of cGMP-gated inward current is reminiscent of classical CNG channels

Subsequently, to shed some light on the ion selectivity of the cGMP-gated early current, I performed cGMP uncaging at different voltages in *P. irradians* ciliary photoreceptors under voltage clamp. Ciliary photoreceptors were superfused with 4-AP in ASW to block the cGMP-gated delayed outward current. The cGMP-gated early current reversed sign at 30 mV (Figure 3.1.5.1-A-B) which is similar to classical CNG channels (Kaupp and Seifert, 2002). Figure 3.1.5.1-B shows the current-voltage (I-V) relation of the cGMP-gated early current ( $n = 1$ ); interestingly, despite the high extracellular  $\text{Ca}^{2+}$  concentration (10 mM), the cGMP-gated early current does not seem to have the characteristic outward and inward rectification due to  $\text{Ca}^{2+}$  blockage of classical CNG channels (Picones and Korenbrot, 1995; Finn et al., 1997; Kaupp and Seifert, 2002).

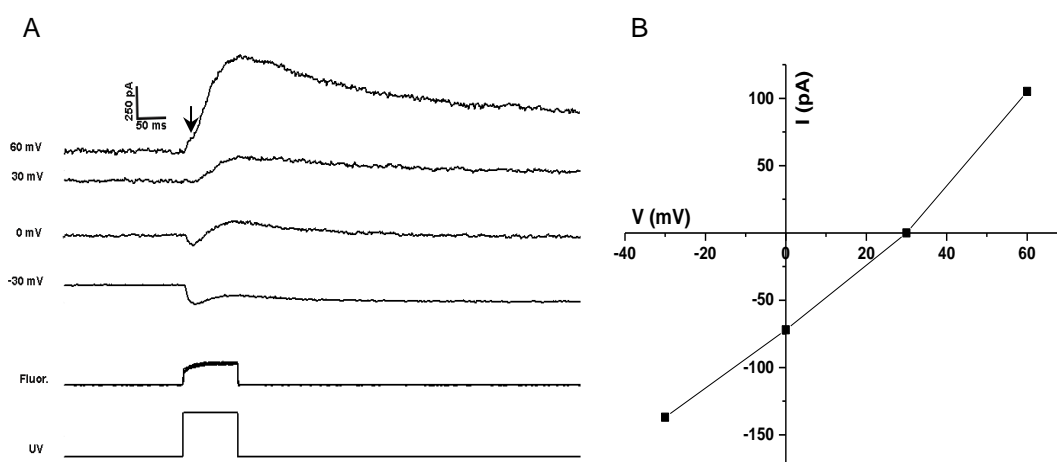


**Figure 3.1.5.1:** Current-voltage relation of the cGMP-gated inward current of ciliary photoreceptors of *P. irradians*. A: cGMP-gated currents recorded in voltage-clamped ciliary photoreceptor at four different voltages. The cGMP-gated outward current was blocked using 10  $\mu\text{M}$  4-AP. B: current-voltage relation of the cGMP-gated inward current. Current amplitudes were obtained from the traces shown on the left.

## 3.2 Analysis of the transcriptome of *P. irradians* retinas

### 3.2.1 GetORF and UFO analysis

The *de-novo* transcriptome assembly produced 49777 Contigs. Although a normalized mRNA library was used for the transcriptome (see materials and methods), some transcripts were underrepresented. In order to analyze the transcriptome, I used the open software GetORF available in the European Molecular Biology Open Software Suite (EMBOSS) to obtain all the possible open reading frames (ORFs) of each assembled contig present in the transcriptome. Subsequently, GetORF output was run in the open source software UFO (Meinicke, 2009), which predicts conserved domains present in the ORFs submitted to analysis. This analysis predicted 89 putative ion channel genes of which 20 were potassium channels (Table 6.1).

### 3.2.2 Homology search using sea urchin CNGKs

Considering that the CNGK channel of sea urchin sperm shares many functional features with the light-activated channels of scallop ciliary photoreceptors, a CNGK-like channel may also be mediating the light response in scallop ciliary photoreceptors. Therefore, I searched for putative genes that may code for a CNGK channel ortholog. I performed a tBLASTn search using the amino acid sequence of the CNGK of the sea urchin, *Arbacia punctulata* (ApCNGK). This search found 8 different contigs (E-value < 1e-5) coding for cyclic-nucleotide gated (CNG) channels and hyperpolarization-activated and cyclic-nucleotide gated (HCN) channels, as well as for members of the Ether-a-go-go (EAG) K<sup>+</sup>-channel family; however none of the hits were orthologue genes to ApCNGK channels.

### **3.2.3 Homology search using K<sup>+</sup>-channels pore region and CNBD of CNG channels**

Because putative genes similar to CNGK channels were not found in the transcriptome, I decided to use conserved protein domains to look for potential candidates that may have both functions: cNMPs binding and potassium selectivity. The structural domains responsible for cNMP binding (CNBD) and potassium selectivity (pore-loop sequence) are highly conserved among species (Kaupp and Seifert, 2002; MacKinnon, 2003). In order to find a consensus sequence of the CNBD, I performed an alignment using CNG channels from eight different species that have been already functionally characterized. The list included, human, rat, bovine, mouse CNG channels (Kaupp et al., 1989; Dhallan et al., 1992; Pittler et al., 1992; Barnstable and Wei J-Y, 1995). Subsequently, I performed a tBLASTn search using the consensus amino acid sequence against *P. irradians* retina transcriptome. This search strategy retrieved the same ion channels already found (CNG, HCN, EAG and ERG channels). Subsequently, I decided to use the pore region of all known K<sup>+</sup> channels. Every single “contig” was used to perform a BLASTx search against all non-redundant protein sequences present in PubMed. This approach retrieved many putative K<sup>+</sup>-channels, however only the putative EAG and ERG K<sup>+</sup> channels harbored both a K<sup>+</sup>-selectivity signature sequence in the pore region and a CNBD at the C-terminus.

### **3.2.4 Molecular cloning of ERG, HCN, and CNG channels**

The *P. irradians* retina transcriptome contains: three putative CNG channels (two alpha and one beta subunits), one putative HCN channel, one putative Ether a-go-go (EAG) K<sup>+</sup> channel and one putative EAG-related K<sup>+</sup> (ERG) channel. Although all these channels harbor a conserved CNBD, homology among these channels is not particularly high (Figure 6.1).

However they are highly conserved compared to their respective consensus sequences (Figure 6.2).

The putative ERG, EAG, HCN and CNG channels harbor a CNBD; however only channels pertaining to the EAG channel family (namely EAG and ERG channels) also bear the K<sup>+</sup>-selectivity signature sequence (Figure 6.1). Recent reports have shown that although some members of the murine EAG-channel family bind cNMPs, they are not activated by cNMPs (Brelidze et al., 2009, 2012). However, the putative ERG (PectERG) channel found in *P. irradians* retina has slight differences in the amino acid sequence of the CNBD (Figure 6.1 & 6.3). Such differences might be sufficient to make PectERG channels responsive to cNMPs, which makes them particularly interesting ion channels to study.

Moreover, the amino acid sequence of the putative HCN (PectHCN) channel of *P. irradians* is highly conserved (70% homology) when compared to other invertebrate HCN channels (Gauss et al., 1998; Robinson and Siegelbaum, 2003). It contains all the characteristic features of other HCN channels, such as: a voltage-sensing domain, a CIGYG sequence in the pore region and a CNBD in the C-terminus (Figure 6.1 & 6.4). Likewise, *P. irradians* CNG-channel subunits are highly conserved (Figure 6.1); however, PectCNG1 alpha-subunit harbors a striking mutation in the pore region, the selectivity filter of the channel is GER instead of GET (Figure 6.1 & 6.5), which, due to the positive charge of the Arginine side chain, may dramatically change the selectivity properties of this ion channel. Considering that the CNBDs of PectERG, PectHCN and PectCNG channels are highly conserved (Figure 6.1), this makes them interesting to study in the context of a photo-transduction cascade of *P. irradians* ciliary photoreceptors, which uses cGMP as second messenger (Gomez & Nasi, 1995).

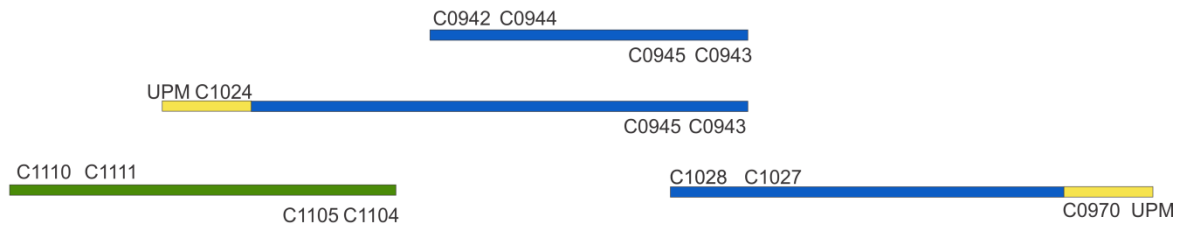
### 3.3 Molecular cloning of PectERG, PectHCN, and PectCNG channels

Because the assembled transcriptome of *P. irradians* does not contain the full-length gene sequence for PectERG, PectHCN and PectCNG1 channels, I used PCR to amplify the known portion of the channels based on the transcriptome sequence-information. To amplify the first fragment of PectERG channel (Figure 3.3.1 A-B), I used primers C0942 and C0943. To discard unspecific amplicons I performed a nested PCR, using primers C0944 and C0945. The PCR product C0944-C0945 was cloned and sequenced. The sequence was identical to the one found in the transcriptome. Subsequently, I used the Rapid Amplification of cDNA Ends (RACE) technique to obtain the 5' and 3' ends of the PectERG-channel gene. To amplify the 3' end of PectERG, I performed the 3' RACE-reaction using the gene-specific primer C1028 and the Universal Primer Mix (UPM). Moreover, to perform the 3' nested RACE I used primers C1027 and C0970. The amplified 3' nested-RACE products were cloned and sequenced. The sequence of the 3'nested-RACE product C1027-C0970 overlapped perfectly with the known sequence. Furthermore, the sequence of the RACE product C1027-C0970 contained a stop codon in frame several nucleotides before the poly-A tail, which suggests that it is the end of the coding region of the gene.

A



B



C



D



**Figure 3.3.1:** Molecular cloning of PectERG channel. A: PectERG channel domains. S1-6 represent the six transmembrane domains. PAS: Per-Arnt-Sim domain. CNBD: Cyclic Nucleotide Binding Domain. UTR: Untranslated Region. ATG: sequence of the start codon. TAG: sequence of the stop codon. B: RACE and PCR fragments obtained for the cloning of PectERG channel. Characters on top and below the bars represent forward and reverse primers, respectively. C: DNA fragments used to make the constructs for heterologous expression. Characters on top and below the bars represent forward and reverse primers, respectively. D: DNA fragment used for the constructs made for RNA *in-situ* hybridization experiments. Characters on top and below the bars represent forward and reverse primers, respectively.

To obtain the 5' end of PectERG channel, I performed a 5' RACE using the UPM against the 5' cDNA anchor and the gene-specific primer C0943. In order to amplify only the products of interest, I performed a 5' nested-RACE, using primers C1024 and C0945. The amplified products from the 5' nested-RACE were cloned and sequenced. The 5' nested-RACE

products did not have any stop codon before a start codon, which indicates that the RACE product may not contain the 5' Untranslated Region (5' UTR). To amplify the remaining part of the 5' end of PectERG channel, I performed a tBLASTn search against the retina transcriptome of *P. irradians* using the amino acid sequence of the human ERG (hERG) channel. I found a sequence with high similarity to the N-terminus of the hERG channel. Furthermore, the longest open reading frame (ORF) contained a triplet coding for a Methionine residue preceded by several stop codons in frame, suggesting that it was the beginning of the gene. Therefore, I designed gene-specific forward primers (C1110 and C1111) against the 5' end of the read from the transcriptome. Subsequently, I performed a PCR using primers C1110 and C1104, followed by a nested PCR with primers C1111 and C1105. The nested PCR-products were cloned and sequenced. The sequences overlapped perfectly with the known portion of PectERG gene. In addition, the PCR products contained a start codon preceded by a stop codon, suggesting that it was the beginning of the gene. The full-length gene of PectERG channel consists of 3828 bp, which encoded a protein of 1246 amino acids (Figure 3.3.1-A; Figure 6.3).

In order to clone PectHCN channel gene, I performed several PCRs using primer pairs C1341-C1343, C1031-C1032 and C0975-C1118 (Figure 3.3.2). Subsequently, I performed nested PCRs using the primer pairs C1342-C1344, C1097-C1098, C0977-C1119, respectively. Nested PCR products were cloned and sequenced. The obtained sequences were identical to the ones found in *P. irradians* retina transcriptome. Furthermore, the sequences covered almost the entire length of PectHCN gene including the 5' Untranslated Region (5' UTR) identified by the presence of several stop codons preceding a start codon in frame with the longest ORF. To obtain the 3' end of PectHCN gene, I performed several 3' RACE reactions. Although all the sequences analyzed harbored a poly-A tail, none of the sequences had a stop codon. Because of premature binding of the poly-T primer during the cDNA

synthesis the stop codon was lacking. In order to tackle this problem, I performed a cDNA synthesis using a modified poly-T primer containing 35 instead of 30 thymines. Although the 3'RACE reactions amplified bigger products, their sequences revealed that none of the products harbored a stop codon. Since polylysine (codons AAA and AAG) stretches are encountered in the C-terminus of several proteins (Chen et al., 2000), poly-T primers used in the cDNA synthesis might have bound to these stretches masking the existence of a stop codon. Because of the lack of a stop codon it is not possible to be absolutely sure that I have the full-length gene; however, PectHCN channel is 166 amino acids longer than the HCN channel of sea urchin, which is the founder member of this ion channel subfamily (Gauss et al., 1998). This supports the notion that I have cloned the full gene of PectHCN channel. PectHCN channel consists of 3516 bp, which coded for a protein of 933 amino acids (Figure 6.4).

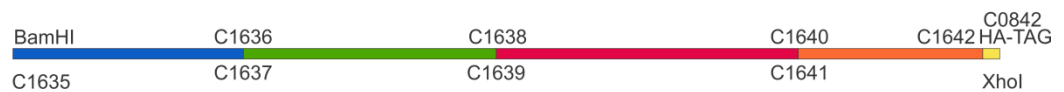
A



B



C



D



**Figure 3.3.2:** Molecular cloning of PectHCN. A: PectHCN channel domains. S1-6 represent the six transmembrane domains. CNBD: Cyclic Nucleotide Binding Domain. UTR: Untranslated Region. ATG: sequence of the start codon. TAG: sequence of the stop codon. B: RACE and PCR fragments obtained for the cloning of PectHCN channel. Characters on top and below the bars represent forward and reverse primers, respectively. C: DNA fragments used to make the constructs for heterologous expression. Characters on top and below the bars represent forward and reverse primers, respectively. D: DNA fragment used for the constructs made for RNA *in-situ* hybridization experiments. Characters on top and below the bars represent forward and reverse primers, respectively.

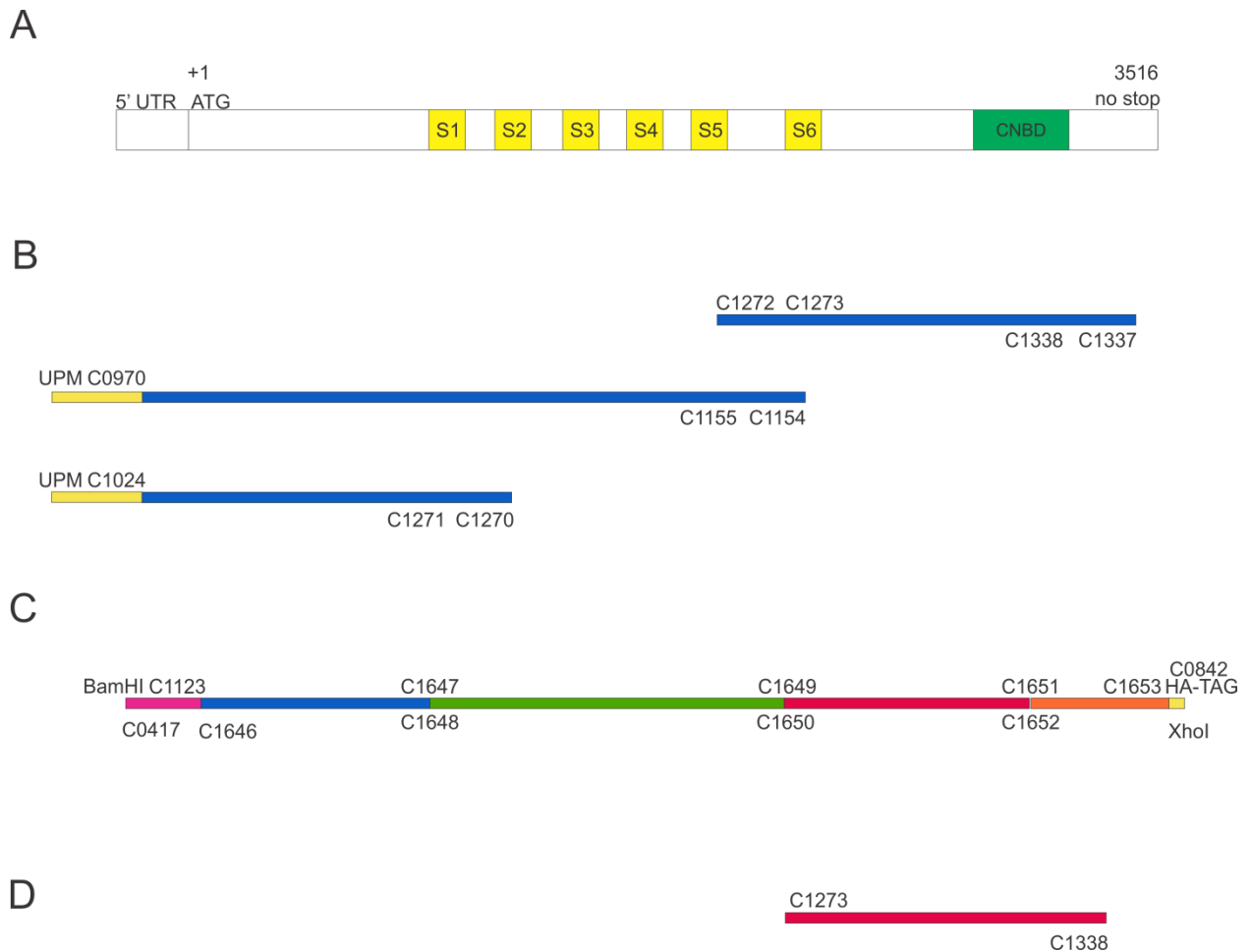


**Figure 3.3.3:** Molecular cloning of PectCNG1. A: PectCNG1 channel domains. S1-6 represent the six transmembrane domains. CNBD: Cyclic Nucleotide Binding Domain. UTR: Untranslated Region. ATG: sequence of the start codon. TAG: sequence of the stop codon. B: RACE and PCR fragments obtained for the cloning of PectCNG1 channel. Characters on top and below the bars represent forward and reverse primers, respectively. C: DNA fragments used to make the constructs for heterologous expression. Characters on top and below the bars represent forward and reverse primers, respectively. D: DNA fragment used for the constructs made for RNA *in-situ* hybridization experiments. Characters on top and below the bars represent forward and reverse primers, respectively.

In order to clone the PectCNG1 channel, I performed a PCR using primers C1272-C1337. Subsequently, I performed a nested PCR using primers C1273 and C1338. Nested PCR products were cloned and sequenced. The sequences were identical to the ones from the transcriptome. Therefore, I designed new gene-specific primers to extend the PCR products. To obtain the 5' end of PectCNG1 channel, I performed 5' RACE reactions using primers UPM-C1154 and UPM-C1270. Next, I performed nested 5' RACE reactions using primers C0970-C1155 and C1024-C1271, using as template the 5' RACE products UPM-C1154 and UPM-C1270, respectively. Nested 5' RACE products were cloned and sequenced. Sequences revealed a start codon preceded by a stop codon. Several attempts to clone the 3' end of PectCNG1 channel were performed, however the same phenomenon as with the cloning of PectHCN gene was encountered; the stop codon was missing. I performed 3' RACE reactions using the cDNA synthesized with a longer poly-T primer (as mentioned above), however this strategy proved unsuccessful. Since several proteins (Chen et al., 2000), including CNG channels (Dai et al., 2013), contain polylysine (codons AAA and AAG) stretches at the C-terminus, the poly-T primers used in the cDNA synthesis might have bound to these stretches masking the existence of a stop codon. Moreover, PectCNG1 harbors a highly conserved CNBD. In addition, hydropathy-index analysis (Kyle and Doolittle; window size = 17) of PectCNG1 amino acid sequence predicted six transmembrane domains (figure 3.2.3-A.). The PectCNG1 gene consists of 3150 bp, which coded for a protein of 711 amino acids (Figure 6.5).

### **3.3.1 Constructs for heterologous expression**

Once the candidate genes were cloned and sequenced, it was necessary to garner functional evidence that they encode viable ion channels and to determine their properties. Therefore, to make the constructs for heterologous expression of PectERG, PectHCN and PectCNG1 channels, I used recombinant PCRs to assemble the products into one ORF. For the PectERG

gene, I used primer pairs C1237 & C1243 and C1242 & C1001. Primers C1243 and C1242 had a EcoRI restriction-site in their 5' end that served as a sticky end for a recombinant PCR using primers C1237 & C1001. Furthermore, primer C1001 introduced the nucleotides in-frame coding for a hemagglutinin tag (HA-tag) that was used as antigen in Western blot and immunocytochemical staining; as well as a stop codon in-frame after the HA-tag (Figure 3.3.1 C.)

For the PectHCN gene, I used primer pairs C1635 & C1636, C1637 & C1638, C1639 & C1640, C1641 & C1642 and C1641 & C0842. Primers C1636, C1638 and C1640 were the reverse complement of C1637, C1639 and C1641, respectively. Recombinant PCRs were used to amplify C1635-C1638 and C1639-C1642 products. Subsequently, these PCR products were assembled using primers C1635 and C1642, which amplified a single PCR product containing the whole PectHCN-channel gene. Furthermore, primer C0842 introduced the nucleotides in-frame coding for a hemagglutinin tag (HA-tag) that was used as antigen in Western blot and immunocytochemical staining, as well as a stop codon after the HA-tag (Figure 3.3.2 C).

For the PectCNG1 gene, I used primer pairs C1646 & C1647, C1648 & C1649, C1650 & C1651, C1652 & C1653 and C1xx & C0842. Primers C1647, C1649 and C1651 were the reverse complement of C1648, C1650 and C1652, respectively. Recombinant PCRs were performed to amplify PCR products C1646-C1649 and C1650-C1653. Subsequently, these PCR products were assembled using primers C1646 and C1653, which amplified a single PCR product containing the whole PectCNG1-channel gene. Furthermore, primer C0842 introduced the nucleotides in-frame coding for a hemagglutinin tag (HA-tag) that was used as antigen in Western blot and immunocytochemical staining, as well as a stop codon after the HA-tag (Figure 3.3.3 C).

### 3.3.2 Western-blot analysis of *P. irradians* ion channels expressed in CHO cells

To test whether PectERG, PectHCN and PectCNG1 proteins have the expected molecular mass, I isolated membrane proteins from CHO-cells transfected with one of the different constructs, as well as from non-transfected CHO cells. Subsequently, I performed Western blot analysis using a  $\alpha$ -HA monoclonal antibody. The  $\alpha$ -HA antibody recognized bands of ~140 KDa (figure 3.3.2.1-A), ~70 KDa (figure 3.3.2.1-B), and ~110 KDa (figure 3.3.2.1-C) similar to the calculated molecular mass of PectERG (139 KDa), PectCNG1 (81 KDa) and, PectHCN (106 KDa), respectively. In membrane proteins from non-transfected CHO cells, the  $\alpha$ -HA antibody did not recognize any protein of the respective molecular mass (Figure 3.3.2.1 A-B).

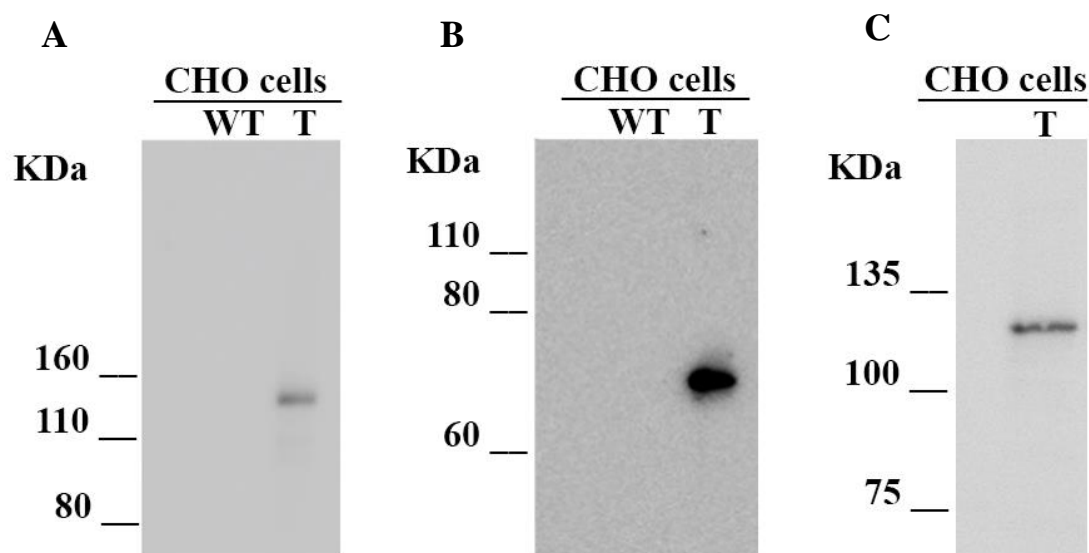


**Figure 3.3.2.1:** Heterologous expression of *P. irradians* ion channels. Western-blot analyses of membrane-protein lysates from CHO cells. A: anti-Hemagglutinin ( $\alpha$ -HA) antibody recognizes the PectERG channel in transfected (T) CHO cells. Absence of staining by  $\alpha$ -HA in lysates of non-transfected (WT) CHO cells. B:  $\alpha$ -HA antibody recognizes the PectCNG1 channel in transfected (T) CHO cells. Absence of staining by  $\alpha$ -HA in lysates of non-transfected (WT) CHO cells. C:  $\alpha$ -HA antibody show specific staining of membrane protein lysates from transfected (T) CHO cells with the PectHCN channel construct.

### 3.4 Localization of PectERG, PectHCN, and PectCNG1 channels in *P.*

#### *irradians* retina

While the molecular identification of putative channels from retinal cDNA provides important clues, it does not establish a link with photo-transduction. A first step in this direction is to localize the putative ion channels. To this end, I used two complementary approaches: RNA in-situ hybridization and immunostainings in *P. irradians* eye cryo-sections.

### **3.4.1 RNA *in-situ* hybridization (ISH) in eye sections of *P. irradians***

#### **3.4.1.1 Constructs for RNA ISH**

In order to generate the constructs for RNA *in-situ* hybridization, I designed primers to amplify a PCR product from nucleotides 2484 to 3121 of PectERG gene (primers C1027 and C1150, 638 bp, Figure 3.3.1 D), nucleotides 2458 to 3059 of the PectHCN gene (primers C1502 and C1119, 602 bp, Figure 3.3.2 D), and nucleotides 1313 to 1961 of the PectCNG1 gene (primers C1273 and C1338, 649 bp, Figure 3.3.3 D). Afterwards, the PCR product was cloned into the pBluescript II SK vector and sequenced to determine its orientation. In order to perform the *in-vitro* transcription, the respective plasmids containing the portion of the gene of interest were linearized. Subsequently, T7 or T3 RNA polymerases were used to synthesize sense or antisense RNA probes. In order to label the RNA probes, Digoxigenin-tagged UTPs were used in the RNA synthesis.

#### **3.4.1.2 RNA ISH experiments indicate that ERG and HCN channels are**

### expressed in ciliary photoreceptors

To identify the cells in the retina expressing PectERG, PectHCN, or PectCNG1 channels, I used the gene-specific RNA probes for hybridization on *P. irradians* eye-sections. Antisense probes against PectERG mRNAs stained the distal retina layer, where ciliary photoreceptors

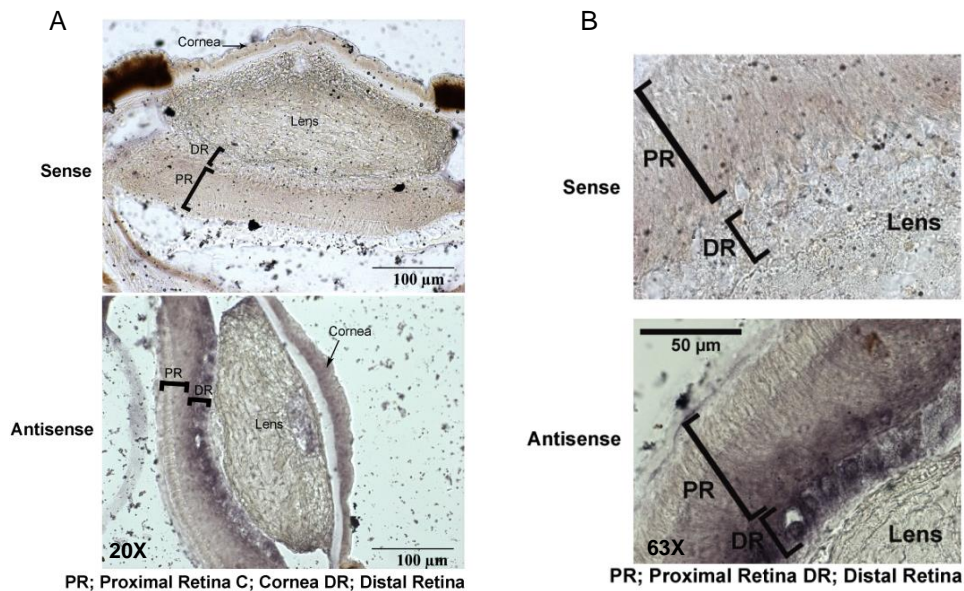


**Figure 3.4.1.2.1:** mRNAs of PectERG channels are expressed in ciliary photoreceptors. Micrographs showing *P. irradians* eye-sections incubated with sense and antisense RNA probes labeled with digoxigenin. A: Specific staining of the distal retina layer, using probes that hybridize with the 3'-end of PectERG channel. B: Micrograph of the staining shown on the left at a higher magnification.

are located (Figure 3.4.1.2.1-A). Furthermore, a closer look at the staining using a higher magnification reveals that PectERG antisense-probes distinctly stained ciliary (Figure 3.4.1.2.1-B; round-shaped cells) photoreceptors. Sense RNA probes showed no staining (Figure 3.4.1.2.1-A-B). A similar staining pattern was obtained in 12 different eye-sections from 4 different *P. irradians* eyes, indicating that the PectERG mRNA is expressed in ciliary photoreceptors of *P. irradians*.

Antisense probes against PectHCN mRNAs also stained the retina layer containing ciliary photoreceptors (DR, Figure 3.4.1.2.2-A). A higher magnification revealed that PectHCN antisense-probes only stained the distal (Figure 3.4.1.2.2-B) but not the proximal retina. Sense RNA probes showed no staining (Figure 3.4.1.2.2). A similar staining pattern was obtained in 12 different eye-sections from 4 different *P. irradians* eyes, indicating that the PectHCN mRNA is expressed in ciliary photoreceptors of *P. irradians*. Finally, one attempt to localize PectCNG1 mRNAs using 12 different eye-sections from 4 different *P. irradians* eyes was performed. However, neither antisense nor sense RNA-probes against the PectCNG1 mRNA showed any staining in *P. irradians* eye-sections. Therefore, the molecular localization of PectCNG1 channels remains to be determined.

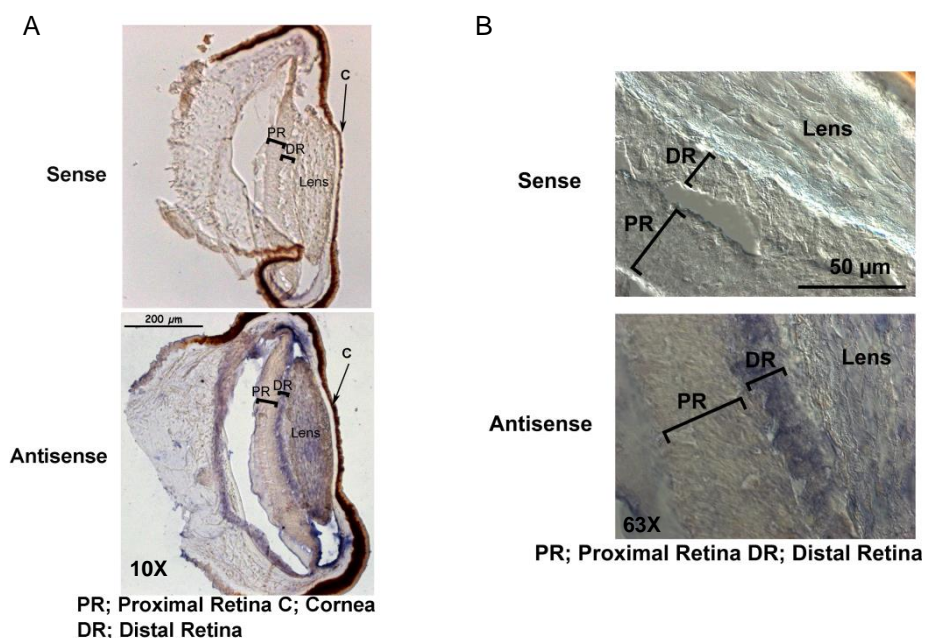


**Figure 3.4.1.2.2:** mRNAs of PectHCN channels are expressed in ciliary photoreceptors. Micrographs showing *P. irradians* eye-sections incubated with sense and antisense RNA probes labeled with digoxigenin. A: Specific staining of the distal retina layer, using probes that hybridize with the 3'-end of PectHCN channel. B: Micrograph of the staining shown on the left at a higher magnification.

### 3.4.2 Immunolocalization of PectERG, PectHCN and PectCNG1 channels

#### 3.4.2.1 Generation of monoclonal antibodies

Although mRNAs of PectERG and PectHCN were localized to ciliary photoreceptors, it was desirable to confirm the identity of the retinal cell type expressing the protein by immunostainings of eye sections of *P. irradians*. Furthermore, this approach might reveal the localization of PectCNG1 channel proteins. Therefore, to corroborate molecular localization of PectERG and PectHCN channels and to reveal the site of expression of PectCNG1

channels; we generated, in collaboration with Dr. Kremmer (Institute for Molecular Immunology, Helmholtz-Zentrum München), specific monoclonal antibodies against each ion channel of interest (Section 2.8). Two different epitopes (FE1 and FE2; Table 3.4.2.2.1) were used to raise antibodies against PectERG channels. Furthermore, one epitope was used to raise antibodies against PectHCN channel, and one epitope to raise antibodies against PectCNG1 channel.

### 3.4.2.2 Primary supernatants screening in CHO cells

**Table 3.4.2.2.1:** Different epitopes used to raise monoclonal antibodies against PectERG, PectHCN and PectCNG1 channels.

Peptide name	Amino acids	Protein target
FE1	970-984	PectERG channel
FE2	1146-1164	PectERG channel
PHCN	899-917	PectHCN channel
PCNG	589-610	PectCNG1 channel

To test the specificity of the different primary supernatants, I performed Western-blot analysis. Four primary supernatants recognized heterologously-expressed PectERG channels: two raised against FE1 and two raised against FE2 (Figure 3.4.2.1.1-A). As a positive control, I used an  $\alpha$ HA antibody, which recognizes the Hemagglutinin-tag (HA-tag) of the recombinant PectERG channel. As shown in Figure 3.4.2.2.1-A, in all cases the antibodies recognized a band of 140 KDa in transfected CHO protein extracts, however the antibodies did not recognize any bands in non-transfected (WT) CHO cells. In addition, three different primary supernatants (shown in figure 3.2.2.1.1-B) recognized heterologously-expressed PectCNG1 channels. Unfortunately, seventy nine primary supernatants from animals

immunized with the peptide from PectHCN channel did not show any positive signal in Western-blot analysis, in all cases  $\alpha$ -HA antibody recognized the PectHCN channel. Therefore, antibodies against PectHCN channels were not obtained.

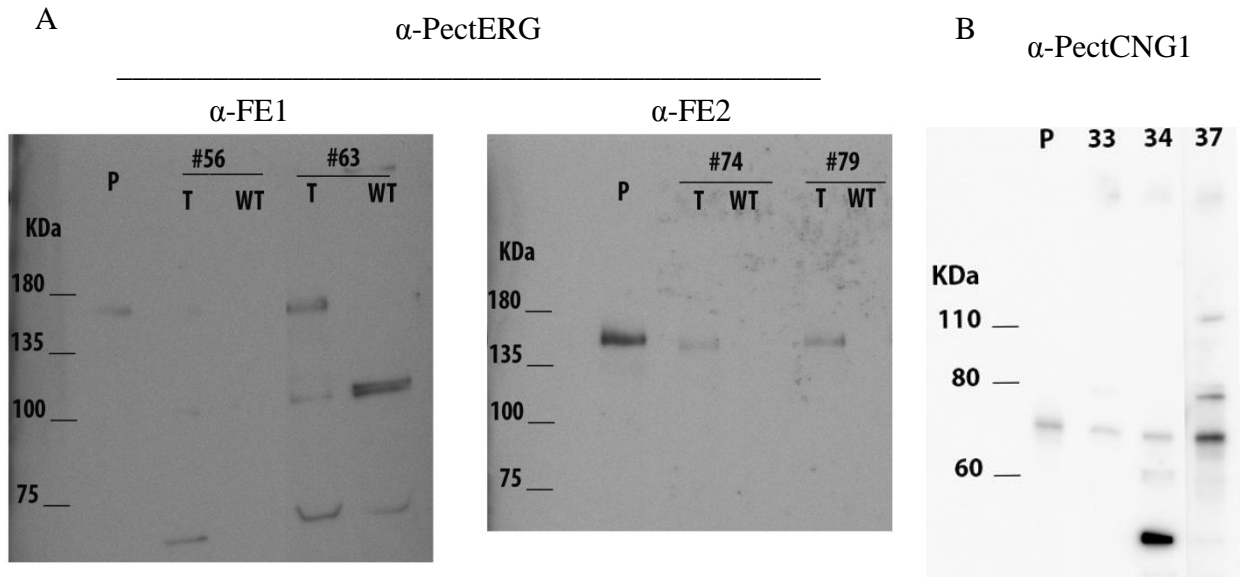


**Figure 3.4.2.2.1:** PectERG and PectCNG1 channels monoclonal antibodies recognized the heterologously-expressed proteins in CHO cells. Western-blot analyses of membrane-protein lysates from CHO cells. A: monoclonal antibodies against epitope 1 (FE1) and epitope 2 (FE2) of PectERG channels recognize the heterologously-expressed protein. P: positive control using anti-Hemagglutinin ( $\alpha$ -HA) antibodies. T: Transfected CHO cells. WT: non-transfected CHO cells. B: monoclonal antibodies against PectCNG1 channels recognize the heterologously-expressed protein. P: positive control using anti-Hemagglutinin ( $\alpha$ -HA) antibodies.

### 3.4.2.3 Immunohistochemical analysis in transfected CHO cells

To test whether the primary supernatants that recognized the heterologously-expressed protein in Western blots also recognized the heterologous protein in immunocytochemical stainings, I performed immunocytochemical analysis using PectERG primary supernatants (undiluted) on PectERG-transfected CHO cells. Four primary antibodies against PectERG recognized the heterologously-expressed channels in transfected CHO-cells (Figure 3.4.2.3.1). Immunocytochemical stainings using  $\alpha$ -PectERG antibodies (Figure 3.4.2.3.1; shown in red) co-localized with GFP fluorescence, which was used as positive control for the transfection procedure (Figure 3.4.2.3.1; shown in green). Furthermore, as a positive control for the immunostaining, I used  $\alpha$ -HA antibodies (Figure 3.4.2.3.1, shown in white) directed against the HA-tag of the recombinant PectERG channel. The fluorescent signals from  $\alpha$ -PectERG stainings (red) colocalized with the fluorescent signal from GFP (green) and  $\alpha$ -HA antibodies (white) (Figure 3.4.2.3.1; third column). In contrast, immunocytochemical stainings of non-transfected (WT) CHO cells using  $\alpha$ -PectERG and  $\alpha$ -HA antibodies showed no stainings (Figure 3.4.2.3.1; WT CHO cells). Therefore,  $\alpha$ -PectERG specifically recognized PectERG channels.

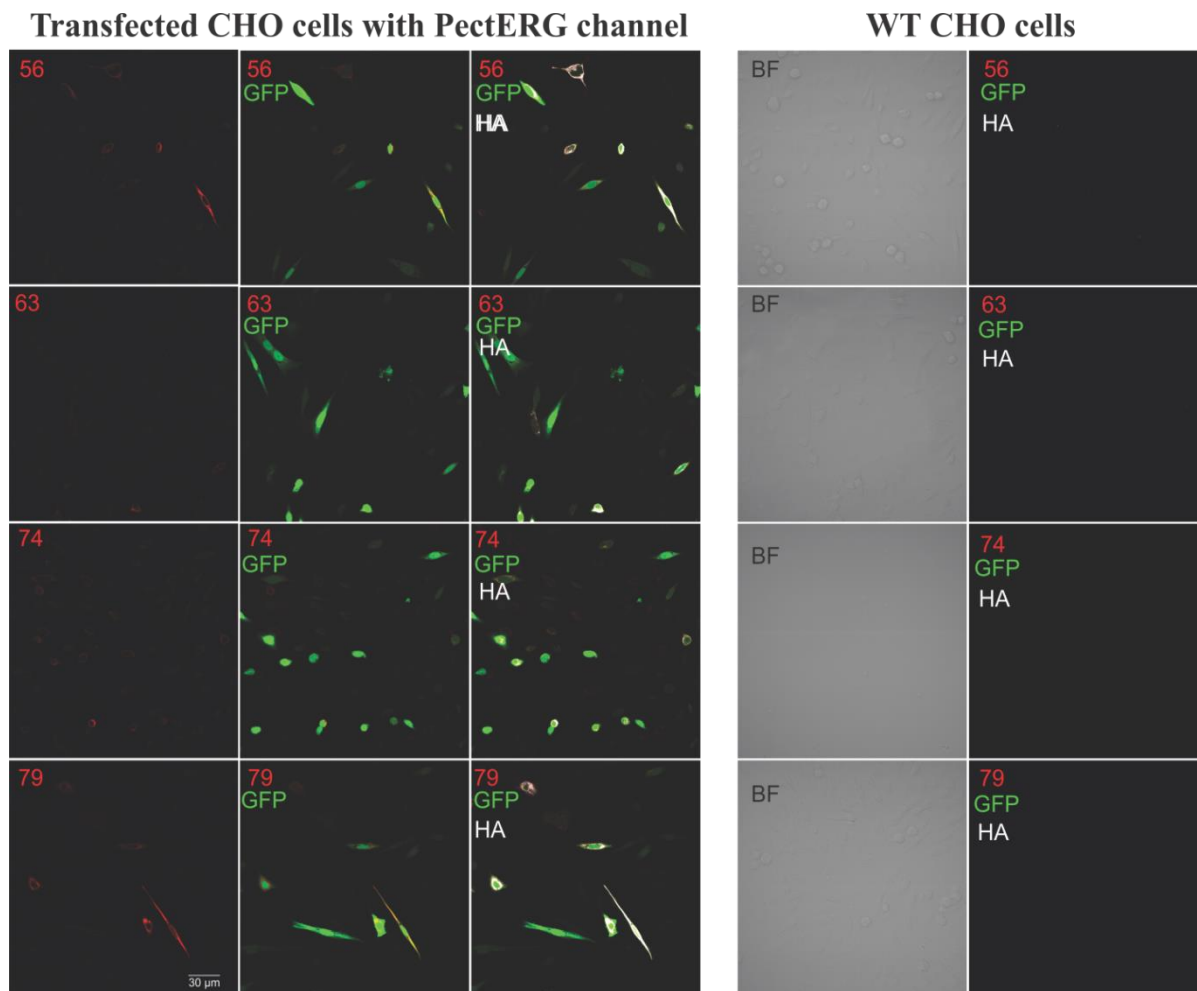


**Figure 3.4.2.3.1:** Immunocytochemical analysis of transfected and non-transfected (WT) CHO cells with PectERG channel constructs. Numbers 56, 63, 74, 79 represent stainings (red) using four different monoclonal antibodies against PectERG channels. GFP was used as reporter of transfection efficiency. HA: stainings using  $\alpha$ -HA antibodies which recognize the HA-tag present in recombinant PectERG channels. BF: bright field image of non-transfected CHO cells.

To test whether  $\alpha$ -PectCNG1 recognized heterologous PectCNG1-channels in immunocytochemical stainings, I performed immunocytochemical analysis using PectCNG1 primary (undiluted) supernatants on PectCNG1-transfected CHO cells. Three primary

antibodies against PectCNG1 channels recognized the heterologously-expressed channels in transfected CHO-cells (Figure 3.4.2.3.2). Immunocytochemical stainings using  $\alpha$ -PectCNG1 antibodies (Figure 3.4.2.3.2; shown in red) co-localized with GFP fluorescence, which was used as positive control for the transfection procedure (Figure 3.4.2.3.2; shown in green). Furthermore, as positive control for the immunostaining, I used  $\alpha$ -HA antibodies (Figure 3.4.2.3.2, last row shown in white) directed against the HA-tag of the recombinant PectCNG1 channel. The fluorescent signals arising from  $\alpha$ -PectCNG1 antibodies (red) colocalized with the fluorescent signal coming from GFP (green) and  $\alpha$ -HA antibodies (white) or DAPI (blue) (Figure 3.4.2.3.2; third column). In contrast, immunocytochemical stainings of non-transfected (WT) CHO cells using the different  $\alpha$ -PectCNG1 and  $\alpha$ -HA antibodies showed no stainings (Figure 3.4.2.3.2; WT CHO cells). Therefore,  $\alpha$ -PectCNG1 antibodies specifically recognized PectCNG1 channels.

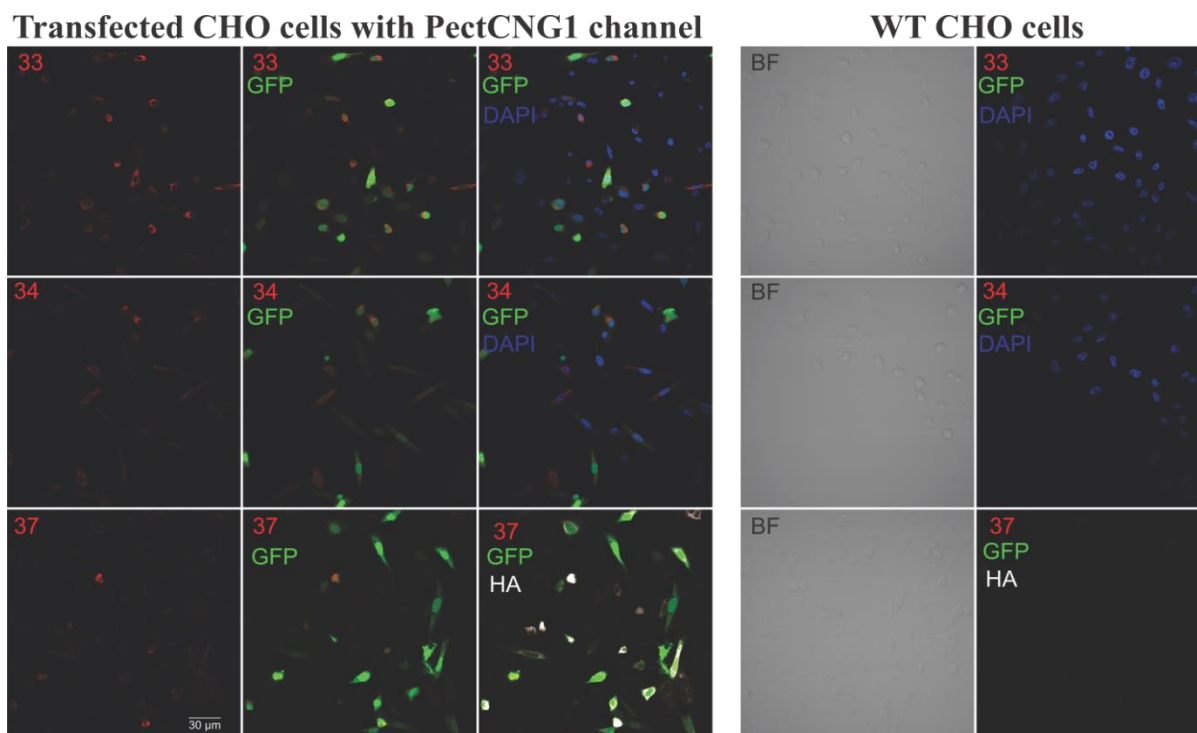


**Figure 3.4.2.3.2:** Immunocytochemical analysis of transfected and non-transfected (WT) CHO cells with PectCNG1 channel constructs. Numbers 33, 34, 37 represent stainings (red) using three different monoclonal antibodies against PectCNG1 channels. GFP was used as reporter of transfection efficiency. DAPI: DNA staining. HA: stainings using  $\alpha$ -HA antibodies which recognize the HA-tag present in recombinant PectERG channels. BF: bright field image of non-transfected CHO cells.

### 3.4.3 Immunohistochemistry in *P. irradians* eye sections

To localize PectERG and PectCNG1 proteins in *P. irradians* retinas, I performed immunohistochemical stainings on *P. irradians* eye-sections using specific monoclonal-antibodies. Using  $\alpha$ -PectERG (56) antibody, I found that PectERG channels are localized in the distal retina layer, which contains ciliary photoreceptors (Figure 3.4.3.1-A). Images at higher magnification (63x) showed a pronounced staining of ciliary photoreceptors (Figure 3.4.3.1-B). In contrast, immunohistochemical stainings using only the secondary antibodies did not show any staining of the proximal or the distal retina layer. Therefore, PectERG

channels are localized in *P. irradians* ciliary photoreceptors. On the other hand,  $\alpha$ -PectCNG1 antibodies did not recognize the native PectCNG1 channels in *P. irradians* retina (data not

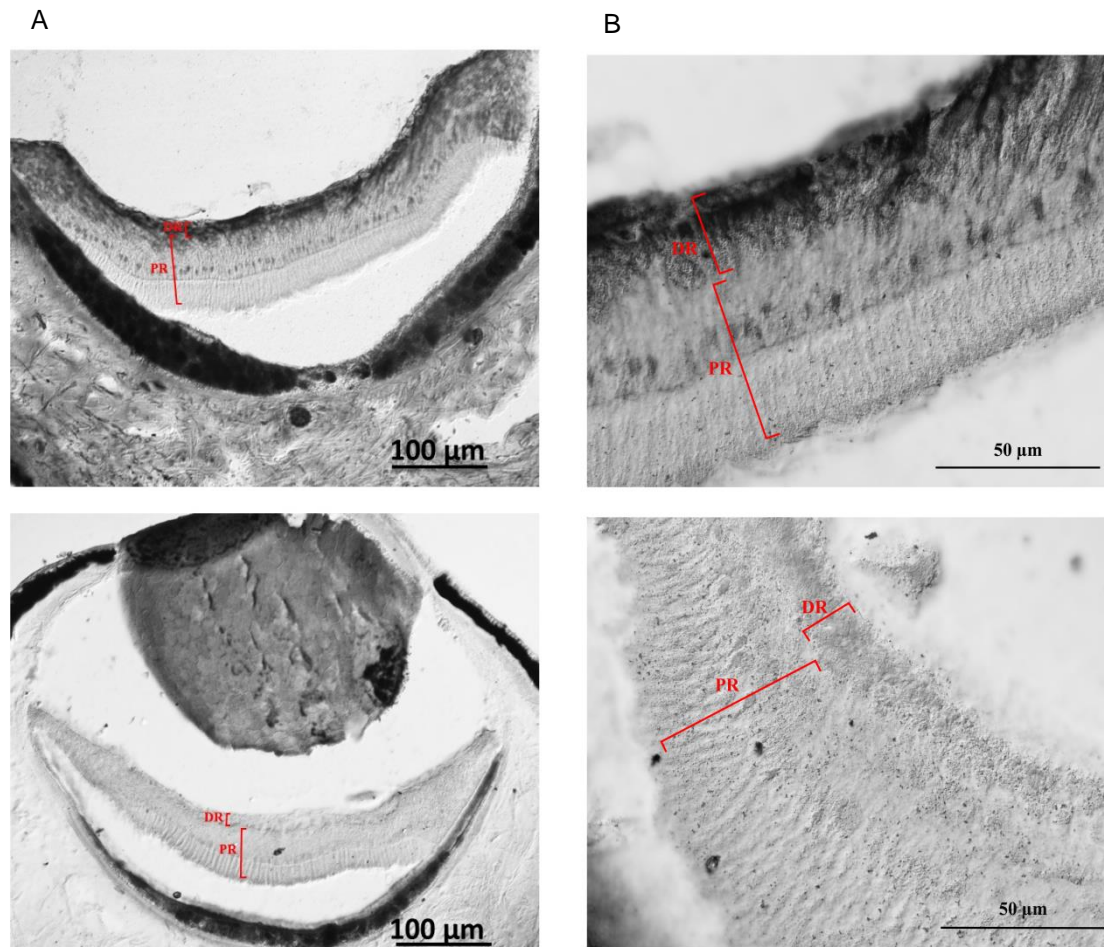


**Figure 3.4.3.1:** PectERG channels are expressed in the distal retina layer of *P. irradians*. Micrographs of *P. irradians* eye-sections. DR: Distal retina layer; PR: Proximal retina layer. Top: immunohistochemical stainings using specific monoclonal antibodies (#56) against PectERG channels. Bottom: immunohistochemical staining using only secondary antibodies. A: Micrographs taken with a 20x objective. B: Micrographs taken with a 63x objective.

shown). Therefore, the localization of PectCNG1 channels remains to be determined.

### 3.5 Electrophysiology on transfected CHO-cells expressing *P. irradians* ion channels

Although PectERG, PectHCN and PectCNG1 channels are highly conserved proteins (Figure 6.1), their functional properties are unknown. Additionally, using Western blot and immunocytochemical analysis, I have shown that transfected CHO-cells express PectERG, PectHCN and PectCNG1 channels (sections 3.3.2, 3.4.2.2 and 3.4.2.3). In order to characterize the electrophysiological properties of PectERG, PectHCN and PectCNG1 channels, I performed patch-clamp recordings on transfected CHO-cells expressing PectERG, PectHCN or PectCNG1 channels.

### **3.5.1 Patch clamp recordings on PectHCN- and PectCNG1-transfected CHO cells**

In order to test whether PectHCN channels functionally express in transfected CHO-cells, I performed patch-clamp recordings on transfected CHO-cells expressing PectHCN channels. To activate PectHCN channels, I used hyperpolarizing voltage-steps (20 to -100 mV) in voltage-clamped ( $V_h = 20$  mV) CHO cells transfected with PectHCN channel constructs. Voltage-clamp recordings showed no hyperpolarization-activated currents. Furthermore, to examine whether PectCNG1 channels are activated by cGMP, I performed patch-clamp recordings on CHO cells expressing PectCNG1 channels. Voltage-clamp recordings using either 8-Br-cGMP (1 mM) or cGMP (1 mM) applied through the patch pipette in the whole-cell configuration, showed no cGMP-activated currents. Furthermore, excised-patch recordings using several (0.05-1 mM) cGMP concentrations superfused to inside-out patches did not show any cGMP-activated currents. The CNBD of PectCNG1 channel harbors the amino acids involved in specific binding of cGMP (Figure 6.1 & 6.5); therefore, I used only cGMP or 8-Br-cGMP on these experiments.

### 3.5.2 Electrophysiological features of *P. irradians* PectERG channels

#### 3.5.2.1 Voltage dependence of PectERG channels

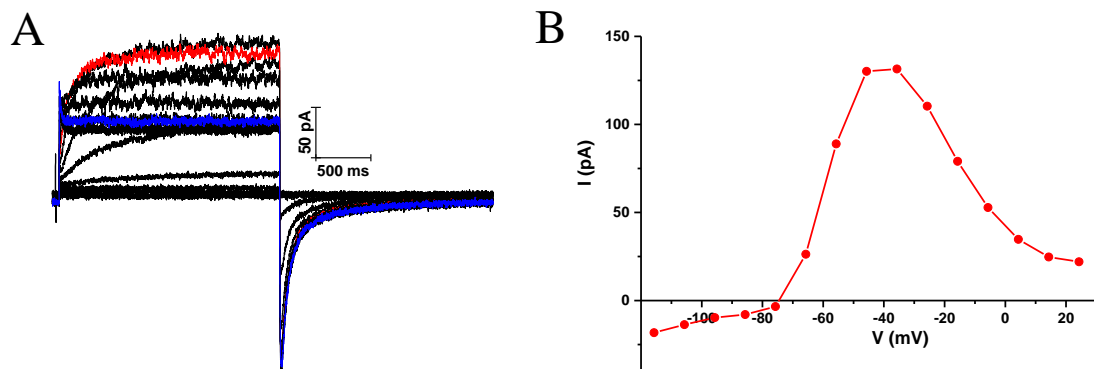


**Figure 3.5.2.1.1:** Voltage-activation of the PectERG channel. A: patch-clamp recordings ( $V_h = -90$  mV) performed on CHO cells expressing PectERG channels. Currents were activated using 10 mV voltage steps from -115 to +25 mV. Trace at -35 mV is depicted in red. Trace at +25 mV is depicted in blue. B: Current-voltage (I-V) relation of the currents from panel A.

Like other members of the ERG family, PectERG channels harbor a voltage-sensing domain and a  $K^+$ -selectivity filter; this suggests that PectERG channels are voltage-dependent  $K^+$  channels. I performed voltage-clamp recordings on transfected CHO-cells expressing PectERG channels. Voltage steps (-115 to 25 mV) elicited outward currents (Figure 3.5.2.1.1-A). The amplitude of the outward currents increased progressively with the holding potential up to -40 mV, and then decreased with holding potentials greater than -40 mV (Figure 3.5.2.1.1-B). Voltage-clamp recordings on non-transfected CHO cells using the same voltage protocol did not activate any voltage-dependent currents. Interestingly, PectERG channel currents rectify, which is more characteristic of mammalian ERG channels rather than invertebrate ERG channels (Martinson et al., 2014).

#### 3.5.2.2 PectERG $K^+$ -selectivity

To determine whether PectERG channels are  $K^+$ -selective channels, I performed whole-cell recordings using different extracellular  $K^+$ -concentrations ( $[K^+]_e$ ). I used voltage-steps (-115 to +25 mV) to activate PectERG channels. As shown in Figure 3.5.2.2.1, an increase in  $[K^+]_e$  from 5.4 to 70 mM or 140 mM shifted the reversal potential ( $V_{rev}$ ) of PectERG channels from  $-68.1 \pm 5.3$  mV to  $-23.3 \pm 2.3$  mV and  $-9.3 \pm 6$  mV, respectively. Figure 3.5.2.2.1-D summarizes the

change in the  $V_{rev}$  of PectERG channels at different  $[K^+]_e$ . Notably, the  $V_{rev}$  shift of PectERG channels at different  $[K^+]_e$  (Table 3.5.2.2.1) changed in a way predicted by the Nernst equation (eq 3.5.1), indicating that PectERG channels are highly  $K^+$ -selective.

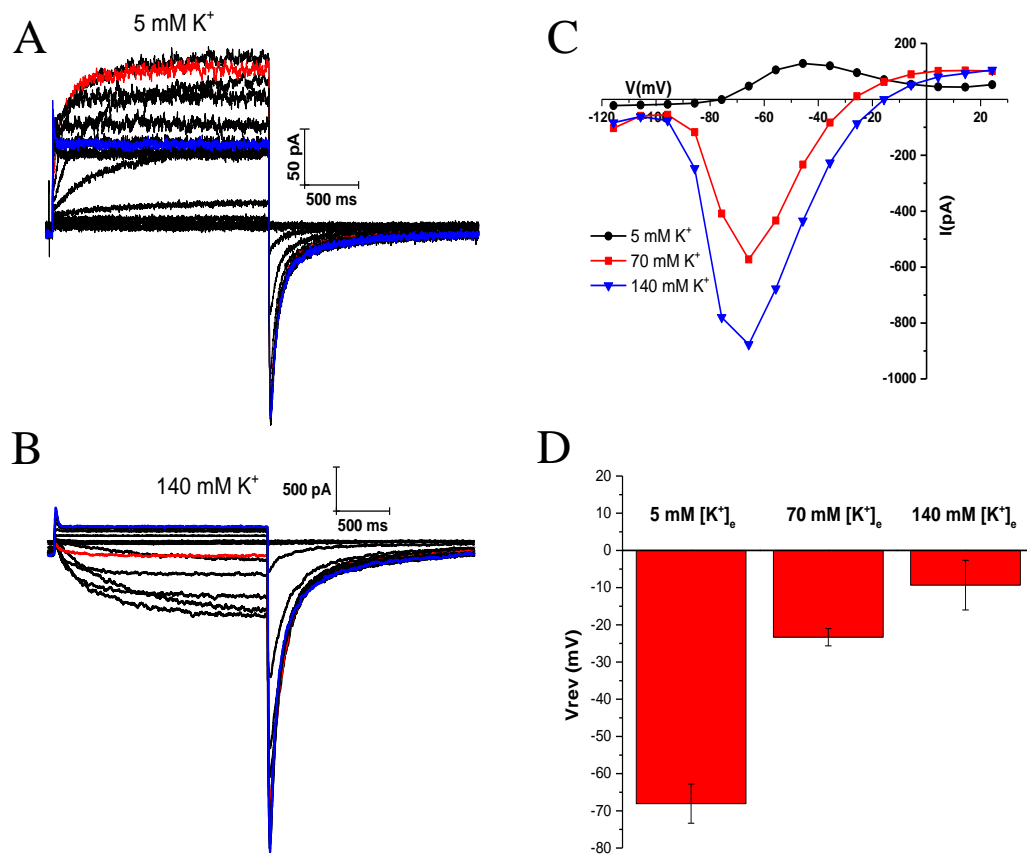


**Figure 3.5.2.2.1:** The PectERG channel is  $K^+$ -selective. A: Patch-clamp recordings performed on CHO cells expressing PectERG channels in presence of 5.4 mM  $[K^+]_e$ . Currents were activated using 10 mV voltage steps from -115 to +25 mV. Trace at -35 mV is depicted in red. Trace at +25 mV is depicted in blue. B: patch-clamp recordings performed on CHO cells expressing PectERG channels in presence of 140 mM  $[K^+]_e$ . Currents were activated using 10 mV voltage steps from -115 to +25 mV. Trace at -35 mV is depicted in red. Trace at +25 mV is depicted in blue. C: Current-voltage relation of PectERG-mediated currents in presence of 5.4, 70 and 140 mM  $[K^+]_e$ . D: Reversal potential ( $V_{rev}$ ) shift of PectERG channels in the presence of 5.4, 70 and 140 mM  $[K^+]_e$ . Error bars represent standard deviation (n = 3).

$$V_{\text{Eq.}} = \frac{RT}{zF} \ln\left(\frac{[X]_{\text{out}}}{[X]_{\text{in}}}\right)$$

**Equation 3.5.1:** Nernst equation.  $V_{\text{Eq.}}$ : equilibrium potential for a given ion X. R: universal gas constant. T: absolute temperature. F: Faraday's constant.  $[X]_{\text{out}}$ : extracellular ion concentration.  $[X]_{\text{in}}$ : intracellular ion concentration. Image adapted from [http://www.physiologyweb.com/calculators/nernst\\_potential\\_calculator.html](http://www.physiologyweb.com/calculators/nernst_potential_calculator.html)

**Table 3.5.2.2.1:** Comparison between calculated reversal potential ( $V_{\text{rev}}$ ) of  $\text{K}^+$  using the Nernst equation and the measured reversal potential ( $V_{\text{rev}}$ ) of PectERG channels. Recordings were performed at room temperature (295 K) and corrected for the Liquid Junction Potential.

$[\text{K}^+]_e$	$[\text{K}^+]_{\text{in}}$	Calculated $V_{\text{rev}}$	Measured $V_{\text{rev}}$
5.4 mM	130 mM	-80.8 mV	$-68.1 \pm 5.3$ mV
70 mM	130 mM	-15.7 mV	$-23.3 \pm 2.3$ mV
140 mM	130 mM	1.88 mV	$-9.3 \pm 6$ mV

### 3.5.2.3 PectERG channels voltage-dependence of activation and inactivation

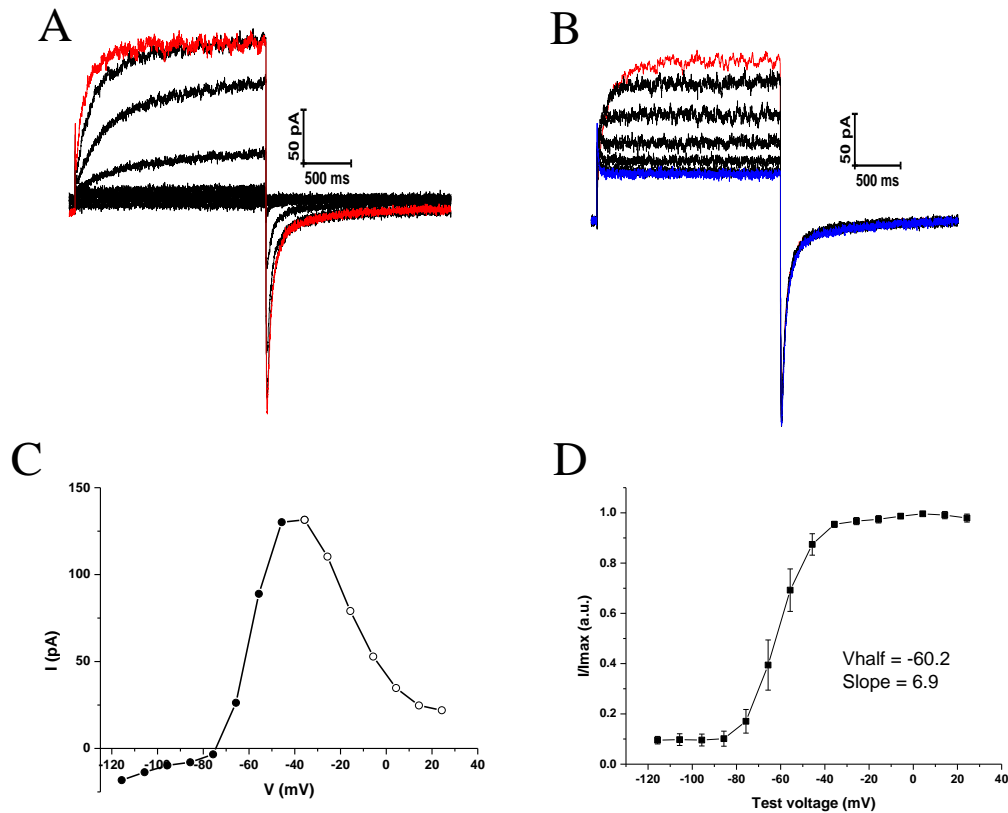


**Figure 3.5.2.3.1:** PectERG channel voltage-dependent activation. A: patch-clamp recordings performed on CHO cells expressing PectERG channels. Currents were activated using voltage steps from -115 to -35 mV at 10 mV increments. Trace at -35 mV is depicted in red. B: patch-clamp recordings performed on CHO cells expressing PectERG channels. Currents were activated using voltage steps from -35 to +25 mV at 10 mV increments. Trace at -35 mV is depicted in red. Trace at +25 mV is depicted in blue. It is worth noticing that there is no difference in the tail currents (inward currents) after return to the holding potential (-105 mV) C: Current-voltage (I-V) relation of the currents shown on A and B. filled and empty circles represent the activation and inactivation of PectERG channels, respectively. D: Normalized tail currents recorded at -105 mV using 10 mV voltage steps ranging from -115 to +25. Tail currents were adjusted to the Boltzmann function.

In order to further characterize the voltage dependence and activation of PectERG channels, I used depolarizing voltage-steps from -115 to 25 mV to activate PectERG channels, then immediately returned to the holding potential (-105 mV) to record tail currents. As mentioned above, PectERG-mediated currents increased from -115 to -35 mV (Figure 3.5.2.3.1-A & C: filled circles) and decreased at voltages greater than -35 mV (Figure 3.5.2.3.1-B & C: empty circles). However, tail currents measured at -105 mV showed that PectERG channels are fully open at voltages more positive than -35 mV (Figure 3.5.2.3.1-A-B). Furthermore, to estimate the voltage-dependence of activation of PectERG channels the relative amplitude of tail currents were plotted as a function of test potential (Figure 3.5.2.3.1 D). Subsequently, the data were fit to the Boltzmann function. The voltage of half-maximal activation of PectERG channel is  $-60.2 \pm 3.4$  mV (Figure 3.5.2.3.1-D). Recordings of tail currents revealed that PectERG channels are open at voltages greater than -35 mV (Figure 3.5.2.3.1 A-B) and yet there is a decrease in conductance at voltages  $> -35$  mV. This decrease in conductance has been described in mammalian ERG channels; it is caused by a voltage-dependent inactivation (Sanguinetti et al., 1995; Smith et al., 1996). Mammalian ERG channels show a recovery from inactivation that is manifested as an increase in conductance when the channels are subjected to repolarizations (Sanguinetti et al., 1995). To examine whether the decrease in conductance of PectERG channels at voltages  $> -35$  mV is due to a voltage-dependent inactivation, I used a voltage step to 25 mV to activate PectERG channels. Subsequently, I applied voltage steps from 25 mV to -105 mV to remove the inactivation. Following repolarization, I applied a voltage step to -105 mV to record tail currents (Figure 3.5.2.3.2-A-B). Like mammalian ERG channels, PectERG channels showed an increase in conductance following repolarization (Figure 3.5.2.3.2-B), meaning that PectERG channels inactivate at voltages  $> -35$  mV. Because there is no difference in the magnitude of the tail currents at voltages  $> -35$  mV (Figure 3.5.2.3.1 and 3.5.2.3.2), it suggests that PectERG channels are

inactivating instead of closing at these voltages. Furthermore, since the inactivation can be removed by repolarizing voltage-steps, it suggests that PectERG channels undergo a voltage-dependent inactivation at depolarized voltages. It is remarkable that PectERG channels of *P. irradians*, an invertebrate, are functionally more similar to vertebrate ERG channels (Sanguinetti et al., 1995) than to other ERG channels from invertebrates, like *Drosophila* ERG channels (Martinson et al., 2014).

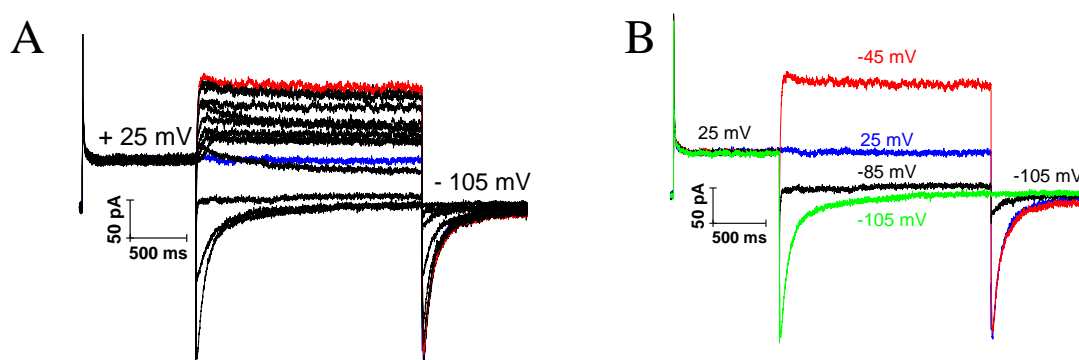


**Figure 3.5.2.3.2:** Voltage-dependent inactivation of PectERG channels. A: Voltage clamp recordings performed on CHO cells expressing PectERG channels. A voltage step to +25 mV was applied. Subsequently 10 mV voltage steps from +25 to -105 mV were applied, followed by a voltage step to -105 mV. Traces at -45 and +25 mV are depicted in red and blue, respectively. B: a few recordings from panel A, showing the removal of the voltage-dependent inactivation. Channels were activated using a depolarizing voltage-step to +25 mV. Subsequently, voltage steps to +25, -45, -85 and -105 mV were applied, followed by a voltage step to -105 mV. These are representative results of three different recordings.

### 3.5.2.4 Modulation of PectERG channels by 8-Br cGMP & cGMP

In order to test whether PectERG channels are modulated by cGMP, I applied 1 mM cGMP through the recording pipette and recorded PectERG-channel tail currents after activation by depolarizing voltage pulses. PectERG channels voltage-dependence remained unaffected in presence of cGMP (Figure 3.5.2.4.1-A) in the recording pipette. In order to rule out potential cGMP cleavage, I also recorded tail currents using 8-Br-cGMP (1 mM) applied through the patch pipette, which is a hydrolysis-resistant cGMP-analog. In presence of 8-Br-cGMP, PectERG channel voltage-dependence shifted to more depolarized voltages (Figure 3.5.2.4.1-B-C). In order to calculate the  $V_{\text{half}}$  of activation of PectERG channels in the presence and absence of cyclic nucleotides, the data were fit to the Boltzmann function using pClamp 10 software. cGMP caused a shift in the  $V_{\text{half}}$  activation of PectERG channels from  $-60.1 \pm 3.4$  mV in absence of cGMP to  $-64.6 \pm 3$  mV in presence of 1 mM cGMP (Figure 3.5.2.4.1-D); a Kolmogorov-Smirnov test showed that these data sets showed no statistically significant difference. Surprisingly, 8-Br-cGMP caused a statistically-significant (Kolmogorov-Smirnov test; P-value  $<0.05$ ) shift in the  $V_{\text{half}}$  activation of PectERG channels from  $-60.1 \pm 3.4$  mV in absence of cGMP to  $-52.4 \pm 1.8$  mV in presence of 1 mM 8-Br-cGMP (3.5.2.4.1-D), suggesting that 8-Br-cGMP inhibits rather than activates PectERG channels. Although 8-Br-cGMP had a statistically significant effect on the  $V_{\text{half}}$  of activation, there is still a 5% chance that this result is a false positive (Colquhoun, 2014). Moreover, a small sample size ( $n = 5$ ) increases the error rate in this type of statistical test (Colquhoun, 2014). More importantly, the fact that cGMP had no effect and that other ERG channels are not modulated by cGMP suggest that this may be a false positive. Further studies need to be performed to determine whether the PectERG channel is indeed modulated by 8-Br-cGMP.

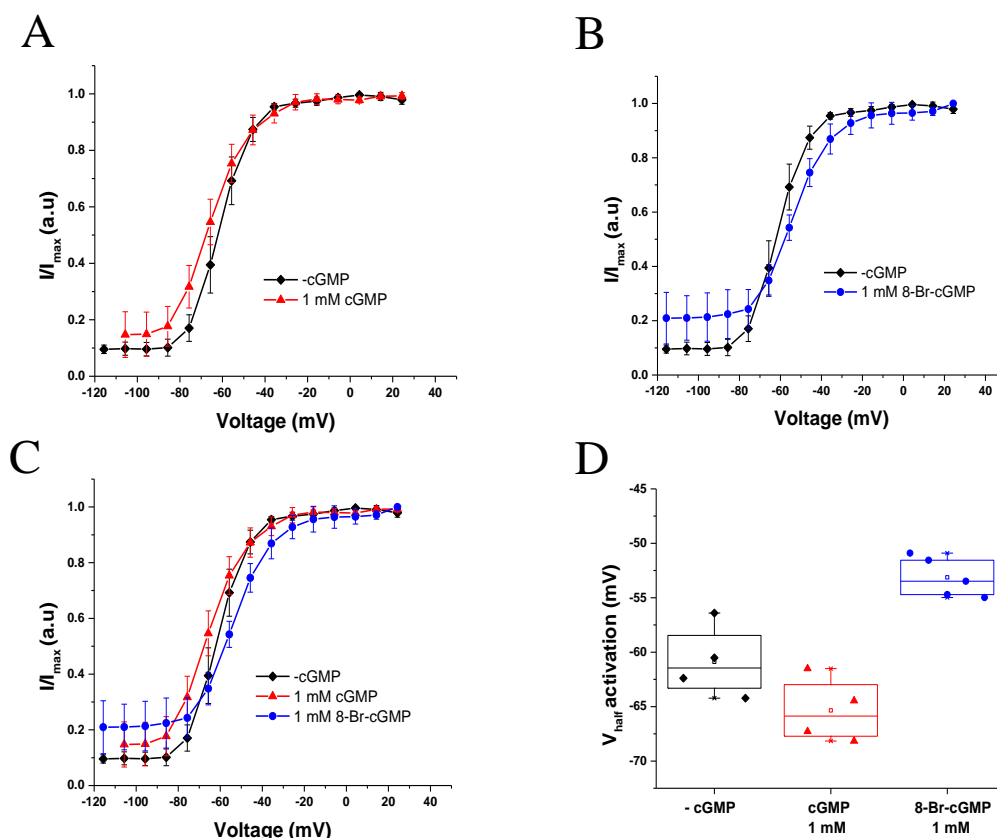


**Figure 3.5.2.4.1:** PectERG channels voltage-dependence in presence of cyclic nucleotides. A. patch-clamp recordings performed on CHO cells expressing PectERG channels. Normalized tail currents recorded at -105 mV using voltage steps ranging from -115 to +25 mV in presence (red triangles) and from -105 to +25 mV in absence (black diamonds) of cGMP applied through the patch pipette at a concentration of 1 mM. Tail currents were adjusted to the Boltzmann function. B. Normalized tail currents recorded at -105 mV using voltage steps ranging from -115 to +25 in presence (blue circles) and absence (black diamond) of 1 mM 8-Br-cGMP. Tail currents were adjusted to the Boltzmann function. C. Normalized tail currents recorded at -105 mV using 10 mV voltage steps ranging from -115 to +25 in presence of 1 mM 8-Br-cGMP (blue circles), 1 mM of cGMP (red triangles) and absence (black diamond) cyclic nucleotides. Tail currents were adjusted to the Boltzmann function. D: Box plot showing the  $V_{\text{half}}$  of activation of PectERG channels in presence of 1 mM 8-Br-cGMP (blue circles,  $n = 5$ ), 1 mM of cGMP (red triangles,  $n = 4$ ) and in absence of cyclic nucleotides (black diamonds,  $n = 4$ ).

### 3.6 Functional characterization of the human Slo3 K<sup>+</sup> channel of sperm

#### 3.6.1 Human Slo3 K<sup>+</sup> channels are activated by Ca<sup>2+</sup>

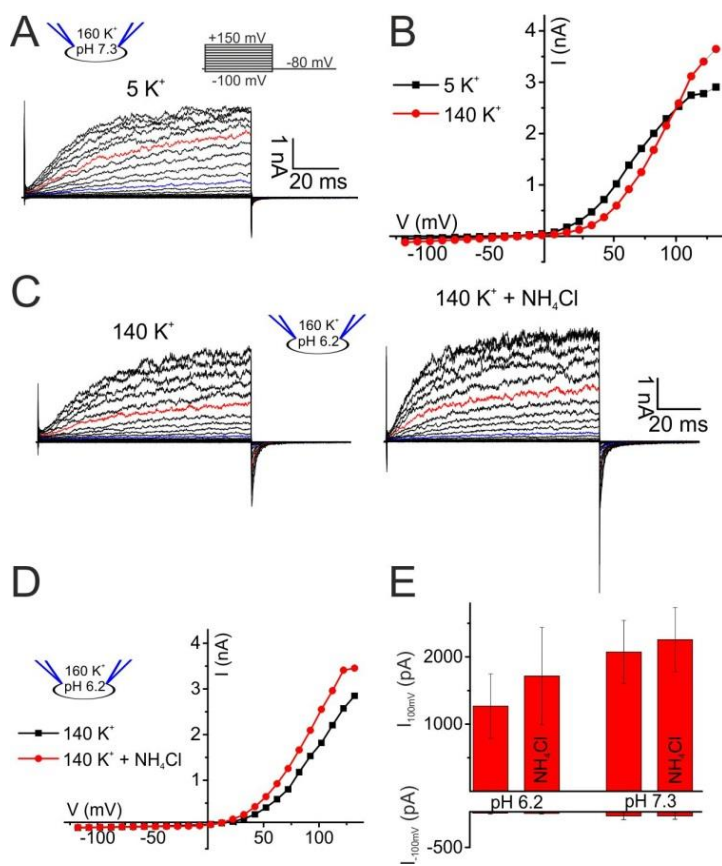


**Figure 3.6.1.1:** Currents carried by hSlo3 co-expressed with hLRRC52 in CHO cells. A: Whole-cell hSlo3 + hLRRC52 currents at pH<sub>i</sub> 7.3. Traces at +35 mV and +85 mV are depicted in blue and red, respectively. B: Current-voltage relation of hSlo3 + hLRRC52 currents recorded in 140 mM and 5 mM [K<sup>+</sup>]<sub>o</sub>. C: Currents recorded at pH<sub>i</sub> 6.2, before and after intracellular alkalization by NH<sub>4</sub>Cl (10 mM). D: Current-voltage relation of recordings from panel C. E: Mean current amplitudes at pH<sub>i</sub> 6.2 and pH<sub>i</sub> 7.3 before and after application of NH<sub>4</sub>Cl (10 mM). Error bars represent the standard deviation (n = 3).

Functional K<sub>Sper</sub> channels in sperm are composed of the pore-forming subunit Slo3 and its auxiliary subunit hLRRC52. It has been shown by heterologous expression that hLRRC52 is necessary for Slo3 channels to have a physiologically relevant (-100 to +100 mV) voltage-dependence (Yang et al., 2011). To study the functional properties of human Slo3 (hSlo3) K<sup>+</sup> channel, I performed patch-clamp recordings on transfected CHO cells expressing hSlo3 channels and the hLRRC52 auxiliary subunit. Whole-cell recordings on hSlo3-transfected CHO cells using different extracellular K<sup>+</sup> concentrations showed that depolarizing voltage-steps elicited K<sup>+</sup>-selective outward currents (Figure 3.6.1.1 A-C). Because intracellular pH

(pH<sub>i</sub>) modulates the murine Slo3 K<sup>+</sup> channel (Navarro et al., 2007), I tested whether hSlo3-mediated currents on transfected CHO cells are sensitive to changes in intracellular pH (pH<sub>i</sub>), using divalent-free intracellular solutions with pH values of 6.2 and 7.3. In comparison to mouse I<sub>K<sub>Sper</sub>, intracellular alkalization from pH<sub>i</sub> 6.2 to 7.3 only modestly enhanced hSlo3-mediated currents (Figure 3.6.1.1 A-D). At both pH values (pH 6.2 and 7.3), hSlo3 currents were enhanced by intracellular alkalization with 10 mM of NH<sub>4</sub>Cl. Before application of NH<sub>4</sub>Cl, the mean current amplitude at 130 mV was 1430 ± 590 pA at pH 6.2 and 3492 ± 1332 pA at pH 7.3. After application of NH<sub>4</sub>Cl (10 mM), hSlo3 currents increased to 1859 ± 575 pA and 4189 ± 1461 pA at pH values of 6.2 and 7.3 respectively (Figure 3.6.1.1 C). Current amplitudes at -100 mV and 100 mV were -63 ± 50 pA and 2074 ± 467 pA, respectively (n = 3) (Figure 3.6.1.1 E). Because changes in intracellular Ca<sup>2+</sup> concentration play a critical role in sperm physiology, Ca<sup>2+</sup> might modulate hSlo3 K<sup>+</sup> channels (Schreiber et al., 1998; De Jonge, 2005). In order to test whether Ca<sup>2+</sup> modulates the hSlo3 channel; I performed whole-cell recordings using different intracellular Ca<sup>2+</sup> concentrations. Indeed, in the presence of Ca<sup>2+</sup>, hSlo3 currents were activated at more negative voltages (Figure 3.6.1.2 A-B); intracellular Ca<sup>2+</sup> concentrations of 70 μM and 1 mM caused a shift of the voltage activation curve of hSlo3 channels of 20 and 50 mV, respectively (Figure 3.6.1.2 C). It is worth to mention that in the absence of divalent ions, hSlo3-mediated currents did not saturate at depolarized voltages (+120 mV) (Figure 3.6.1.1 B); in contrast, in the presence of 1 mM [Ca]<sub>i</sub> hSlo3-mediated currents reached saturation at +50 mV (Figure 3.6.1.2 B). Furthermore to test that Ca<sup>2+</sup> has an effect on the Slo3-mediated current and not on other type of outward like Ca<sup>2+</sup>-activated Cl<sup>-</sup> currents (Hartzell et al., 2005), I increased the extracellular K<sup>+</sup> concentration (140 mM) in the presence of Ca<sup>2+</sup>. The current switched its reversal potential to more depolarized values, which suggests that Ca<sup>2+</sup> activates the Slo3 K<sup>+</sup> currents. Additionally, to test the specificity of the effect of Ca<sup>2+</sup> in the activation of hSlo3 channels, I</sub>

performed whole-cell recordings using 2 mM of intracellular  $\text{Mg}^{2+}$  at pH 7.3. Intracellular  $\text{Mg}^{2+}$  had no effect on the hSlo3-mediated currents (Figure 3.6.1.2 D), suggesting that the hSlo3 channel is specifically regulated by  $\text{Ca}^{2+}$ .

Taken together, these results show that in contrast to the exclusively alkaline-activated mouse (mSlo3) Slo3  $\text{K}^+$  channel (Navarro et al., 2007; Zeng et al., 2011), the human Slo3  $\text{K}^+$  channel is moderately activated by alkalization and strongly by intracellular  $\text{Ca}^{2+}$ .

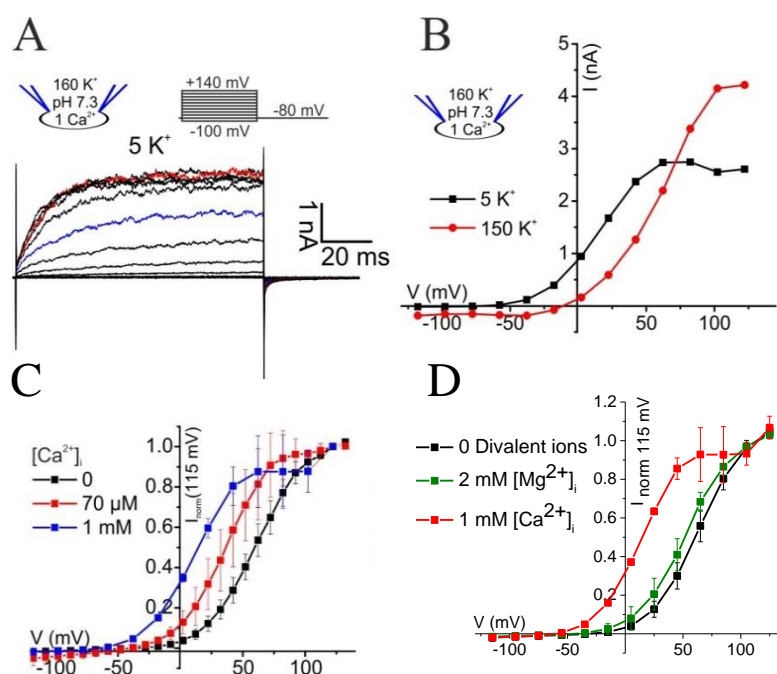


**Figure 3.6.1.2:** hslo3 currents are activated by  $\text{Ca}^{2+}$ . A: Currents recorded at 1 mM  $[\text{Ca}^{2+}]_i$  and 5 mM  $[\text{K}^+]_o$ . B: Current-voltage relation of recordings at 1 mM  $[\text{Ca}^{2+}]_i$  in 140 mM and 5 mM  $[\text{K}^+]_o$ . C: Current-voltage relation of steady-state hSlo3 + hLRRC52 currents in CHO cells at pH<sub>i</sub> 7.3 and 0, 70 μM, and 1 mM  $[\text{Ca}^{2+}]_i$ . Currents were normalized to the amplitude evoked at +115 mV. D: Current-voltage relation of steady-state hSlo3 + hLRRC52 currents in CHO cells at pH<sub>i</sub> 7.3 and 0 intracellular divalent ions, 2 mM  $[\text{Mg}^{2+}]_i$ , and 1 mM  $[\text{Ca}^{2+}]_i$ . Currents were normalized to the amplitude evoked at +115 mV. Normalized as in panel (C). Error bars represent the standard deviation (n = 3).

### 3.6.2 Pharmacological properties of the human Slo3 channel

During the course of this work, a paper by Mannowetz et al., 2013 was published suggesting that the principal  $K^+$  channel in human sperm is the Slo1 channel. Our findings together with Mannowetz *et al.*, agree on that  $I_{K_{Sper}}$  of human sperm is activated by  $Ca^{2+}$ . However, there are some discrepancies. We found that human sperm  $K^+$  currents have a modest pH

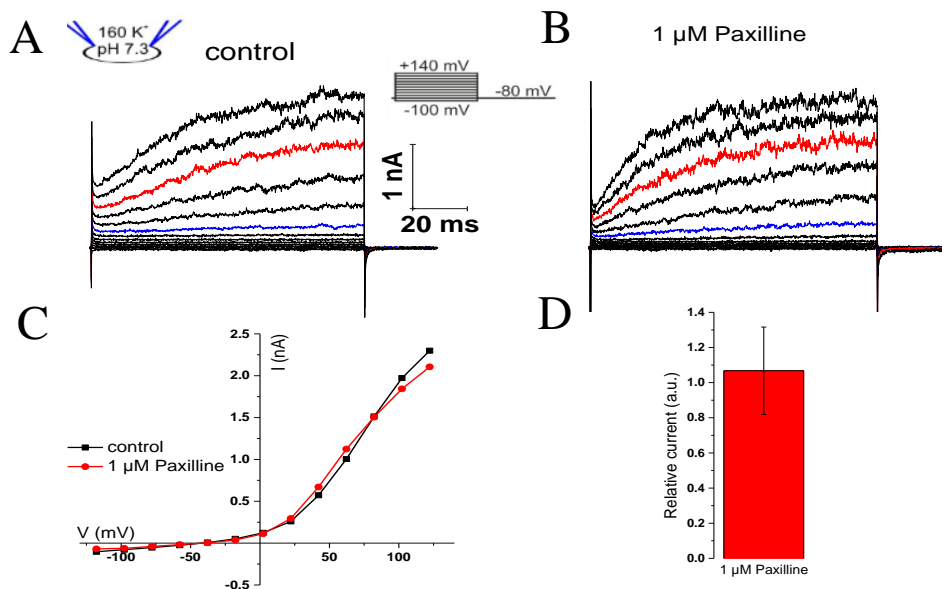


**Figure 3.6.2.1:** Lack of inhibition on hSlo3-mediated currents by Paxilline. hSlo3 was co-expressed with hLRRC52 in CHO cells. A: Whole-cell hSlo3 + hLRRC52 currents at  $pH_i$  7.3 in the absence of Paxilline. Traces at +35 mV and +85 mV are depicted in blue and red, respectively. B: Whole-cell hSlo3 + hLRRC52 currents at  $pH_i$  7.3 in the presence of Paxilline (1  $\mu$ M) in the extracellular solution. Traces at +35 mV and +85 mV are depicted in blue and red, respectively. C: Current-voltage relation of recordings from panel A and B. D: Relative current amplitude of hSlo3 + hLRRC52 currents (at 80 mV) before and after superfusion with 1  $\mu$ M of Paxilline. Error bars represent the standard deviation ( $n = 3$ ).

dependence, which is consistent with the small pH dependence of the heterologously expressed hSlo3 channel. Furthermore, there are some conflicting pharmacological results regarding the molecular identity of the channel. To challenge these findings, I used the same Slo1 channel blockers that were used by Mannowetz et al., to test whether they block the

hSlo3 currents. Paxilline blocks Slo1-channels with a  $K_i = 1.9$  nM (Knaus et al., 1994). I used 1  $\mu$ M of extracellularly applied Paxilline and observed no inhibition on hSlo3 mediated currents (Figure 3.6.2.1).

Furthermore Charybdotoxin (CTX) blocks Slo1-channels with a  $K_i$  value of 2.1 nM (Gimenez-Gallego et al., 1988). I performed whole cell recordings on Slo3 channels in the absence and presence of CTX (100 nM). The hSlo3 currents were not affected by the extracellular application of CTX (Figure 3.6.2.2).

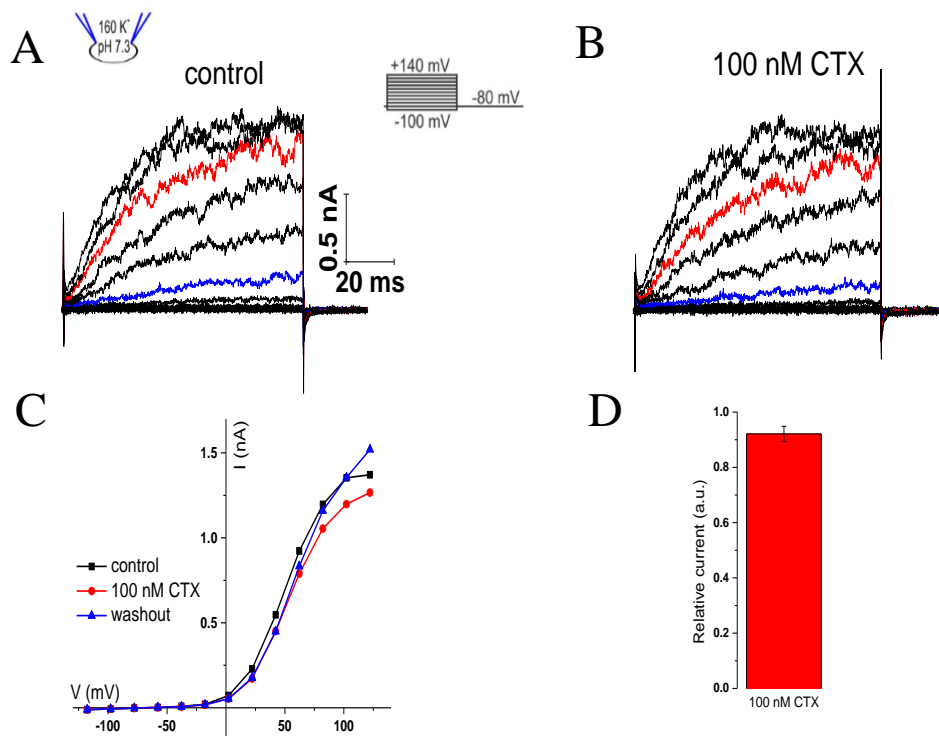


**Figure 3.6.2.2:** Lack of inhibitory effect of CTX on hSlo3 currents. hSlo3 was co-expressed with hLRRC52 in CHO cells. A: Whole-cell hSlo3 + hLRRC52 currents at pH<sub>i</sub> 7.3 in the absence of CTX. Traces at +35 mV and +85 mV are depicted in blue and red, respectively. B: Whole-cell hSlo3 + hLRRC52 currents at pH<sub>i</sub> 7.3 in the presence of CTX (100 nM) in the extracellular solution. Traces at +35 mV and +85 mV are depicted in blue and red, respectively. C: Current-voltage relation of recordings from panel A and B. D: Relative current amplitude of hSlo3 + hLRRC52 currents (at 80 mV) before and after superfusion with 100 nM of CTX. Error bars represent the standard deviation (n = 3).

In addition, the Slo1-channel blocker Iberitoxin (IbTX) (100 nM) had no inhibitory effect on hSlo3 currents (Figure 3.6.2.3). Altogether, Slo1 channel blockers did not show any inhibition on hSlo3 currents. In contrast, patch-clamp recordings on hSlo1-transfected CHO cells showed that IbTX (100 nM) blocks hSlo1 currents by about  $84\% \pm 10\%$ ,  $n = 3$  (Figure 3.6.2.4).

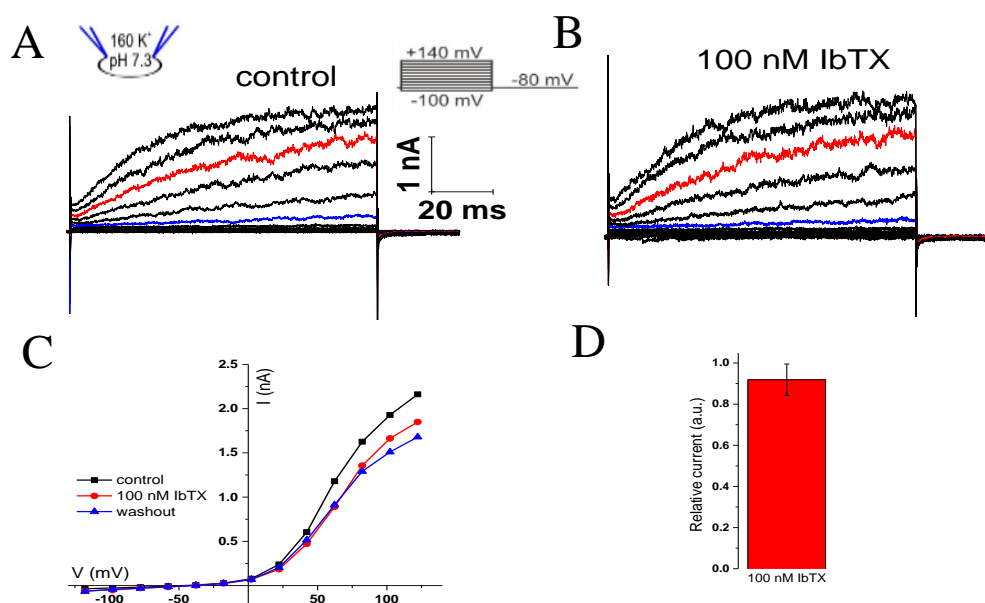


**Figure 3.6.2.3:** IbTX does not inhibit hSlo3 currents. hSlo3 was co-expressed with hLRRC52 in CHO cells. A: Whole-cell hSlo3 + hLRRC52 currents at pH<sub>i</sub> 7.3 in the absence of IbTX. Traces at +35 mV and +85 mV are depicted in blue and red, respectively. B: Whole-cell hSlo3 + hLRRC52 currents at pH<sub>i</sub> 7.3 in the presence of IbTX (100 nM) in the extracellular solution. Traces at +35 mV and +85 mV are depicted in blue and red, respectively. C: Current-voltage relation of recordings from panel A and B. D: Relative current amplitude of hSlo3 + hLRRC52 currents (at 80 mV) before and after superfusion with 100 nM of IbTX. Error bars represent the standard deviation ( $n = 3$ ).

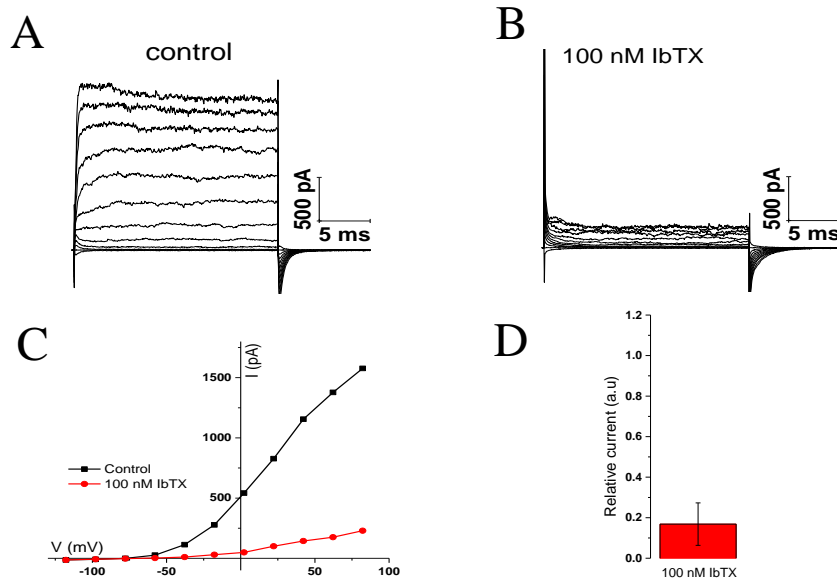


**Figure 3.6.2.4:** Inhibition of hSlo1 currents by IbTX. hSlo1 was expressed in CHO cells. A: hSlo1 currents recorded in outside-out patches excised from hSlo1-transfected CHO cells at  $\text{pH}_i$  7.3 and  $70 \mu\text{M} [\text{Ca}^{2+}]_i$  in the absence of IbTX. B: hSlo1 currents recorded in outside-out patches excised from hSlo1-transfected CHO cells at  $\text{pH}_i$  7.3 and  $70 \mu\text{M} [\text{Ca}^{2+}]_i$  after superfusion with 100 nM of IbTX in the extracellular solution. C: Current-voltage relation of recordings from panel A and B. D: Relative current amplitude of hSlo1 (at 80 mV) before and after superfusion with 100 nM of IbTX. Error bars represent the standard deviation ( $n = 3$ ).

### 3.6.3 hSlo3 channel is inhibited by Progesterone

In addition, in the same paper, Mannowetz et al., 2013 reported an inhibitory effect of progesterone on  $I_{K_{Sper}}$ . To test whether progesterone inhibits hSlo1 and hSlo3 currents; I used different progesterone concentrations while recording whole-cell currents on CHO cells

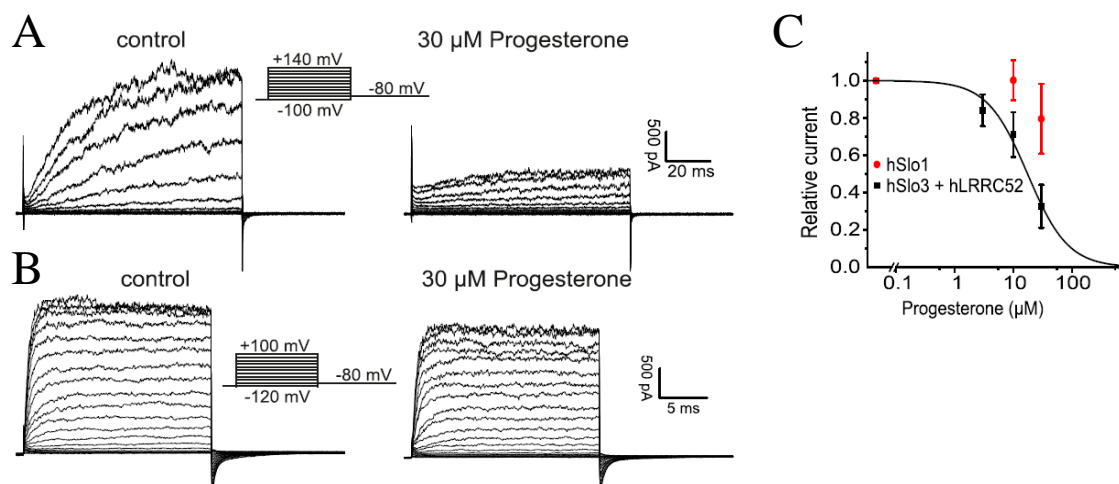


**Figure 3.6.3.1:** Progesterone inhibits hSlo3 but not hSlo1 channels. A: Whole-cell hSlo3 + hLRRC52 currents recorded in hSlo3-transfected CHO cells at  $pH_i$  7.3 before and after perfusion with 30  $\mu$ M progesterone. B: hSlo1 currents recorded in outside-out patches excised from hSlo1-transfected CHO cells at  $pH_i$  7.3 and 70  $\mu$ M  $[Ca^{2+}]_i$  before and after perfusion with 30  $\mu$ M progesterone. C: Relative amplitude of hSlo1 and hSlo3 + hLRRC52 currents at 80 mV in CHO cells in the presence of progesterone.

expressing either hSlo3 or hSlo1 channels. Progesterone inhibited hSlo3-mediated currents (Figure 3.6.3.1 A) in a concentration dependent manner. In contrast, progesterone had only a weak inhibitory effect on hSlo1-mediated currents (Figure 3.6.3.1 B). Finally, hSlo3 is inhibited by progesterone with a  $K_i$  of 17  $\mu$ M (Figure 3.6.3.1 C), which greatly agrees with the progesterone inhibition ( $K_i = 7.5\mu$ M) of  $I_{K_{Sper}}$  reported by Mannowetz et al.

### 3.6.4 hSlo3-mediated currents resemble the $K^+$ currents ( $I_{KSper}$ ) of human sperm

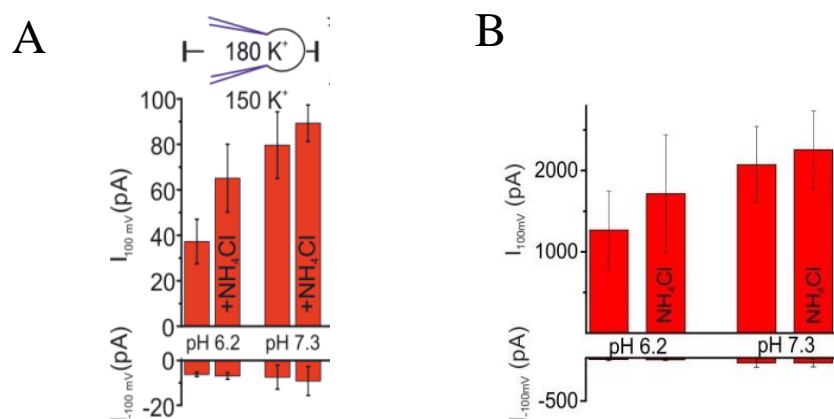


**Figure 3.6.4.1:** A: Whole-cell recordings of sperm currents before and after extracellular application of  $NH_4Cl$  (10 mM) at  $pH_i$  of 6.2 and 7.3 ( $n = 3-6$ ). Adapted from Brenker et al 2014. B: Whole cell recordings performed on CHO cells expressing hSlo3 + hLRRC52. Mean current amplitudes at  $pH_i$  6.2 and  $pH_i$  7.3 before and after application of  $NH_4Cl$  (10 mM) ( $n = 3$ ). Error bars represent the standard deviation.

The  $K^+$  current of human sperm ( $I_{KSper}$ ) and hSlo3 currents share several features. The pH dependence of both currents is similar. At  $pH_i$  6.2, intracellular alkalization with  $NH_4Cl$  enhanced  $I_{KSper}$  by  $1.8 \pm 0.9$ -fold (at +100 mV,  $n = 4$ ) (Figure 3.6.4.1 A), whereas at  $pH_i$  7.3, alkalization by  $NH_4Cl$  had a less pronounced effect (Figure 3.6.4.1 A). Similarly, hSlo3 currents are enhanced by alkalization with  $NH_4Cl$  at pH 6.2 and to a lower extent at pH 7.3 (Figure 3.6.4.1 B).

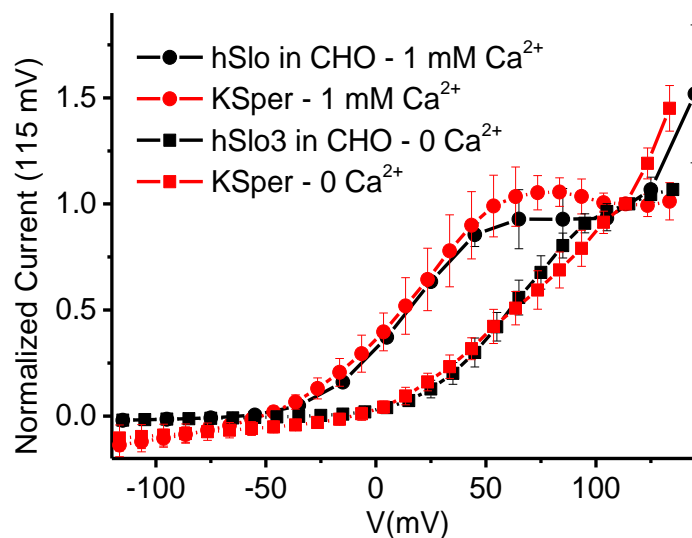


**Figure 3.6.4.2:** Activation of  $I_{K_{Sper}}$  by  $Ca^{2+}$  is identical to hSlo3  $K^+$  channels. Current-voltage relation of hSlo3 + hLRRC52 currents in CHO cells and  $I_{K_{Sper}}$  recorded from human sperm at 0 and 1 mM  $[Ca^{2+}]_i$  ( $pH_i$  7.2). Currents were normalized to the amplitude evoked at +115 mV ( $n = 3$ ). Error bars represent the standard deviation. Adapted from Brenker et al 2014.

Furthermore, the human  $I_{K_{Sper}}$  and Slo3 are modulated by  $Ca^{2+}$ . The  $Ca^{2+}$ -dependence of activation of human  $I_{K_{Sper}}$  and hSlo3 are strikingly similar. Normalized currents from hSlo3-transfected CHO cells and  $I_{K_{Sper}}$  in the presence of 1 mM  $Ca^{2+}$  shifted 50 mv to the left, compared to the recordings in divalent-free intracellular solution (Figure 3.6.4.2).

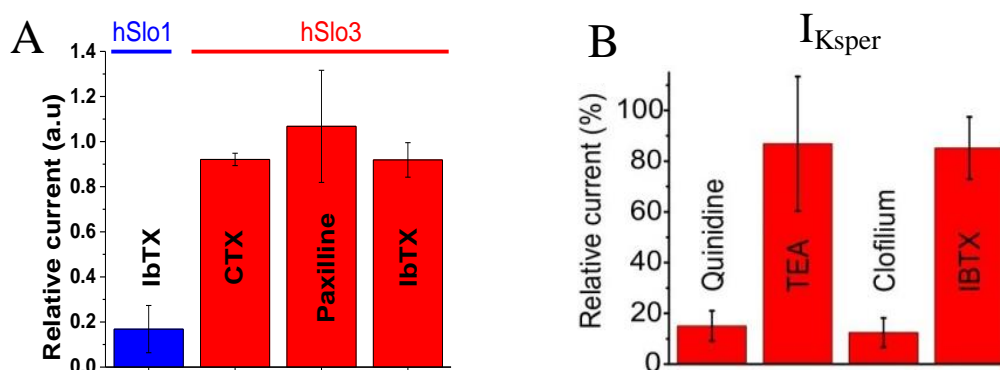


**Figure 3.6.4.3:**  $I_{Ksper}$  of human sperm shows the pharmacological profile of hSlo3 rather than hSlo1 channels. A: Blue histogram: relative current amplitude of hSlo1 (at 80 mV) before and after superfusion with IbTX (100 nM). Red histograms: relative current amplitude of hSlo3 + hLRRC52 currents (at 120 mV) before and after superfusion with IbTX (100 nM), CTX (100 nM), or Paxilline (1  $\mu$ M). hSlo1 and hSlo3 + hLRRC52 were expressed in CHO cells. Error bars represent the standard deviation (n = 3). B: Mean outward currents at 65 mV in the presence of 500  $\mu$ M quinidine, 10 mM TEA, 50  $\mu$ M clofilium, or 100 nM IBTX. Error bars represent the standard deviation (n = 3). Adapted from (Brenker et al., 2014).

Finally, several Slo1 channel blockers had no effect on hSlo3 currents (Figure 3.6.4.3). More importantly, the specific Slo1-channel blocker IbTX had no inhibitory effect on  $I_{Ksper}$ , suggesting that  $I_{Ksper}$  is not mediated by Slo1 (Figure 3.6.4.3). It is remarkable that  $I_{Ksper}$  together with the hSlo3-mediated currents are both weakly enhanced by alkalization and activated by  $Ca^{2+}$ . Moreover, the fact that progesterone inhibits  $I_{Ksper}$  and hSlo3 but not hSlo1, together with the lack of inhibition of  $I_{Ksper}$  and hSlo3 by several Slo1 channel blockers, strongly suggests that  $I_{Ksper}$  is mediated by hSlo3 and not hSlo1.



---

## 4 Discussion

### 4.1 Light-activated K<sup>+</sup> channel of ciliary photoreceptors

Ciliary photoreceptors of *P. irradians* respond to light with a hyperpolarization (McReynolds and Gorman, 1970; Gomez and Nasi, 1995). The hyperpolarization induced by light is caused by an increase in membrane conductance due to the activation of a K<sup>+</sup>-selective channel (McReynolds and Gorman, 1970; Gomez and Nasi, 1994b). Several reports suggest that the phototransduction cascade of ciliary photoreceptors of *P. irradians* use cGMP as second messenger. Voltage-clamp recordings using the patch-clamp technique showed that 8-Br-cGMP, applied via the patch pipette, elicits the activation of a K<sup>+</sup> current and a non-selective cation current (Gomez & Nasi, 1995; Gomez and Nasi, 1997b). The non-selective cation current shall be discussed later. This chapter will focus on the K<sup>+</sup>-selective current. The K<sup>+</sup> current activated by 8-Br-cGMP is reminiscent of the light activated current of ciliary photoreceptors of *P. irradians*. Both currents have commonalities such 4-AP blockade, high selectivity for K<sup>+</sup> and outward rectification (Gomez and Nasi, 1995). More importantly, after internal perfusion of ciliary photoreceptors with 8-Br-cGMP, the light response has a smaller amplitude, which suggests that 8-Br-cGMP activates the light-dependent channels, leaving a smaller number of channels available to be activated by the phototransduction cascade. In addition, I could show that fast photorelease of cGMP rapidly activates a K<sup>+</sup> conductance. This K<sup>+</sup> conductance, like the light-activated conductance of *P. irradians* ciliary photoreceptors, is blocked by 4-AP (10 μM) (Section 3.1). All together, these results suggest that the light-activated K<sup>+</sup> channel of ciliary photoreceptors of *P. irradians* is a cGMP-gated K<sup>+</sup> channel. Attempts to find a cGMP-gated K<sup>+</sup> channel in the transcriptome of *P. irradians* retina failed. How can these results be reconciled?

One possible scenario is that the transcriptome lacks the transcript of the cGMP-activated K<sup>+</sup> channel responsible for the photoresponse. It has been shown that the turnover rate of proteins in murine rods is 24 h (Bok and Young, 1972). Furthermore, the rod outer segments of mouse renew completely in 10-12 days (Young, 1967). It is possible that the proteins of ciliary photoreceptors of *P. irradians* have a similar turnover rate; therefore, it is safe to assume that the main ion channel involved in the phototransduction of ciliary photoreceptors is not a rare transcript. Moreover, to increase the likelihood of sequencing rare transcripts, *P. irradians* retina transcriptome was obtained from a normalized cDNA library (see materials and methods).

Another scenario is that the cGMP-gated K<sup>+</sup> channel of *P. irradians* harbors an unconventional CNBD. I performed BLAST searches in *P. irradians* retina transcriptome using the cyclic nucleotide binding (GAF) domain of phosphodiesterases (Heikaus et al., 2009); although there were several hits, the contigs found were putative phosphodiesterases; none of the contigs had a putative ion channel function or a putative transmembrane domain. It is worth to mention that all the approaches I used to search in the transcriptome to find the cGMP K<sup>+</sup> channel were based on sequence homology. Therefore, protein domains that do not have sequence homology to domains of known function were not detected (Mathé et al., 2002). Thus, there is still a chance that a K<sup>+</sup> channel with a CNBD completely different to any known CNBD could be the light-transduction channel of *P. irradians* ciliary photoreceptors.

Another scenario is that some subunits of CNG channels and K<sup>+</sup> channels form heteromers, where the CNG channel subunit confers the sensitivity to cyclic nucleotides and the K<sup>+</sup> channel subunit the K<sup>+</sup> selectivity. Although members of the two-pore channel family form heteromers of  $\alpha$ -subunits (Levitz et al., 2016), heteromers between CNG channels and members of other channel families have not been reported.

An additional possible explanation might be that cGMP induces a fast change in intracellular pH ( $[pH]_i$ ) that leads to the opening of a pH-dependent  $K^+$  channel causing the hyperpolarizing response of *P. irradians* ciliary photoreceptors, and, therefore, leading to the false premise that cGMP directly gates the  $K^+$  channel. Recent reports have shown that *Drosophila* rhabdomeric photoreceptors use  $pH_i$  changes as part of their phototransduction cascade (Huang et al., 2010; Hardie and Juusola, 2015). *Drosophila* rhabdomeric photoreceptors respond to light with a depolarization. Light activates rhodopsin, which in turn activates heterotrimeric Gq proteins. Gq proteins activate phospholipase C (PLC) that hydrolyses phosphatidyl-inositol 4,5 bisphosphate ( $PIP_2$ ). PLC-mediated cleavage of  $PIP_2$  yields diacylglycerol (DAG), inositol 1,4,5 trisphosphate ( $IP_3$ ) and a proton, which activate TRP and TRPL cation-channels leading to the depolarization of the cell. The molecular mechanism of activation of TRP and TRPL channels remains controversial (Hardie and Juusola, 2015). It has been proposed that protons and stretch of the cell membrane due to  $PIP_2$  depletion activate TRP channels (Huang et al., 2010; Hardie and Juusola, 2015). Although some invertebrate photoreceptors use  $pH_i$  changes in their phototransduction cascade, the phosphoinositide-signaling cascade of rhabdomeric photoreceptors is dramatically different to the cGMP transduction pathway of ciliary photoreceptors (Yau and Hardie, 2009b). A recent report in sea urchin sperm might shed light onto the possible molecular mechanism for fast pH changes in the context of cGMP signaling (Seifert et al., 2015).

In sea urchin sperm, the chemoattractant (resact) activates a guanylate cyclase (GC) that is embedded in the membrane of the sperm flagellum. Upon activation, the GC rapidly increases the cGMP levels inside the flagellum (Kaupp et al., 2003). In turn, cGMP activates a  $K^+$ -selective channel (CNGK) which hyperpolarizes the cell due to the efflux of  $K^+$  ions (Strücker T et al, 2006). Subsequently, hyperpolarization elicits two different signals; rapid

intracellular alkalization via  $\text{Na}^+/\text{H}^+$  exchangers (sNHE) and depolarization via HCN channels. Alkalization shifts the voltage dependence of sperm-specific  $\text{Ca}^{2+}$  (CatSper) channels to more negative values, which causes the opening of CatSper channels by the HCN channel-induced depolarization. Likewise, CatSper-channel activation causes further depolarization and a concomitant increase in  $[\text{Ca}^{2+}]_i$ , modifying the flagellar beat of sperm cells (Strünker *et al.*, 2015; Seifert *et al.*, 2015).

Similar to the photoresponse of scallop ciliary photoreceptors, the resact-induced alkalization of sea urchin sperm happens rapidly (30-100 ms) (Brenker *et al.*, 2012; Seifert *et al.*, 2015). More importantly, like resact, photorelease of cGMP elicits intracellular alkalization of sperm. cGMP directly activates the CNGK channel, which hyperpolarizes the cell; in turn, this hyperpolarization activates the voltage-dependent  $\text{Na}^+/\text{H}^+$  exchanger (Seifert *et al.*, 2015).

Intracellular pH regulates several  $\text{K}^+$  channels. Two-pore  $\text{K}^+$  channels form homo- and heterodimers (Levitz *et al.*, 2016) that are modulated by  $\text{pH}_i$  changes; either an increase or decrease in  $\text{pH}_i$  modulates different members of the two-pore  $\text{K}^+$  channel family (Noël *et al.*). For instance, intracellular acidification stimulates both Twik-related  $\text{K}^+$  channel 1 (TREK1) and TREK2, whereas intracellular alkalization activates the Twik-related arachidonic acid stimulated  $\text{K}^+$  channel (TRAAK) (Noël *et al.*; Maingret *et al.*, 1999; Kim *et al.*, 2001). Currents carried by TREK1 and TREK2 increase one-fold by one unit decrease in pH from  $\text{pH} = 7.4$ . In contrast, currents mediated by TRAAK channels increase 10-fold when  $\text{pH}_i$  increases from 7.4 to 8.8 (Levitz *et al.*, 2016).

A possible scenario in *P. irradians* ciliary photoreceptors might be that cGMP activates a  $\text{Na}^+/\text{H}^+$  exchanger (NHE), which produces an alkalization of  $\text{pH}_i$ . In turn, the alkalization activates two-pore  $\text{K}^+$  (TRAAK) channels which hyperpolarize the cell membrane due to  $\text{K}^+$  efflux. For this scenario to be plausible *P. irradians* ciliary photoreceptors need to express

---

NHEs and TRAAK channels. Surprisingly, the transcriptome of *P. irradians* retina reveal that both, a  $\text{Na}^+/\text{H}^+$  exchanger and several TRAAK channels are expressed in the scallop retina. Because there is only a partial sequence of *P. irradians* NHE, which contains a portion of the CNBD it is not possible to know whether the CNBD is conserved or not. However, the partial sequence reveals that the CNBD contains crucial amino acids for cyclic nucleotide binding, such as the glycine, glutamate and arginine homologous to G543, E544, R559 of the CNBD of the bovine CNGA1 channel (Kaupp et al., 1989; Kaupp and Seifert, 2002). Therefore, it might be possible that the NHE of *P. irradians* is modulated by cyclic nucleotides. In addition, TRAAK channels found in *P. irradians* retina are activated by alkalization of the  $\text{pH}_i$  (Noël et al.; Levitz et al., 2016). Further studies need to be performed to determine whether  $\text{Na}^+/\text{H}^+$  exchangers and two-pore  $\text{K}^+$  channels have a physiological role in *P. irradians* ciliary photoreceptors.

## **4.2 Functional role of classical CNG channels in *P. irradians* ciliary photoreceptors**

Like vertebrate rods and cones, ciliary photoreceptors of *P. irradians* use cGMP as second messenger (Yau and Hardie, 2009a). The light sensitivity of ciliary photoreceptors is more similar to cones than to rods (Gomez and Nasi, 1997a). For instance, scallop ciliary photoreceptors are less sensitive to light than their rhabdomic counterpart; quantum bumps, the electrical response to the absorption of a single photon cannot be resolved in *P. irradians* ciliary photoreceptors (Gomez and Nasi, 1997a). It is noteworthy that *P. irradians* ciliary photoreceptors have ciliary appendages analogous to the outer segments of rods and cones (MILLER, 1958; Gomez and Nasi, 1997b). Furthermore, it has been suggested that the

phototransduction machinery of *P. irradians* ciliary photoreceptors is located inside the cilia (Gomez & Nasi, 1995; Gomez and Nasi, 1997a).

Because of their pivotal role in phototransduction of rods and cones, vertebrate classical CNG-channels have been extensively characterized. Although classical CNG-channels are found in invertebrates, their function in invertebrate photoreceptors is less clear (Yau and Hardie, 2009). Bay scallops (*P. irradians*) express classical CNG channels in their retina. Although attempts to localize the expression site of CNG channels using RNA in-situ hybridization and immunohistochemistry were unsuccessful, the transcriptome of *P. irradians* retina suggest that two alpha and one beta CNG-channel subunits are expressed in the retina. Moreover, patch-clamp recordings combined with uncaging of cGMP in ciliary photoreceptors of *P. irradians* showed that cGMP activates the light-dependent current and a current reminiscent of classical CNG channels. In addition, patch-clamp recordings performed on ciliary photoreceptors showed that intracellular perfusion of 8-Br-cGMP activates a non-selective cation current, similar to classical CNG-channels, followed by a K<sup>+</sup>-selective current (Gomez and Nasi, 1995). This suggests that classical CNG channels and the light-dependent channels are both located in ciliary photoreceptors. Similarly to currents mediated by classical CNG-channels, *P. irradians* CNG current is gated by cGMP in a concentration-dependent manner (Figure 3.1.3.2), it is likely non-cation selective and it has no apparent voltage dependence (Figure 3.1.5.1). What is its function in photoreceptors?

Vertebrate CNG channels are the phototransduction channels in rods and cones; however, CNG channels of cones have an additional function than their rod counterparts (Rieke and Schwartz, 1994). CNG channels expand the dynamic range of cones by regulating, at least in part, the neurotransmitter (glutamate) release at synaptic sites (Rieke and Schwartz, 1994; Kaupp and Seifert, 2002). Light gradually hyperpolarizes rods and cones by up to 35 mV in amplitude. However, the whole response range is not effectively transmitted to postsynaptic

cells in the retina. In rods the output of the glutamatergic synapse is highly nonlinear. This phenomenon is mainly accounted by the voltage dependence of pre-synaptic  $\text{Ca}^{2+}$  channels (Attwell et al., 1987; Kaupp and Seifert, 2002). At the resting voltage in the dark (-35 mV), some of the  $\text{Ca}^{2+}$  channels are active, the continuous  $\text{Ca}^{2+}$  entry maintains a tonic release of the neurotransmitter glutamate from the synaptic terminal (Attwell et al., 1987). Because  $\text{Ca}^{2+}$  channels from rods have an activation threshold of approximately -45 mV; light hyperpolarizes rods to values more negative than -45 mV, which close voltage-gated  $\text{Ca}^{2+}$  channels and inhibit synaptic transmission (Barnes and Kelly, 2002). Conversely, synaptic transmission in cones continues as the light-induced voltage response grows to -70 mV (Korenbrodt and Rebrük, 2002). Although the overlap in the voltage range of  $\text{Ca}^{2+}$  channel-activation and the voltage range produced by light can explain signal clipping at the rod synapse, it fails to explain the broader voltage range over which synaptic transmission operates in cones (Kaupp and Seifert, 2002). This enigma has been solved to some extent by the discovery of CNG channels at the inner segment and synaptic terminal of cones (Rieke and Schwartz, 1994). Whereas the density of CNG channels in the inner segment is low, at the cone terminal these channels come in clusters (Savchenko et al., 1997). Experimental maneuvers that activate CNG channels induce glutamate release from cone synaptic terminals (Rieke and Schwartz, 1994; Savchenko et al., 1997). Therefore by providing a sustained  $\text{Ca}^{2+}$  influx at very negative voltages, CNG channels might extend the voltage range over which synaptic transmission operates.

Whether CNG channels are involved in the modulation of synaptic release of *P. irradians* ciliary photoreceptors in a similar manner as classical CNG channels at the inner segment of cones needs to be addressed in future work.

### **4.3 ERG channels of *P. irradians* ciliary photoreceptors**

ERG channels are voltage-gated  $K^+$  channels. Mammalian and invertebrate ERG channels differ in their gating properties. Mammalian ERG channels inactivate at depolarized voltages whereas invertebrate ERG channels do not inactivate (Gustina and Trudeau, 2013; Haitin et al., 2013). The structural cause of inactivation of ERG channels has been elucidated. ERG channels bearing an EAG domain at the N-terminus inactivate at depolarized potentials, whereas ERG channels lacking the EAG domain do not inactivate (Martinson et al., 2014). During my doctoral studies, I have studied the molecular localization and function of *P. irradians* ERG channel (PectERG channel). By using transcriptomics, I have molecularly cloned the alpha subunit of PectERG channel from *P. irradians* retina cDNA. Surprisingly, PectERG bears an EAG domain at the N-terminus suggesting that the channel is more closely related to mammalian rather than to other invertebrate ERG channels. Furthermore, using a specific probe against the 3' end of PectERG mRNA in *in-situ* RNA hybridization experiments performed in *P. irradians* eye-sections, I could show that PectERG channels are expressed in the ciliary photoreceptors of *P. irradians* (Section 3.4.1.2). This result was corroborated by immunohistochemical stainings performed on *P. irradians* eye sections using specific monoclonal antibodies against PectERG channels (Section 3.4.3); To test whether PectERG channels are functionally more similar to mammalian than to invertebrate ERG channels, I have used patch-clamp electrophysiology. I found that indeed, like mammalian ERG channels, PectERG channels inactivate at depolarized voltages. Although I have elucidated the molecular localization in *P. irradians* retina together with the functional properties of heterologously-expressed PectERG channels, the physiological role of PectERG channels on native ciliary photoreceptors of *P. irradians* is still unclear.

ERG channels mediate the rapidly (IKr) activating  $K^+$  current of the delayed-rectifying  $K^+$  current of ventricular myocytes (Sanguinetti and Jurkiewicz, 1990; Sanguinetti et al., 1995). Furthermore, in atrial and ventricular myocytes, ERG channels are involved in plateau

formation and repolarization of the action potential. Because of their inward-rectifier properties, ERG channels carry only a small current during the plateau phase of the ventricular action potential. Such a small current supports the formation of the plateau potential. As repolarization proceeds, ERG-mediated outward currents transiently increase due to fast recovery from inactivation and slow deactivation. The action of ERG channels combined with the activation of the classical cardiac inward rectifier repolarize the action potential (Schwarz and Bauer, 2004).

Although the functional role of ERG channels in the plateau and repolarization of the action potential has been well investigated, an additional functional role of ERG channels has been described. ERG currents are involved in setting the resting membrane potential in different cell types. Blockade of the ERG current using pharmacological agents depolarize the membrane potential. In oesophageal cells, ERG-channel blockade induces spontaneous contractions, presumably due to the opening of voltage-dependent  $\text{Ca}^{2+}$  channels (Akbarali et al., 1999). Furthermore, in gallbladder smooth-muscle cells, application of E-4031, an ERG channel blocker, depolarized muscle fibres, which increased contractility (Parr et al., 2003). Smooth-muscle cells express an ERG1 isoform (ERG1-sm) which lacks 101 amino acids at the C-terminal domain (Shoeb et al., 2003). In comparison to cardiac ERG1 channels, ERG1-sm channels contain an amino acid substitution in the S4 domain, which presumably is responsible for the shift in the voltage dependence of ERG1 activation to more negative membrane potentials (Shoeb et al., 2003). This shift in the voltage dependence of ERG1-sm channels might explain the contribution of the ERG1 current to the maintenance of the relatively negative resting potential of smooth muscle cells (Shoeb et al., 2003).

*P. irradians* ciliary photoreceptors have a relatively depolarized (-30 mV) resting membrane potential (McReynolds and Gorman, 1970; Gomez & Nasi, 1995). Furthermore, these photoreceptors have a Na<sup>+</sup> current active in the dark (Gorman and McReynolds, 1978). Because under physiological conditions the equilibrium potential of Na<sup>+</sup> is around 60 mV, there must be a mechanism that counteracts this Na<sup>+</sup> current to keep the photoreceptor membrane potential at -30 mV. Potassium ions have an equilibrium potential of -80 mV, which could be the ion counteracting the sodium current present in the dark. In fact, in the dark, the K<sup>+</sup> permeability is seven times larger than the Na<sup>+</sup> permeability (Gorman and McReynolds, 1978). Because the open probability of PectERG channels at -30 mV is 0.8 (Section 3.5.2), PectERG channels might be involved in the maintenance of the resting potential by counteracting the action of Na<sup>+</sup>. Further studies must be performed to determine whether this is the function of PectERG channels in ciliary photoreceptors of *P. irradians*.

#### 4.4 Ion channel properties of Slo3 and Slo1: which one underlies I<sub>Ksper</sub>

Although Slo1 and Slo3 channels belong to the same family of ion channels, they differ in several functional features. Slo1 channels are activated by intracellular Ca<sup>2+</sup>; upon binding, Ca<sup>2+</sup> induces a shift to the left of the Slo1 voltage activation curve (Marty, 1981; Pallotta et al., 1981; Díaz et al., 1998), which means that Slo1 channels have a higher probability of opening at negative potentials in the presence than in the absence of Ca<sup>2+</sup> (Cox et al., 1997; Díaz et al., 1998). Moreover, Ca<sup>2+</sup> binds to Slo1 with an affinity ranging from 1 to 10 μM (McManus and Magleby, 1991; Cox et al., 1997). In addition, Slo1 channels are activated by intracellular decrease in pH (increase in proton concentration) (Hou et al., 2008). Several Slo1 channel blockers have been reported. The scorpion toxins IbTX and CTX block Slo1 channels at nM concentrations; however, only IbTX specifically blocks Slo1 channels (Miller et al., n.d.; Galvez et al., 1990; Candia et al., 1992). Moreover, the mycotoxin Paxilline blocks Slo1 channels at nM concentrations (Knaus et al., 1994). Likewise, extracellular TEA and 4-aminopyridine (4-AP) block Slo1 channels (Tang et al., 2010).

On the other hand, Slo3 channels have been shown to be activated by alkalization (decrease in proton concentrations) and lack sensitivity to intracellular Ca<sup>2+</sup> (Navarro et al., 2007). However, we have shown that the human Slo3 channel is the exception to the rule (Brenker et al., 2014). Micromolar concentrations of intracellular Ca<sup>2+</sup> activate the human Slo3 channel. Moreover, the human Slo3 channel has a weaker pH-dependence compared to its mouse counterpart. Finally, Slo3 channels are blocked by quinidine, and the above-mentioned Slo1 channel blockers have no inhibitory effect on Slo3 channels (Tang et al., 2010). I<sub>Ksper</sub>, like hSlo3, is activated by Ca<sup>2+</sup> ions and only weakly activated by intracellular alkalization (Figure 3.6.4.1 & 3.6.4.2). This observation together with the remarkable similarity in the voltage dependence of hSlo3 and human I<sub>Ksper</sub> in the absence and presence of intracellular Ca<sup>2+</sup> (Figure 3.6.4.2) strongly suggests that hSlo3 channels mediate human I<sub>Ksper</sub>.

Additionally, the lack of inhibitory effect on hSlo3 and human  $I_{K_{sper}}$  of saturating concentrations of the specific Slo1-channel blocker IbTX, the progesterone inhibition of hSlo3 and human  $I_{K_{sper}}$ , and the lack of inhibition of Slo1 by progesterone support the notion that hSlo3 but not hSlo1 underlies human  $I_{K_{sper}}$ .

#### 4.5 What is the physiological role of Slo3 channels in human sperm?

Slo3 channel controls the membrane potential in mouse sperm (Navarro et al., 2007). Moreover, because Slo3 channel is  $K^+$  selective, its activation leads to a  $K^+$  efflux, which in turn hyperpolarizes sperm cells. The murine Slo3-channel is activated by alkalization of  $pH_i$  (Navarro et al., 2007; Zeng et al., 2011), a condition that has been shown to be essential for capacitation, hyperactivation, and acrosomal exocytosis of mouse sperm (Nishigaki et al., 2014). Alkalization activates the sperm-specific  $Ca^{2+}$  channel (CatSper) and the Slo3 channel (Carlson et al., 2003; Navarro et al., 2007). It has been hypothesized that due to the increase in the driving force of  $Ca^{2+}$ , the Slo3-induced hyperpolarization enhances the  $Ca^{2+}$  entry through CatSper channels (Navarro et al., 2007).

On the other hand, human Slo3 and CatSper channels are modestly activated by alkalization. Furthermore, Slo3 channel is activated by intracellular  $Ca^{2+}$ . We have proposed that  $Ca^{2+}$  entry through CatSper activates the Slo3 channel, which hyperpolarizes sperm causing CatSper channels to close (Brenker et al., 2014). This works under the premise that the intracellular  $Ca^{2+}$  concentration will be high enough to shift voltage dependence of activation of the hSlo3 channel to more hyperpolarized values. However there are other scenarios of physiological relevance, where the intracellular  $Ca^{2+}$  concentration may not be high enough to induce the shift in the voltage dependence of hSlo3 channels.

Prostasomes are calcium-containing, cholesterol-enriched vesicles that are produced by the prostate and contributed to the seminal plasma (Arienti et al., 2004). It has been proposed that upon fusion with sperm, prostasomes stimulates the acrosome reaction (Palmerini et al., 2003). Furthermore, after fusion with sperm, prostasomes caused an increase of intracellular  $\text{Ca}^{2+}$  from 130 nM to 300 nM; human Slo3 channels are not activated by these  $\text{Ca}^{2+}$  concentrations (Arienti et al., 2001; Brenker et al., 2014). In addition, it was shown that the fusion of prostasomes prior to incubation with progesterone potentiates the progesterone-induced  $\text{Ca}^{2+}$  response (Arienti et al., 2001). Of note, to promote fusion of prostasomes with sperm, acidic (pH 5–6) conditions are necessary (Arienti et al., 1997; Carlini et al., 1997). Remarkably, at the periovulatory period the vaginal pH of 4.5–6 is very similar to the pH needed for prostasome fusion; hence, a plausible scenario might be that upon deposit of the ejaculate into the acidic environment of the vagina, prostasomes fuse with sperm, which provides sperm with intracellular  $\text{Ca}^{2+}$  for their encounter with the progesterone-rich cumulus–oocyte–complex (De Jonge, 2005). We have shown that progesterone increases the  $\text{Ca}^{2+}$  concentration to levels sufficient to activate the hSlo3 channel (Brenker et al., 2014). Moreover, several reports have shown that CatSper channels are activated by submicromolar concentrations of progesterone, which are similar to physiological progesterone levels (Lishko et al., 2011; Strünker et al., 2011). It is, therefore, possible that the  $\text{Ca}^{2+}$  sensitivity of hSlo3 is tuned with the  $\text{Ca}^{2+}$  levels reached due to activation of CatSper channels. Thereby, in the absence of progesterone, hSlo3 channels would inhibit CatSper channels by curtailing the depolarization induced by the opening of CatSper channels. In contrast, because progesterone shifts the voltage dependence of CatSper to more hyperpolarized potentials, in the presence of progesterone, hSlo3 would act like a positive feedback by increasing the driving force for  $\text{Ca}^{2+}$ .



---

## 5 References

- Akbarali HI, Thatte H, He XD, Giles WR, Goyal RK (1999) Role of HERG-like K<sup>+</sup> currents in opossum esophageal circular smooth muscle. *Am J Physiol Cell Physiol* 277:C1284-1290.
- Alvarez L, Friedrich BM, Gompper G, Kaupp UB (2014) The computational sperm cell. *Trends Cell Biol* 24:198–207.
- Arendt D (2003) Evolution of eyes and photoreceptor cell types. *Int J Dev Biol* 47:563–571.
- Arendt D, Hausen H, Purschke G (2009) The “division of labour” model of eye evolution. *Philos Trans R Soc Lond B Biol Sci* 364:2809–2817.
- Arienti G, Nicolucci A, Santi F, Carlini E, Palmerini CA (2001) Progesterone-induced increase of sperm cytosolic calcium is enhanced by previous fusion of spermatozoa to prostasomes. *Cell Calcium* 30:222–227.
- Attwell D, Borges S, Wu SM, Wilson M (1987) Signal clipping by the rod output synapse. *Nature* 328:522–524.
- Barnes S, Kelly MEM (2002) Calcium channels at the photoreceptor synapse. *Adv Exp Med Biol* 514:465–476.
- Barnstable CJ, Wei J-Y (1995) Isolation and characterization of the alpha-subunit of the rat rod photoreceptor cGMP-gated cation channel. *J Mol Neurosci* 6:289–302.
- Bezánilla F (2008) Ion Channels: From Conductance to Structure. *Neuron* 60:456–468.
- Biel M, Michalakis S (2009) Cyclic nucleotide-gated channels. *Handb Exp Pharmacol* 191:111–136.
- Birnboim HC, Doly J (1979) A rapid alkaline extraction procedure for screening recombinant plasmid DNA. *Nucleic Acids Res* 7:1513–1523.
- Bok D, Young RW (1972) The renewal of diffusely distributed protein in the outer segments

- of rods and cones. *Vision Res* 12:161–IN5.
- Bönigk W, Bradley J, Müller F, Sesti F, Boekhoff I, Ronnett G V, Kaupp UB, Frings S (1999) The native rat olfactory cyclic nucleotide-gated channel is composed of three distinct subunits. *J Neurosci* 19:5332–5347.
- Bönigk W, Loogen A, Seifert R, Kashikar N, Klemm C, Krause E, Hagen V, Kremmer E, Strünker T, Kaupp UB (2009) An atypical CNG channel activated by a single cGMP molecule controls sperm chemotaxis. *Sci Signal* 2:ra68.
- Brelidze TI, Carlson AE, Sankaran B, Zagotta WN (2012) Structure of the carboxy-terminal region of a KCNH channel. *Nature* 481:530–533.
- Brelidze TI, Carlson AE, Zagotta WN (2009) Absence of direct cyclic nucleotide modulation of mEAG1 and hERG1 channels revealed with fluorescence and electrophysiological methods. *J Biol Chem* 284:27989–27997.
- Brenker C, Goodwin N, Weyand I, Kashikar ND, Naruse M, Krähling M, Müller A, Kaupp UB, Strünker T (2012) The CatSper channel: a polymodal chemosensor in human sperm. *EMBO J* 31:1654–1665.
- Brenker C, Zhou Y, Müller A, Echeverry FA, Trötschel C, Poetsch A, Xia X, Bönigk W, Lingle CJ, Kaupp UB, Strünker T (2014) The Ca<sup>2+</sup>-activated K<sup>+</sup> current of human sperm is mediated by Slo3. :1–19.
- Burns ME, Baylor DA (2001) ACTIVATION, DEACTIVATION, AND ADAPTATION IN VERTEBRATE PHOTORECEPTOR CELLS. *Annu Rev Neurosci* 24:779–805.
- Candia S, Garcia ML, Latorre R (1992) Mode of action of iberiotoxin, a potent blocker of the large conductance Ca(2+)-activated K<sup>+</sup> channel. *Biophys J* 63:583–590.
- Carlson AE et al. (2003) CatSper1 required for evoked Ca<sup>2+</sup> entry and control of flagellar function in sperm. *Proc Natl Acad Sci* 100:14864–14868.
- Catterall WA (1995) Structure and Function of Voltage-Gated Ion Channels. *Annu Rev*

- Biochem 64:493–531.
- Chen Z, Otto JC, Bergo MO, Young SG, Casey PJ (2000) The C-terminal polylysine region and methylation of K-Ras are critical for the interaction between K-Ras and microtubules. *J Biol Chem* 275:41251–41257.
- Colquhoun D (2014) An investigation of the false discovery rate and the misinterpretation of p-values. *R Soc Open Sci* 1.
- Cornwall MC, Gorman AL (1983) The cation selectivity and voltage dependence of the light-activated potassium conductance in scallop distal photoreceptor. *J Physiol* 340:287–305.
- Cox DH, Cui J, Aldrich RW (1997) Allosteric gating of a large conductance Ca-activated K<sup>+</sup> channel. *J Gen Physiol* 110:257–281.
- Cukkemane A, Seifert R, Kaupp UB (2011) Cooperative and uncooperative cyclic-nucleotide-gated ion channels. *Trends Biochem Sci* 36:55–64.
- Dai G, Peng C, Liu C, Varnum MD (2013) Two structural components in CNGA3 support regulation of cone CNG channels by phosphoinositides. *J Gen Physiol* 141:413–430.
- De Jonge C (2005) Biological basis for human capacitation. *Hum Reprod Update* 11:205–214.
- del Pilar Gomez M, Nasi E (2005) Calcium-independent, cGMP-mediated light adaptation in invertebrate ciliary photoreceptors. *J Neurosci* 25:2042–2049.
- Dhallan RS, Macke JP, Eddy RL, Shows TB, Reed RR, Yau KW, Nathans J (1992) Human rod photoreceptor cGMP-gated channel: amino acid sequence, gene structure, and functional expression. *J Neurosci* 12:3248–3256.
- Dhallan RS, Yau K-W, Schrader KA, Reed RR (1990) Primary structure and functional expression of a cyclic nucleotide-activated channel from olfactory neurons. *Nature* 347:184–187.
- Díaz L, Meera P, Amigo J, Stefani E, Alvarez O, Toro L, Latorre R (1998) Role of the S4

- segment in a voltage-dependent calcium-sensitive potassium (hSlo) channel. *J Biol Chem* 273:32430–32436.
- Doerner JF et al. (2015) Ion channels and calcium signaling in motile cilia. *Elife* 4:130052.
- Finn JT, Solessio EC, Yau K-W (1997) A cGMP-gated cation channel in depolarizing photoreceptors of the lizard parietal eye. *Nature* 385:815–819.
- Galvez A, Gimenez-Gallego G, Reuben JP, Roy-Contancin L, Feigenbaum P, Kaczorowski GJ, Garcia ML (1990) Purification and characterization of a unique, potent, peptidyl probe for the high conductance calcium-activated potassium channel from venom of the scorpion *Buthus tamulus*. *J Biol Chem* 265:11083–11090.
- Gauss R, Seifert R, Kaupp UB (1998) Molecular identification of a hyperpolarization-activated channel in sea urchin sperm. *Nature* 393:583–587.
- Gerstner A, Zong X, Hofmann F, Biel M (2000) Molecular cloning and functional characterization of a new modulatory cyclic nucleotide-gated channel subunit from mouse retina. *J Neurosci* 20:1324–1332.
- Gimenez-Gallego G, Navia MA, Reuben JP, Katz GM, Kaczorowski GJ, Garcia ML (1988) Purification, sequence, and model structure of charybdotoxin, a potent selective inhibitor of calcium-activated potassium channels. *Proc Natl Acad Sci U S A* 85:3329–3333.
- Gomez M d. P, Espinosa L, Ramirez N, Nasi E (2011) Arrestin in Ciliary Invertebrate Photoreceptors: Molecular Identification and Functional Analysis In Vivo. *J Neurosci* 31:1811–1819.
- Gomez MD, Nasi E (1994a) Blockage of the light-sensitive conductance in hyperpolarizing photoreceptors of the scallop. Effects of tetraethylammonium and 4-aminopyridine. *J Gen Physiol* 104:487–505.
- Gomez MDP, Nasi E (2005) On the gating mechanisms of the light-dependent conductance in Pecten hyperpolarizing photoreceptors: does light remove inactivation in voltage-

- dependent K channels? *J Gen Physiol* 125:455–464.
- Gomez MP, Nasi E (1994b) The light-sensitive conductance of hyperpolarizing invertebrate photoreceptors: a patch-clamp study. *J Gen Physiol* 103:939–956.
- Gomez MP, Nasi E (1997a) Light adaptation in Pecten hyperpolarizing photoreceptors. Insensitivity to calcium manipulations. *J Gen Physiol* 109:371–384.
- Gomez MP, Nasi E (1997b) Antagonists of the cGMP-gated conductance of vertebrate rods block the photocurrent in scallop ciliary photoreceptors. *J Physiol* 500 ( Pt 2:367–378.
- Gomez MP, Nasi E (2000) Light transduction in invertebrate hyperpolarizing photoreceptors: possible involvement of a Go-regulated guanylate cyclase. *J Neurosci* 20:5254–5263.
- Gomez & Nasi (1995) Activation of light-dependent K<sup>+</sup> channels in ciliary invertebrate photoreceptors involves cGMP but not the IP<sub>3</sub>/Ca<sup>2+</sup> cascade. *Neuron* 15:607–618.
- Gorman AL, McReynolds JS (1969) Hyperpolarizing and depolarizing receptor potentials in the scallop eye. *Science* 165:309–310.
- Gorman AL, McReynolds JS (1978) Ionic effects on the membrane potential of hyperpolarizing photoreceptors in scallop retina. *J Physiol* 275:345–355.
- Gustina AS, Trudeau MC (2013) The eag domain regulates hERG channel inactivation gating via a direct interaction. *J Gen Physiol* 141:229–241.
- Hagen V, Dekowski B, Nache V, Schmidt R, Geißler D, Lorenz D, Eichhorst J, Keller S, Kaneko H, Benndorf K, Wiesner B (2005) Coumarinylmethyl esters for ultrafast release of high concentrations of cyclic nucleotides upon one- and two-photon photolysis. *Angew Chemie - Int Ed* 44:7887–7891.
- Haimo LT, Rosenbaum JL (1981) Cilia, flagella, and microtubules. *J Cell Biol* 91.
- Haitin Y, Carlson AE, Zagotta WN (2013) The structural mechanism of KCNH-channel regulation by the eag domain. *Nature* 501:444–448.
- Hardie RC, Juusola M (2015) Phototransduction in *Drosophila*. *Curr Opin Neurobiol* 34:37–

45.

- Hartzell C, Putzier I, Arreola J (2005) Calcium-Activated Chloride Channels. *Annu Rev Physiol* 67:719–758.
- Heginbotham L, Abramson T, MacKinnon R (1992) A functional connection between the pores of distantly related ion channels as revealed by mutant K<sup>+</sup> channels. *Science* 258:1152–1155.
- Heginbotham L, Lu Z, Abramson T, MacKinnon R (1994) Mutations in the K<sup>+</sup> channel signature sequence. *Biophys J* 66:1061–1067.
- Heikaus CC, Pandit J, Klevit RE (2009) Cyclic nucleotide binding GAF domains from phosphodiesterases: structural and mechanistic insights. *Structure* 17:1551–1557.
- Hille B (2001) Ion channels of excitable membranes.
- Hou S, Xu R, Heinemann SH, Hoshi T (2008) Reciprocal regulation of the Ca<sup>2+</sup> and H<sup>+</sup> sensitivity in the SLO1 BK channel conferred by the RCK1 domain. *Nat Struct Mol Biol* 15:403–410.
- Huang J, Liu C-H, Hughes SA, Postma M, Schwiening CJ, Hardie RC (2010) Activation of TRP channels by protons and phosphoinositide depletion in *Drosophila* photoreceptors. *Curr Biol* 20:189–197.
- Jan LY, Jan YN (2012) Voltage-gated potassium channels and the diversity of electrical signalling. *J Physiol* 590:2591–2599.
- Jiang Y, Ruta V, Chen J, Lee A, MacKinnon R (2003) The principle of gating charge movement in a voltage-dependent K<sup>+</sup> channel. *Nature* 423:42–48.
- Kaupp UB, Niidome T, Tanabe T, Terada S, Bönigk W, Stühmer W, Cook NJ, Kangawa K, Matsuo H, Hirose T (1989) Primary structure and functional expression from complementary DNA of the rod photoreceptor cyclic GMP-gated channel. *Nature* 342:762–766.

- Kaupp UB, Seifert R (2002) Cyclic Nucleotide-Gated Ion Channels. *Physiol Rev* 82:769–824.
- Kaupp UB, Solzin J, Hildebrand E, Brown JE, Helbig A, Hagen V, Beyermann M, Pampaloni F, Weyand I (2003) The signal flow and motor response controlling chemotaxis of sea urchin sperm. *Nat Cell Biol* 5:109–117.
- Khanna H (2015) Photoreceptor Sensory Cilium: Traversing the Ciliary Gate. *Cells* 4:674–686.
- Kim Y, Gnatenco C, Bang H, Kim D (2001) Localization of TREK-2 K<sup>+</sup> channel domains that regulate channel kinetics and sensitivity to pressure, fatty acids and pH. *Pflügers Arch Eur J Physiol* 442:952–960.
- Knaus HG, McManus OB, Lee SH, Schmalhofer WA, Garcia-Calvo M, Helms LM, Sanchez M, Giangiacomo K, Reuben JP, Smith AB (1994) Tremorgenic indole alkaloids potently inhibit smooth muscle high-conductance calcium-activated potassium channels. *Biochemistry* 33:5819–5828.
- Kojima D, Terakita A, Ishikawa T, Tsukahara Y, Maeda A, Shichida Y (1997) A novel G<sub>o</sub>-mediated phototransduction cascade in scallop visual cells. *J Biol Chem* 272:22979–22982.
- Korenbrod JI, Rebrik TI (2002) Tuning outer segment Ca<sup>2+</sup> homeostasis to phototransduction in rods and cones. *Adv Exp Med Biol* 514:179–203.
- Land MF (1965) Image formation by a concave reflector in the eye of the scallop, *Pecten maximus*. *J Physiol* 179:138–153.
- Levitz J, Royal P, Comoglio Y, Wdziekonski B, Schaub S, Clemens DM, Isacoff EY, Sandoz G (2016) Heterodimerization within the TREK channel subfamily produces a diverse family of highly regulated potassium channels. *Proc Natl Acad Sci U S A*:1522459113-.
- Liman ER, Buck LB (1994) A second subunit of the olfactory cyclic nucleotide-gated

- channel confers high sensitivity to cAMP. *Neuron* 13:611–621.
- Lishko P V, Botchkina IL, Kirichok Y (2011) Progesterone activates the principal Ca<sup>2+</sup> channel of human sperm. *Nature* 471:387–391.
- Lishko P V, Kirichok Y, Ren D, Navarro B, Chung J-J, Clapham DE (2012) The control of male fertility by spermatozoan ion channels. *Annu Rev Physiol* 74:453–475.
- Loogen A (2009) Klonierung und Charakterisierung eines ungewöhnlichen K<sup>+</sup>-selektiven zyklisch Nukleotid-gesteuerten Ionenkanals aus Seeigelspermien.
- MacKinnon R (2003) Potassium channels. *FEBS Lett* 555:62–65.
- Maingret F, Patel AJ, Lesage F, Lazdunski M, Honoré E (1999) Mechano- or acid stimulation, two interactive modes of activation of the TREK-1 potassium channel. *J Biol Chem* 274:26691–26696.
- Mandel M, Higa A (1970) Calcium-dependent bacteriophage DNA infection. *J Mol Biol* 53:159–162.
- Mangmool S, Kurose H (2011) G(i/o) protein-dependent and -independent actions of Pertussis Toxin (PTX). *Toxins (Basel)* 3:884–899.
- Mannowetz N, Naidoo NM, Choo SAS, Smith JF, Lishko P V. (2013) Slo1 is the principal potassium channel of human spermatozoa. *Elife* 2:e01009.
- Martinson AS, van Rossum DB, Diatta FH, Layden MJ, Rhodes SA, Martindale MQ, Jegla T (2014) Functional evolution of Erg potassium channel gating reveals an ancient origin for IKr. *Proc Natl Acad Sci U S A* 111:5712–5717.
- Marty A (1981) Ca-dependent K channels with large unitary conductance in chromaffin cell membranes. *Nature* 291:497–500.
- Mathé C, Sagot M-F, Schiex T, Rouzé P (2002) Current methods of gene prediction, their strengths and weaknesses. *Nucleic Acids Res* 30:4103–4117.
- McManus OB, Magleby KL (1991) Accounting for the Ca(2+)-dependent kinetics of single

- large-conductance  $\text{Ca}^{2+}$ -activated  $\text{K}^+$  channels in rat skeletal muscle. *J Physiol* 443:739–777.
- McReynolds JS, Gorman AL (1970) Photoreceptor potentials of opposite polarity in the eye of the scallop, *Pecten irradians*. *J Gen Physiol* 56:376–391.
- McReynolds JS, Gorman AL (1974) Ionic basis of hyperpolarizing receptor potential in scallop eye: increase in permeability to potassium ions. *Science* 183:658–659.
- Meinicke P (2009) UFO: a web server for ultra-fast functional profiling of whole genome protein sequences. *BMC Genomics* 10:409.
- Miki K, Clapham DE (2013) Rheotaxis guides mammalian sperm. *Curr Biol* 23:443–452.
- Miller C, Moczydlowski E, Latorre R, Phillips M (n.d.) Charybdotoxin, a protein inhibitor of single  $\text{Ca}^{2+}$ -activated  $\text{K}^+$  channels from mammalian skeletal muscle. *Nature* 313:316–318.
- MILLER WH (1958) Derivatives of cilia in the distal sense cells of the retina of *Pecten*. *J Biophys Biochem Cytol* 4:227–228.
- Mullis K, Faloona F, Scharf S, Saiki R, Horn G, Erlich H (1986) Specific enzymatic amplification of DNA in vitro: the polymerase chain reaction. *Cold Spring Harb Symp Quant Biol* 51 Pt 1:263–273.
- Navarro B, Kirichok Y, Clapham DE (2007) KSper, a pH-sensitive  $\text{K}^+$  current that controls sperm membrane potential. *Proc Natl Acad Sci* 104:7688–7692.
- Nishigaki T, José O, González-Cota AL, Romero F, Treviño CL, Darszon A (2014) Intracellular pH in sperm physiology. *Biochem Biophys Res Commun* 450:1149–1158.
- Noël J, Sandoz G, Lesage F Molecular regulations governing TREK and TRAAK channel functions. *Channels (Austin)* 5:402–409.
- Pallotta BS, Magleby KL, Barrett JN (1981) Single channel recordings of  $\text{Ca}^{2+}$ -activated  $\text{K}^+$  currents in rat muscle cell culture. *Nature* 293:471–474.

- Palmerini CA, Saccardi C, Carlini E, Fabiani R, Arienti G (2003) Fusion of prostasomes to human spermatozoa stimulates the acrosome reaction. *Fertil Steril* 80:1181–1184.
- Parr E, Pozo MJ, Horowitz B, Nelson MT, Mawe GM (2003) ERG K<sup>+</sup> channels modulate the electrical and contractile activities of gallbladder smooth muscle. *Am J Physiol Gastrointest Liver Physiol* 284:G392-8.
- Pichlo M et al. (2014) High density and ligand affinity confer ultrasensitive signal detection by a guanylyl cyclase chemoreceptor. *J Cell Biol* 206:541–557.
- Picones A, Korenbrot JI (1995) Permeability and interaction of Ca<sup>2+</sup> with cGMP-gated ion channels differ in retinal rod and cone photoreceptors. *Biophys J* 69:120–127.
- Pittler SJ, Lee AK, Altherr MR, Howard TA, Seldin MF, Hurwitz RL, Wasmuth JJ, Baehr W (1992) Primary structure and chromosomal localization of human and mouse rod photoreceptor cGMP-gated cation channel. *J Biol Chem* 267:6257–6262.
- Rieke F, Schwartz EA (1994) A cGMP-gated current can control exocytosis at cone synapses. *Neuron* 13:863–873.
- Robinson RB, Siegelbaum SA (2003) Hyperpolarization-activated cation currents: from molecules to physiological function. *Annu Rev Physiol* 65:453–480.
- Sanguinetti MC, Jiang C, Curran ME, Keating MT (1995) A mechanistic link between an inherited and an acquired cardiac arrhythmia: HERG encodes the IK<sub>r</sub> potassium channel. *Cell* 81:299–307.
- Sanguinetti MC, Jurkiewicz NK (1990) Two components of cardiac delayed rectifier K<sup>+</sup> current. Differential sensitivity to block by class III antiarrhythmic agents. *J Gen Physiol* 96:195–215.
- Savchenko A, Barnes S, Kramer RH (1997) Cyclic-nucleotide-gated channels mediate synaptic feedback by nitric oxide. *Nature* 390:694–698.
- Schreiber M, Wei A, Yuan A, Gaut J, Saito M, Salkoff L (1998) Slo3, a novel pH-sensitive

- K<sup>+</sup> channel from mammalian spermatocytes. *J Biol Chem* 273:3509–3516.
- Schwarz JR, Bauer CK (2004) Functions of erg K<sup>+</sup> channels in excitable cells. *J Cell Mol Med* 8:22–30.
- Seifert R, Flick M, Bönigk W, Alvarez L, Trötschel C, Poetsch A, Müller A, Goodwin N, Pelzer P, Kashikar ND, Kremmer E, Jikeli J, Timmermann B, Kuhl H, Fridman D, Windler F, Kaupp UB, Strünker T (2015) The CatSper channel controls chemosensation in sea urchin sperm. *EMBO J* 34:379–392.
- Shoeb F, Malykhina AP, Akbarali HI (2003) Cloning and functional characterization of the smooth muscle ether-a-go-go-related gene K<sup>+</sup> channel. Potential role of a conserved amino acid substitution in the S4 region. *J Biol Chem* 278:2503–2514.
- Smith PL, Baukrowitz T, Yellen G (1996) The inward rectification mechanism of the HERG cardiac potassium channel. *Nature* 379:833–836.
- Solzin J, Helbig A, Van Q, Brown JE, Hildebrand E, Weyand I, Kaupp UB (2004) Revisiting the role of H<sup>+</sup> in chemotactic signaling of sperm. *J Gen Physiol* 124:115–124.
- Strünker T, Alvarez L, Kaupp UB (2015) At the physical limit - chemosensation in sperm. *Curr Opin Neurobiol* 34:110–116.
- Strünker T, Goodwin N, Brenker C, Kashikar ND, Weyand I, Seifert R, Kaupp UB (2011) The CatSper channel mediates progesterone-induced Ca<sup>2+</sup> influx in human sperm. *Nature* 471:382–386.
- Strünker T, Weyand I, Bönigk W, Van Q, Loogen A, Brown JE, Kashikar N, Hagen V, Krause E, Kaupp UB (2006) A K<sup>+</sup>-selective cGMP-gated ion channel controls chemosensation of sperm. *Nat Cell Biol* 8:1149–1154.
- Tang Q-Y, Zhang Z, Xia X-M, Lingle CJ (2010) Block of mouse Slo1 and Slo3 K<sup>+</sup> channels by CTX, IbTX, TEA, 4-AP and quinidine. *Channels (Austin)* 4:22–41.
- Towbin H, Staehelin T, Gordon J (1979) Electrophoretic transfer of proteins from

- 
- polyacrylamide gels to nitrocellulose sheets: procedure and some applications. *Proc Natl Acad Sci U S A* 76:4350–4354.
- Trudeau MC, Warmke JW, Ganetzky B, Robertson GA (1995) HERG, a human inward rectifier in the voltage-gated potassium channel family. *Science* 269:92–95.
- Warmke J, Drysdale R, Ganetzky B (1991) A distinct potassium channel polypeptide encoded by the *Drosophila* eag locus. *Science* 252:1560–1562.
- Weitz D, Ficek N, Kremmer E, Bauer PJ, Kaupp UB (2002) Subunit stoichiometry of the CNG channel of rod photoreceptors. *Neuron* 36:881–889.
- Yang C, Zeng X-H, Zhou Y, Xia X-M, Lingle CJ (2011) LRRC52 (leucine-rich-repeat-containing protein 52), a testis-specific auxiliary subunit of the alkalization-activated Slo3 channel. *Proc Natl Acad Sci U S A* 108:19419–19424.
- Yau KW, Hardie RC (2009a) Phototransduction Motifs and Variations. *Cell* 139:246–264.
- Yau K-W, Hardie RC (2009b) Phototransduction motifs and variations. *Cell* 139:246–264.
- Young RW (1967) The renewal of photoreceptor cell outer segments. *J Cell Biol* 33:61–72.
- Zeng X-H, Yang C, Kim ST, Lingle CJ, Xia X-M (2011) Deletion of the Slo3 gene abolishes alkalization-activated K<sup>+</sup> current in mouse spermatozoa. *Proc Natl Acad Sci U S A* 108:5879–5884.
- Zheng J, Trudeau MC, Zagotta WN (2002) Rod cyclic nucleotide-gated channels have a stoichiometry of three CNGA1 subunits and one CNGB1 subunit. *Neuron* 36:891–896.
- Zhong H, Molday LL, Molday RS, Yau K-W (2002) The heteromeric cyclic nucleotide-gated channel adopts a 3A:1B stoichiometry. *Nature* 420:193–198.

## 6 Appendix

**Table 6.1:** List of contigs corresponding to the putative K<sup>+</sup> channels found on *P. irradians* retina transcriptome

<b>Name Transcriptome</b>	<b>Putative function</b>
contig05186	voltage-gated potassium channel
contig05549	Inward rectifier potassium channel
contig07204	voltage-gated potassium channel
contig09613	Girk2 potassium channel
contig12007	voltage-gated potassium channel
contig14505	Inward rectifier potassium channel
contig16762	voltage-gated potassium channel
contig17187	KCNQ voltage-gated potassium channel
contig17606	voltage-gated potassium channel
contig17622	Calcium-activated SK potassium channel
contig18241	voltage-gated potassium
contig18597	Shaw-related voltage-gated potassium
contig18871	voltage-gated potassium channel
contig21848	voltage-gated potassium channel
contig22584	shaker related delayed rectifier potassium channel
contig26719	Shaw-related voltage-gated potassium
contig30583	potassium inwardly-rectifying channel
contig31721	Shaw-related voltage-gated potassium
contig32394	Kv2 voltage-gated potassium channel
contig32865	KCNQ voltage-gated potassium channel

```

      10      20      30      40      50      60      70      80
PectERG  MP-VRRGHVAPPNIFIDTIIRKPFDEQNRKRFVIANA-----QVETCPILFCNDGFCELTGSSRAEVIKSCICDFLHGP
PectEAG  MPGARRGLVAPQNTFLENIIRRSQGHSFLLANA-----RIVEYPIVVCNDGFCKLSGYNRAEVMOKSCTCSFMYGD
PectHCN  MANIRNPSSQPLIDI SEHDRPVSYSSDEESSNQNSPYRRAPEPPRNTPPVPHRSKGVSEATSSVVESFAS TLQQVHLS P
PectCNG1 -----MFHPVKRLNSRTVPVSRRTWSNSSSKRS-----EELEDDDDVDDA---KLEDTTTRRNVKLMDSHRVSDTA
PectCNG2 -----MATSPPTTSKPPDKVNHKSFPDDEVEVIEN-----GGLSPQLSLRTD---DDTCSEIIRIEKQSYDEPQQVSA
PectCNGb -----

      90     100     110     120     130     140     150     160
PectERG  LTSSFGILQIKDALQGSEEKQVEILYRKGSGKFLCSVLTAPVKNEQGEVIMFIINYEDI SEHATAISSKPENNVKIKTK
PectEAG  LTDQDVLKIEQSFEGVEQEQVEILLYKKNRTPPLWLLLVHAPIKNEKQVVLFLCTFFKDI TALK-----
PectHCN  KITRSDSVKFSKANGSAGRKSSHPIGSSQTTPKPSRRVPSLKLKRMNLGVNSDKAEGTMPCLPKPCPNRPTN-----
PectCNG1 VHDGHSPLQLRKLWSG-----IEGTGNHT-----
PectCNG2 LERIAITLQVIKSWASGRWRSRTLPQRPDSFL-----
PectCNGb -----NYP-----

      170     180     190     200     210     220     230     240
PectERG  SGRI GSFKLR LPS IRRDFNRFKSCGMDKSPDENPPIPEEA VPLNSLPYLDNEI PPNSPIFRYKKTGSDI PAPNSRTGAY
PectEAG  -----QPIDEEGG-----KAGMSKFARLARS-----
PectHCN  -----
PectCNG1 -----
PectCNG2 -----
PectCNGb -----

      250     260     270     280     290     300     310     320
PectERG  IRRASSMEGLEAEQLTPTSGTGNHVKSNCI NQTCSDSELAKHRTKQLTDSG NLLADSLQVGWTPDRDGAMP GSGKGVFL
PectEAG  -----VTRNKSTLLQFSS-----HI-----
PectHCN  -----PSITITIE SDEESIYSDYLS PDMNYNNDIKVHFVGD EQSLYGT PK EELLPGSGET
PectCNG1 -----
PectCNG2 -----
PectCNGb -----

      330     340     350     360     370     380     390     400
PectERG  PNVQNMKHN VSEKVAQGSCHDGRSSAAAEVLSLGADVLPEYK LQSPRIHRLTILHYS PFAVWDWI LLLLVITAIFFTP
PectEAG  PNTK-----FDNSKPSQLANMMNLNADVLPQYRLEAPKTPPHIILHYCL EKTIDWKMILTLTFYTA VIVP
PectHCN  SSTDQKTSPTS YLKEQFISFFQPSDKLAMKLFGNRNSLMREKMRHRKRVGNWVIHPCSNRFYWDLFMLVLLIANLIIILP
PectCNG1 -----SDMINTSKSPQNETMEALHTNLSTR-----VLDPDGNWCYNWMIIVTMAALYNIVVII
PectCNG2 -----ERVAMGGQDTKDGHGDRKARKISDIRYWKGFVVDPSQRFYRRLVVISISVLVAVVIFII
PectCNGb -----PGLNIPCSI PR-----KLEPQSKLYMTLFIIVT PCFMVNAWVIVP

      410     420     430     440     450     460     470     480
PectERG  YAAAFLLSEENSRNRDGNKSI EYRYQNPMITIDLI VDI MPFIIDILNFRRTTYVNKND-----EVVSHPGK
PectEAG  YNTAFRN-----KTMDQVPLIVDSDIVDVVFSW- ISYLFPPYD ICRPSG-----EII SDHKI
PectHCN  VAISFFNDLDS-----THWIVVNCISDI VVFLDIVINFRGTGFQISHDDQENVNSVILNDFADEI ILDPKL
PectCNG1  LRLAFAEMRE-----HVL PSTLFTV D LGDAVYI IDIVVQS-RVSHYEDG-----CI VSDVHN
PectCNG2  ARSVFWELQK-----SYLS--LWLADYLS DALYI IDMGISF-RTGYLEEG-----LIVR DATK
PectCNGb  LRGVFPYQNG-----SNLIY--WLI CDYTCDAIYHLDIMLVKPHLTYLNSG-----IVETD PKL

      490     500     510     520     530     540     550     560
PectERG  IAVHYFKG-WFLIDVVAIIPFDLL-LFGSET-----DETATLIGLKRARLLR LRV
PectEAG  IRNHYLRS-WFVIDLLSCLPYDFVNAFYVD-----DGI STLFSALRVVRLRLGRV
PectHCN  IARHYVKS-WFFD LISSIPMDYIFLMWDAEADFNQLFHAGTTASMG PSSYWQGRALRMLRLAKLLSLIRLRLSRLVRY
PectCNG1  VSERVWRTRFKIDMLSI LPLHTVIFICQGM LRCINVSIG-----IDQYRFYIAITRLRDLKARTVSEF
PectCNG2  LRRHYMTSTMFKTDILSIIPD LFYFLIG-----LDKPELRFNRIRFRNLEF
PectCNGb  MRNHYMQRMFKFLVLSLPLD LFYMLG-----VVPWFRLPRLRFKIQTFWEF

      570     580     590     600     610     620     630     640
PectERG  VRKIDRYSEYG-----AAVLLDLMATPALIAWLA CIWYAGNV ERPHLPPPKIGWLDQLA
PectEAG  VRKIDHYLEYG-----AAMIVLILLVFILFAWFA CIWYSTGLTELQSG--LEYCGLSTLA
PectHCN  VQDFEEMAKNFEGSPCFAMCGRRRRPGLAFAGKFMRI FNLLCLMFLLGWRNGCLQPLIPMLQ EYPD---DQVMSIEG
PectCNG1  FDIIDSRTSNPN-----FVRAKRLTYLYLIVHWIGCLYYM VSLYEGIGS-----TEWYASSG
PectCNG2  FDRFATRTSFTN-----MIRILNIVLYIILIIHWNACIYPAISNSIGFGS---DIWYYPNV
PectCNGb  YQRIDQAVKSAH-----VLRIRIKMTYMLLLILETCEYYAVSVYEG-----

```

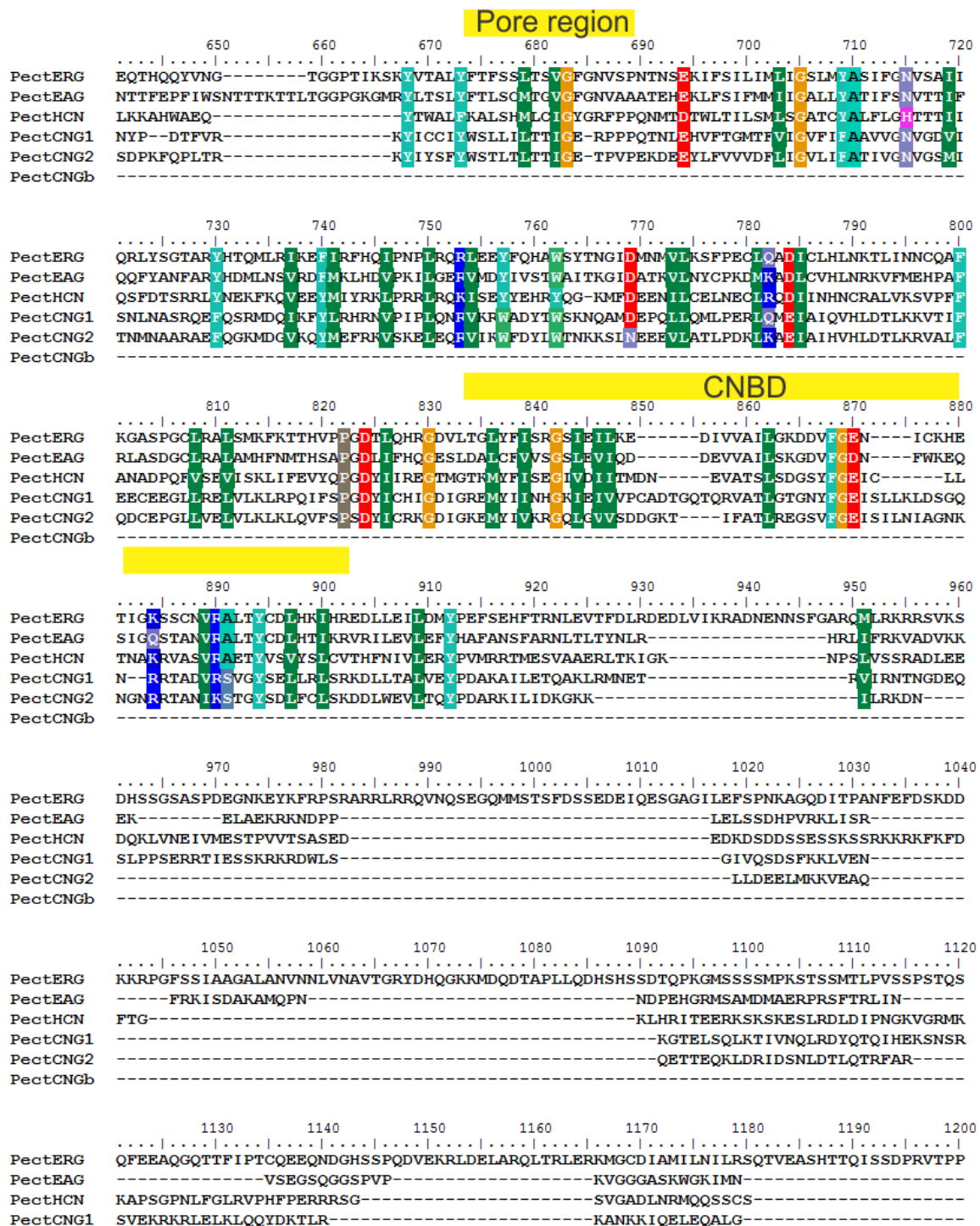


**Figure 6.1:** Alignment of *P. irradians* putative cNMP-modulated channels. PectERG: putative EAG-related  $K^+$  channel. PectEAG: Putative EAG  $K^+$ -channel. PectHCN: Putative HCN channel. PectCNG1-2: putative CNG channel  $\alpha$ -subunits; PectCNG-b: Putative CNG-channel  $\beta$ -subunit.

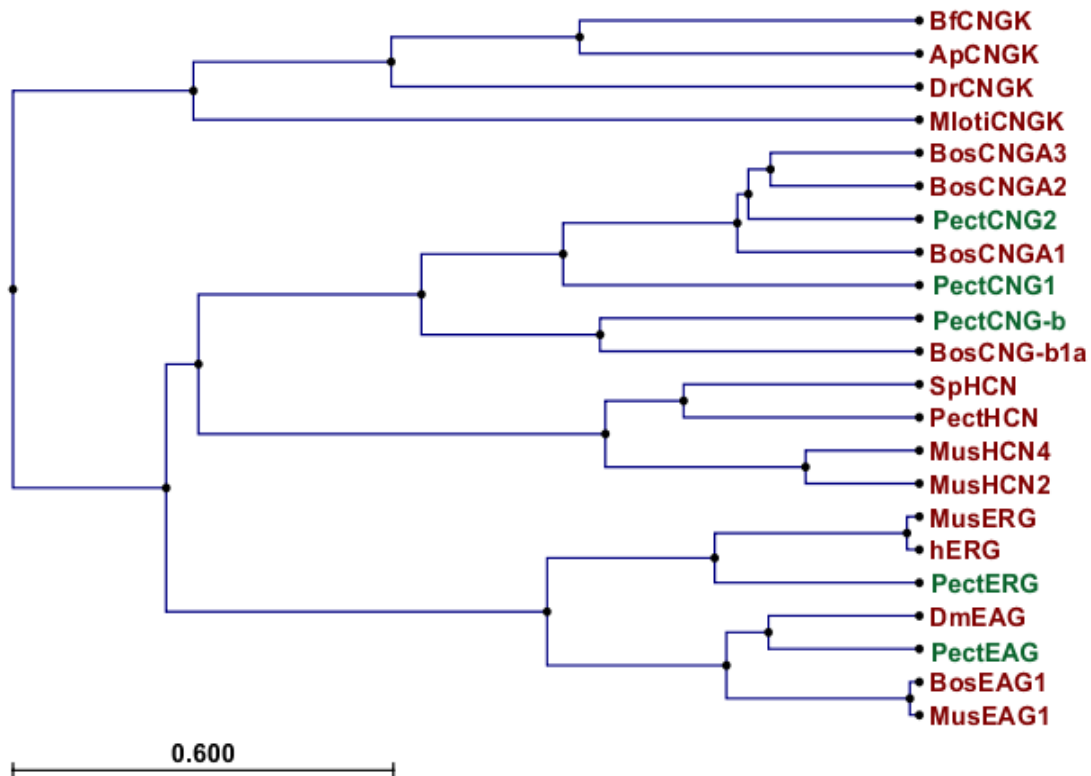


**Figure 6.2:** Phylogenetic tree of relevant ion channels. BfCNGK: Putative amphioxus CNGK channel; ApCNGK: CNGK channel from sea urchin (*Arbacia punctulata*); DrCNGK: Putative zebrafish CNGK channel; MlotiCNGK: *Mesorhizobium loti* CNGK channel; BosCNGA1: cattle rod CNG-channel  $\alpha$ -subunit; BosCNGA2: cattle olfactory CNG-channel  $\alpha$ -subunit; BosCNGA3: cattle cone CNG-channel  $\alpha$ -subunit; PectCNG1-2: putative scallop (*P. irradians*) CNG channel  $\alpha$ -subunits; PectCNG-b: Putative scallop (*P. irradians*) CNG-channel  $\beta$ -subunit; BosCNG-b1a: cattle CNG-channel  $\beta$ -subunit isoform a; SpHCN: Sea urchin HCN channel (*Strongylocentrotus purpuratus*); PectHCN: Putative scallop (*P. irradians*) HCN channel; MusHCN 2 & 4: Murine HCN channel isoforms 2 & 4; MusERG: Murine ERG  $K^+$ -channel; hERG: Human ERG  $K^+$  channel; PectERG: scallop (*P. irradians*) ERG  $K^+$ -channel; DmEAG1: *Drosophila melanogaster* EAG  $K^+$ -channel; PectEAG: Putative scallop (*P. irradians*) EAG  $K^+$ -channel; BosEAG1: Cattle EAG  $K^+$ -channel; MusEAG1: Murine EAG  $K^+$ -channel.

MPVRRGHVAPPNIFIDTIIRKFDEQNRKFVIANAQVETCPILFCNDGFCELTGSSRAEVI -60  
 QKSCICDFLHGPLTSSFGILQIKDALQGSEEQVEILYYRKDGSKFLCSVLTAPVKNEQG -120  
 EVIMFIINYEDISEHATTAISSKPENNVKITKSGRIGSFKLRLPSIRRDFNRFKSCGMDK -180  
 SPDPENPPPIPEEAVPLNSLPYLDNEIPPNSPIFRYKKTGSDIPAPNSRTGAYIRRASSME -240  
 GLEAEQLTPTSGTGNHVKSNCINQTCSDSELAKHRTKQLTDSSGNLLADSLQVGWTPDRD -300  
 GAMPGSGKGVFLPNVQNMKHNVSEKVAQGSCHDGRSSSSAAEVLSLGADVLPEYKQLQSPR -360  
 IHRLTILHYS PFKAVWDWIILLVVIYTAIFTPYAAAFLLSEENSRNRDGNKSIEVRYQNP -420  
 MTIIDLIVDIMFIIDILINFR'TTYVNKNDEVVSHPGKIAVHYFKGWFLIDVVAIIPFDLL -480  
 LFGSETDETATLIGLLK**TARLLRLVRVVRKLD**RYSEYGAAVLLLLMATFALIAHWLACIW -540  
 YAIGNVERPHLPPPKIGWLDQLAEQTHQOQYVNGTGGPTIKSKYVTALY**FTFSSLTSVGF**G -600  
**NVS**PNTNSEKIFSIILIMLIGSLMYASIFGNVSAIIQRLYSGTARYHTQMLRIKEFIRFHQ -660  
 IPNPLRQRLEEFQHAWSYTNPIDMMVLKSFPECLQADICLHLNKTILINNCQAFKQASP -720  
 GCLRALSMKFKTTHVPPGDTLQHR**GDVLTGLYFISRGSIEILKEDIVVAILGKDDVFG**EN -780  
**ICKHETIGKSSCNVRALTYCDLHKIHRED**LLEILDMPYEFSEHFTRNLEVTDFDLRDEDLV -840  
 IKRADNENNSFGARQMLRKRRSVKS DHSSGSASPDEGNKEYKFRPSRARRLRQVNQSEG -900  
 QMMSTSFDSSEDEIQESGAGILEFSPNKAGQDITPANFEFDSKDDKKRPGFSSIAAGALA -960  
 NVNNLVNAVGTGRYDHQKMDQDTAPLLQDHS HSSDTQPKGMSSSSMPKSTSSMTLPVSS -1020  
 PSTQSQFEEAQGQTTFIPTCQEEQNDGHSSPQDVEKRLDELARQLTRLERKMGCDIAMIL -1080  
 NILRSQTVEASHTTQISSDPRVTPPDGNLPPPPDYNQIQEDDDTFGYQDTADKSGKSQDS -1040  
 AKQSKMVS DTDSEEDGPWKPR TDCDIVSPLSTIPTSDNSISCDPTDSTHSSSFSQSQTVS -1200  
 PLSEAVSPISQSEDPAQSQFSQSQSSTLSPTTRRRRLGIPDGVD MRNTIV -1249  
  
 Number of residues of PectERG channel: 1249  
 Molecular mass: 139.08 kDa

**Figure 6.3:** Amino acid sequence of the PectERG channel. Amino acids corresponding to the voltage-sensing domain, the pore region and the cyclic nucleotide-binding domain (CNBD) are depicted in yellow.

MANIRNPSSQPLIDISEHDRPVSYSSDEESSNQNSPYRRAPEPPRNTPPVPHRSKGVSE -60  
 ATSSVVESEASTLQQVHLSPKITRSDSVKFSKSANGSAGRKSSHPIGSSQTPPKPSRRVP -120  
 SLKLRMNLGVNSDKAEGTMPCLPKCPNRPTNPSITITITIESEESIYS DYLS PDMN YNND -180  
 IKVHFGDEQSLYGTPEKELLPGSGETSSTDQKTSPTS YLKEQFISFFQPSDNKLAMKLF -240  
 GNRNSLMREKMRHKRVGNWVIHPCSNFRFYWDLFMLVLLIANLIILPVAISFFNDDLSTH -300  
 WIVENCISD TVFFLDIVINFR TGFQISHDDQENVNSVILNDFADEIILD PKLIARHYVKS -360  
 WFFLDLISSIPMDYIFLMWDAEADFNQLFHAGTTASMGPS **Voltage-sensing domain**  
**SSYWQGRALRMLRLAKLLSLL** -420  
**RLRLSRLVRYVQWEE**HMAKNFEGSPCFAMCGRRRRPGFLAFAGKFMRIFNLLCLMFL -480  
**Pore region**  
**WALFKALSHMLCIGYGR**FPPQN -540  
 GHWNGCLQFLIPMLQEYPDDCWVSIEGLKKAHWAEQYTWALFKALSHMLCIGYGRFPPQN -540  
 MTDTWLTILSMLSGATCYALFLGHTTTIIQSFDTSRRLYNEKFKQVEEYMIYRKLPRRLR -600  
 QKISEYYEHRYQGKMFDEENILCELNECLRQDIINHNCRALVKSVPFFANADPQFVSEVI -660  
**CNBD**  
**SKLIFEVYQPGDYIIREGTMGTKMYFISEGIVDIIITMDNEVATSLSDGSYFGEICLLTNA** -720  
**KRVASVRAETYVSVVSLCVTHFNIVLERYPVMRRTMESVAAERLTK**IGKNPSLVSSRADL -780  
 EEDQKLVNEIVMESTPVVTSASEDEDKSDSDSSESSKSSRKRKFKFDFTGKLHRITEER -840  
 KSKSKESLRDLDIPNGKVGRMKKAPSGPNLFGLRVPHFPERRRSGSVGADLNRMQQSSCS -900  
 DESRRSDPEDMKDGSRRSSFLGTKLFPSEQK -933  
  
 Number of residues of PectHCN channel: 933  
 Molecular mass: 106.72 kDa

**Figure 6.4:** Amino acid sequence of the PectHCN channel. Amino acids corresponding to the voltage-sensing domain, the pore region and the cyclic nucleotide-binding domain (CNBD) are depicted in yellow.

MFHPVKRLNSRTVPVSRRTSSNSSKRSEELEDDDDVDDAKLEDTTTRRNVKLMDSHRVS -60  
 DTAVHDGHSPLQLRKLWSGIEGTEGNHTSDMTNTSKSPQNETMEALHTNLSTRVLDPDGN -120  
 WCYNWMIIVTMAALYNIVVVIILRLAFAEMREHVLPTLFTVLDLGCDAVYLIDIVVQSRV -180  
 SHYEDGCLVSDVHNVSERYWRRTRFRKLDMLSILPLHTVIFICQGLRCINVSIGIDQYRF -240  
 YIAITRLPRLKARTVSEFFDITDSRTSNPNFVRAIKLTLYLLLVIHWIGCLYIMVSLYE -300  
**Pore region**  
 GIGSTEWAYSSGNYPDTFVRKYICCIYWSLLILTTIGERPPPQTNLEHVFTGMTFVIGVF -360  
 IFAAVVGNVGDVISNLNASRQEFQSRMDQIKFYLRHRNVPIPLQNRVKRWADYTWSKNQA -420  
 MDEPQLLQMLPERLQMEIAIQVHLDTLKKVTFEECEEGLLRELVLKLRPQIFSPGDYIC -480  
**CNBD**  
 HIGDIGREMYIINHKGIEIVVPCADTGQTQRVATLGTGNYFGEISLLKLD SGQNRRTADV -540  
 RSVGYSELLRLSRKDLLTALVEYPAKAILETQAKLRMNETRVIRNTNGDEQSLPPSERR -600  
 TIESSKRKRDWLSGIVQSDSFKKLVENKGTLSQLKTIVNQLRDYQTIHEKSNSRSVEK -660  
 RKRLLEKLQOYDKTLRKANKKIQEQALGASCACGKVSNSVDTASSYRKS -711

Number of residues of PectCNG1 channel: 711  
 Molecular mass: 81.62 kDa

**Figure 6.5:** Amino acid sequence of the PectCNG1 channel. Amino acids corresponding to the pore region and the cyclic nucleotide-binding domain (CNBD) are depicted in yellow.



# Acknowledgments

This work was performed at the Department of Molecular Sensory Systems of the Research Center caesar in Bonn. I thank all the employees of the Research Center caesar for their support, whose help made this research possible.

I want to thank Prof. Dr. Benjamin Kaupp for giving me the opportunity to work in his group and for all his support throughout the course of my PhD thesis. Since I was an undergraduate student, Prof. Kaupp was a source of inspiration; his papers were always fascinating.

I would like to thank Prof. Dr. Michael Pankratz for taking over the role of second reviewer of my PhD thesis.

I would like to also thank PD. Dr. Dagmar Wachten and Prof. Dr. Ulrich Kubitscheck for being part of my doctoral committee.

I would like to thank Dr. Reinhard Seifert for all his support from the beginning to the end of this work. Dr. Seifert supervision of my PhD thesis was outstanding, his scientific advice was critical for my development as a scientist.

In addition, I would like to thank Prof Dr. Timo Strünker and Dr. Christoph Brenker for their support in the hSlo3-channel project.

I also would like to thank Dr. Wolfgang Bönigk for teaching me all the tricks that make a superb Molecular Biologist.

I would like to thank Drs. Enrico Nasi and Maria Gomez for all the summers at the MBL in Woods Hole and their support throughout my scientific career. I cannot thank you enough!

I would like to thank the Grass Foundation for the best summer of my life. The Grass Fellowship was a life-changing experience; the scientific community at the MBL is truly inspiring.

I would like to thank Dr. Alberto Pereda for his support in my career and life in general.

I would like to thank Dr. Luis Alvarez for his help through my PhD thesis and when I first moved to Germany.

I would like to also thank all the Postdocs and PhD students of the Dept. Molecular Sensory Systems. I would like to specially thank Shatanik and Diana for their support and understanding of the difficulties one faces as a foreigner living abroad.

I would also like to thank Florian Windler for his friendship and all the Kicker matches after lunch.

I would like to thank David Fusshöller for all his support during the writing of the thesis, without his support during submission this thesis literally would not have been possible. Also, I would like to thank David for all his German and Kicker lessons!

I would like to thank my family; their love and support have given me the strength to pursue my dreams in life. I would like to specially thank my aunt Luz Myriam, who has been my role model my entire life. Thanks for everything!

Last but not least, I would like to thank Meg Younger for all her support and patience during the writing process of my PhD thesis. Thanks a lot!

Ich versichere, dass ich die von mir vorgelegte Dissertation selbständig angefertigt, die benutzten Quellen und Hilfsmittel vollständig angegeben und die Stellen der Arbeit – einschließlich Tabellen, Karten und Abbildungen –, die anderen Werken im Wortlaut oder dem Sinn nach entnommen sind, in jedem Einzelfall als Entlehnung kenntlich gemacht habe; dass diese Dissertation noch keiner anderen Fakultät oder Universität zur Prüfung vorgelegen hat; dass sie – abgesehen von der unten angegebenen Teilpublikation – noch nicht veröffentlicht worden ist, sowie, dass ich eine solche Veröffentlichung vor Abschluss des Promotionsverfahrens nicht vornehmen werde. Die Bestimmungen der Promotionsordnung sind mir bekannt. Die von mir vorgelegte Dissertation ist von Prof. Dr. U. Benjamin Kaupp betreut worden.

Bonn, den 17.11.2016

Fabio Andres Echeverry Bautista

Im Rahmen meiner Doktorarbeit ist folgende Publikation entstanden:

Brenker C, Zhou Y, Müller A, **Echeverry FA**, Trötschel C, Poetsch A, Xia XM, Bönigk W, Lingle CJ, Kaupp UB, Strünker T. The Ca<sup>2+</sup>-activated K<sup>+</sup> current of human sperm is mediated by Slo3. 2014. eLife.

